U.S. Geological Survey
Open File Report # 94-192
April 5, 1994

Geophysical Database of the East Coast of the United States Northern Atlantic Margin: Velocity Analyses

K.D. Klitgord and C.M. Schneider
U.S. Geological Survey
Woods Hole MA 02543

Geophysical Database of the East Coast of the United States Northern Atlantic Margin: Velocity Analyses

K.D. Klitgord and C.M. Schneider
U.S. Geological Survey, Woods Hole MA 02543

Introduction

Acoustic transmission characteristics in the marine environment are influenced by the sound propagation properties of the rock units beneath the sea floor. Geoacoustic models of these rock units are "basic to underwater acoustics and to marine geological and geophysical studies of the earth's crust, including stratigraphy, sedimentology, geomorphology, structural and gravity studies, geologic history, etc." (Hamilton, 1980). Numerous geoacoustic models (e.g., Hamilton, 1980; Stoll, 1980; Hamilton and Bachman, 1982) have been developed from small, local data sets in acoustic transmission studies, but their general utility has been limited by the lack of regional geoacoustic data sets for model parameter determinations. A regional geoacoustic database on the U.S. Atlantic margin has been developed for the U.S. Naval Oceanographic Office by the U.S. Geological Survey as an initial step to meet this need. Multichannel seismic-reflection data are the primary sources of acoustic information used in this construction. It is recognized that these data have limited resolution in the upper 500m of the sedimentary column, critical for transmission studies, but this database can be used in existing geoacoustic models to define the nature and extent of more detailed high-resolution acoustic studies of the upper sedimentary column.

This report describes the velocity data utilized in the construction of the geoacoustic database. Information concerning the stratigraphic, structural, and regional distribution aspects of this geoacoustic database is presented in a companion report (Klitgord and others, 1994). Velocity data for the northern U.S. Atlantic margin have been derived from a combination of normal moveout velocity analyses on a network of multichannel seismic-reflection profiles (Figure 1), sonic logs and velocity checkshot studies at various industry drillholes (Figure 2), and wide-angle seismic data from 2-ship seismic experiments (LASE) (Figure 3). Seismic-refraction data (Figure 3) have been examined for consistency of final seismic velocity vertical profiles, but these data have not been incorporated into the database.

The Geoacoustic Database

The basic database is a suite of geoacoustic parameters (Tables 1, 2 and 3) for a layered set of acoustic stratigraphic units on the continental shelf and adjacent slope and rise of the Atlantic continental margin of the United States (Poag, 1985b, 1992; Schlee, 1984; Klitgord and others, 1988; Sheridan and Grow, 1988; Grow and others, 1988). Each of these units is comprised of rocks with lithologies that can vary across and along the margin. All of the rock units in this data base are sedimentary; we have minimal velocity information from the underlying igneous and metamorphic rocks. Primary input data for the database are 1.)

seismo-stratigraphic horizons (Table 4) from seismic-reflection profiles (Figure 1 and Appendix 1), 2.) bio- and lithostratigraphic information at a sparse set of industry and stratigraphic test drill wells (Appendix 2) and surficial seafloor sampling sites, and 3.) seismic-velocity information from normal-moveout analyses of multichannel seismic-reflection data, sonic logs and checkshot velocity studies at industry and stratigraphic test drill wells (Figure 2 and Appendices 2 and 3) and seismic-refraction studies (Figure 3; Sheridan and others 1988). These data are used to determine the three-dimensional (horizontal and vertical) geometries of stratigraphic units for the database, lithologies and ages of these units, and RMS sound transmission velocities to the surfaces that bound these units. This set of observations is then expanded to include geologic and acoustic parameters that are derived from this initial set of parameters: density (ρ), compressional-wave (p-wave) velocity, shear-wave (s-wave) velocity, p-wave attenuation (k_p), and s-wave attenuation (k_s). The stratigraphic parameters have been determined at a spacing of 5 shot points (250 m on newer seismic-reflection lines and 500 m on older lines as indicated in Appendix 1) and the velocity parameters have been determined at an ~3000-m spacing; both data sets have been merged onto a 5-minute spacing grid (9250 m x 7100 m) for the final database. Thus the database is actually two data sets: one confined to points along individual seismic lines and the second interpolated onto a regional grid.

A basic premise in this study is that the geoacoustic parameters of a given unit or reflector are influenced only by the material above it and the unit just below it. The acoustic units are defined by acoustic reflectors that bound them on top and bottom. Nomenclature has been developed for these units such that parameters are related to the surface (reflector) that defines the base of each unit. Two-way travel times (in seconds; sea level to reflector to sea level), depth below sea level (in meters) and RMS velocities, properties related to the entire overlying crustal column, are given with respect to a particular reflector (Figure 4). Densities, thicknesses, p-wave velocities, s-wave velocities and attenuation properties pertaining to a given unit are relate to the unit directly above a given reflector. Each reflector has been numbered (see Table 4) to facilitate digitizing and identification in the digital arrays. These numbers monotonically increase with depth (and age) but they have no meaning in a geologic sense. Most of these surfaces are erosional unconformities, some of which have eroded deeply enough into the sedimentary wedge to completely remove one or more underlying units on parts of the margin. In such cases, two or more reflectors merge and there could be ambiguity in identifying the age of the boundary between two units. In the situation shown in Figure 5, reflector 60 is the top of Eocene-Paleocene sediments in some places and the top of Cretaceous sediments in others. The mid-Oligocene unconformity (base of Upper Oligocene; reflector 60) has eroded down to the top of the Cretaceous (base of Paleocene-Eocene; reflector 70) and we have referred to that surface as reflector 60 (base of Upper Oligocene). To avoid ambiguity, we always refer to a reflector as the surface that defines the base of the overlying unit rather than as the top of the underlying unit. In this way, when we discuss the properties in the database, we can refer to material that *exists* above a reflector, since it is often possible that the original material below a reflector (in the case of reflector 60 it is Eocene-Paleocene material) is now missing. In this convention, prominent geologic boundaries, such as the surface forming the top of the Cretaceous, will consist of portions of several reflectors (e.g., reflector 70, then reflector 60 and finally reflector 70 again in Figure 5). This nomenclature (referencing to the bottom of units) is different from the standard reference to the top of units, but it eliminates ambiguity in the layer reference frame and simplifies the bookkeeping.

Table 1: Geoacoustic Parameters and Formulas used to calculate them.

For each horizon n (n=1,N) or each layer n bounded by horizons n-1 and n:

$T(n)$ = two-way travel time depth below sea level of reflector n (in seconds);
$T(0)$ = 0.0 = sea surface observed on seismic-reflection records.
$V_{rms}(n)$ = RMS velocity of all units above reflector n (in m/sec)
calculated from NMO analysis of multichannel seismic data.
$A(n)$ = age of unit above reflector n based on correlation of acoustic units to biostratigraphic information at drill sites or dredge sites.
$ST(n)$ = sediment type within unit above reflector n based on correlation of acoustic units to lithostratigraphic information at drill or dredge sites (see symbol codes in Table 4).
$V_i(n)$ = interval velocity of unit above reflector n in m/sec
$= (V_{rms}(n)-V_{rms}(n-1))/(T(n)-T(n-1))$
$V_p(n)$ = compressional-wave velocity for unit above reflector n in m/sec
$= V_i(n)$
$V_p(water)$ = 1500 m/sec on all of profiles.
$DZ(n)$ = thickness of layer n in meters
$= (T(n)-T(n-1))\cdot V_i(n)$
$D(n)$ = depth of reflector n in meters
$= \Sigma (T(j)-T(j-1))\cdot V_i(j)$ for $j=1,n$
$Z(n)$ = depth to midpoint of unit above reflector n in meters
$= D(n) - DZ(n)/2$
$\rho(n)$ = density of rock within unit n in gm/cc
calculated from V_p using the following formulae for terrigenous marine sediments (Hamilton, 1978, p. 368)

$= 14.80\ V_p - 21.014$ gm/cc	at V_p (seafloor)
$= 1.135\ V_p - 0.190$ gm/cc	1.5 km/s < V_p < 2.0 km/s
$= -0.08\ V_p \cdot V_p + 0.744\ V_p + 0.917$ gm/cc	2.0 km/s < V_p < 4.5 km/s

$V_s(n)$ = shear-wave velocity in unit n
calculated from V_p using the following formulae for terrigenous marine sediments (Hamilton, 1979, p. 1095):

$= 3.884\ V_p(n) - 5.757$ km/s	1.512 km/s < V_p < 1.555 km/s
$= 1.137\ V_p(n) - 1.485$ km/s	1.555 km/s < V_p < 1.650 km/s
$= +0.47\ V_p(n)\cdot V_p(n) - 1.136\ V_p(n) + 0.991$ km/s	1.650 km/s < V_p < 2.150 km/s
$= 0.780\ V_p(n) - 0.962$ km/s	2.150 km/s < V_p

for mud stone (Castagna and others, 1985):
$= 0.862\ V_p(n) - 1.172$ km/s

$\alpha_p(n)$ = compressional-wave attenuation in dB/m
$= F(k_0, V_p(n), D(n-1), D(n), f)$
where k_0 is a constant dependent on surface rock type, f is the frequency in kHz (Mitchell and Focke ,1980; Stoll, 1985).
$\alpha_s(n)$ = shear-wave attenuation in dB/m
$= k_s \cdot f$ where k_s is a constant in dB/m-kHz , f is frequency in kHz
(Hamilton, 1976a,b; Castagna and others, 1985)

Geoacoustic Parameters

The digital database contains the following information at a 250-m or 500-m spacing along each seismic-reflection line and at each of the 5-minute grid points in the study area where adequate data are available: labelling by line number, shot point, latitude-longitude pairs and an array of geoacoustic parameters at each of these points. This parameter array includes information determined from seismic or sample data: reflector number, two-way travel time (T) of each reflector, RMS velocity (V_{rms}) between sea surface and this reflector, layer age (A) and sediment type (ST). From these data we have calculated at each location: depth (D) in meters to the reflector and thickness (DZ), density (ρ), p-wave velocity (V_p), s-wave velocity (V_s), p-wave attenuation (k_p), and s-wave attenuation (k_s) for each layer (Tables 1, 2 and 3).

Table 2: Example of Profile Geoacoustic Database

Line No.	Shot Point No.	Latitude (deg.)	Longitude (deg.)	Layer No.	Sed. Type	Travel Time (sec.)	Depth (m)	Thick-ness (m)	Density (gm/cc)	RMS Vel. (m/s)	P-Wave Vel. (m/s)	S-Wave Vel. (m/s)	Surface Atten.	P-Wave Atten. (dB/m-kHz)	S -Wave Atten.
22	915	-71.0864	41.1034	001	02	0.070	052	052	1.000	1500	1500	-	0.01138	-	-
22	915	-71.0864	41.1034	020	02	0.210	169	117	1.715	1620	1678	408	-	0.01302	0.18339
22	915	-71.0864	41.1034	070	04	0.240	196	026	1.830	1641	1780	458	-	0.01672	0.12278
22	915	-71.0864	41.1034	080	04	0.400	350	153	1.989	1758	1920	542	-	0.04559	0.17813
22	915	-71.0864	41.1034	090	04	0.470	423	073	2.123	1811	2090	669	-	0.06491	0.14818
22	1002	-71.0644	41.0658	001	02	0.070	052	052	1.000	1500	1500	-	0.01150	-	-
22	1002	-71.0644	41.0658	020	02	0.211	171	118	1.727	1628	1689	413	-	0.01305	0.16945
22	1002	-71.0644	41.0658	070	04	0.250	206	035	1.859	1657	1805	471	-	0.01527	0.09843
22	1002	-71.0644	41.0658	080	04	0.420	372	166	2.028	1783	1954	565	-	0.03864	0.13345
22	1002	-71.0644	41.0658	090	04	0.510	468	095	2.138	1848	2127	701	-	0.05020	0.10421
22	1062	-71.0486	41.0406	001	02	0.070	052	052	1.000	1500	1500	-	0.01193	-	-
22	1062	-71.0486	41.0406	020	02	0.237	194	141	1.741	1643	1701	418	-	0.01364	0.16263
22	1062	-71.0486	41.0406	070	04	0.274	229	034	1.909	1673	1849	497	-	0.03769	0.19713
22	1062	-71.0486	41.0406	080	04	0.442	396	167	2.080	1804	2000	599	-	0.03401	0.10081
22	1062	-71.0486	41.0406	090	04	0.550	514	117	2.158	1883	2177	736	-	0.06548	0.12066
22	1122	-71.0339	41.0148	001	02	0.070	052	052	1.000	1500	1500	-	0.01279	-	-
22	1122	-71.0339	41.0148	020	02	0.260	214	162	1.750	1655	1709	422	-	0.01906	0.21511
22	1122	-71.0339	41.0148	070	04	0.300	252	037	1.939	1686	1876	513	-	0.07267	0.33819
22	1122	-71.0339	41.0148	080	04	0.460	415	163	2.101	1816	2039	628	-	0.05726	0.15071
22	1122	-71.0339	41.0148	090	04	0.572	540	124	2.178	1904	2228	775	-	0.11813	0.19468
22	1182	-71.0194	40.9890	001	02	0.070	052	052	1.000	1500	1500	-	0.01422	-	-
22	1182	-71.0194	40.9890	020	02	0.270	224	171	1.759	1663	1717	426	-	0.01929	0.20641
22	1182	-71.0194	40.9890	070	04	0.320	271	047	1.957	1701	1892	524	-	0.09098	0.39647
22	1182	-71.0194	40.9890	080	04	0.470	426	154	2.112	1825	2065	649	-	0.06493	0.15867
22	1182	-71.0194	40.9890	090	04	0.580	551	125	2.196	1918	2275	812	-	0.12349	0.18506
22	1242	-71.0040	40.9639	001	02	0.071	053	053	1.000	1500	1500	-	0.01642	-	-
22	1242	-71.0040	40.9639	020	02	0.260	215	161	1.753	1656	1712	423	-	0.01905	0.21069
22	1242	-71.0040	40.9639	070	04	0.312	264	049	1.964	1699	1898	528	-	0.07685	0.32696
22	1242	-71.0040	40.9639	080	04	0.470	428	164	2.116	1833	2074	656	-	0.06336	0.15102
22	1242	-71.0040	40.9639	090	04	0.600	577	148	2.202	1942	2292	825	-	0.11758	0.17052
22	1302	-70.9893	40.9386	001	02	0.072	053	053	1.000	1500	1500	-	0.02031	-	-
22	1302	-70.9893	40.9386	020	02	0.267	220	166	1.749	1654	1708	421	-	0.04753	0.54013
22	1302	-70.9893	40.9386	070	04	0.310	261	040	1.962	1689	1896	526	-	0.09897	0.42444
22	1302	-70.9893	40.9386	080	04	0.480	436	175	2.113	1831	2066	650	-	0.07543	0.18382
22	1302	-70.9893	40.9386	090	04	0.610	586	149	2.203	1940	2296	828	-	0.02376	0.03420
22	1302	-70.9893	40.9386	105	04	0.618	595	009	2.250	1947	2424	928	-	0.01955	0.02256
22	1362	-70.9747	40.9128	001	02	0.073	054	054	1.000	1500	1500	-	0.02491	-	-

Table 3: Example of Gridded Geoacoustic Database

Latitude (degrees): 40.500000
Longitude (degrees): -71.000000

Layer No.	Surface (Age)	Sed. Type	Travel Time (sec)	Depth (m)	Thick-ness (m)	Density (gm/cc)	Velocity RMS (m/s)	Velocity P-Wave (m/s)	Velocity S-Wave (m/s)	Atten. Surface	Atten. P-Wave (db/m-kHz)	Atten S-Wave
001	Seafloor	02	0.106	79	79	1.000	1500	1500	-	0.021	-	-
020	Base Quaternary	02	0.240	189	110	1.676	1581	1644	384	-	0.036	0.665
045	Base Mid Miocene	02	0.342	280	91	1.840	1646	1788	462	-	0.078	0.545
070	Base Tertiary	04	0.420	354	73	1.945	1692	1881	517	-	0.176	0.802
080	Base Campanian	04	0.671	619	264	2.133	1861	2115	691	-	0.167	0.358
090	Base Coniacian	04	0.982	1000	381	2.259	2065	2447	947	-	0.013	0.015
105	Base Aptian	04	1.126	1202	201	2.378	2175	2815	1234	-	0.010	0.007
140	Base Kimmeridgian	08	1.159	1252	49	2.431	2203	3007	1383	-	0.010	0.006
190	Base Aalenian	12	2.977	5236	3984	2.641	3690	4382	2456	-	0.010	0.003

Latitude (degrees): 40.583333
Longitude (degrees): -71.000000

Layer No.	Surface (Age)	Sed. type	Travel Time (sec)	Depth (m)	Thick-ness (m)	Density (gm/cc)	Velocity RMS (m/s)	Velocity P-Wave (m/s)	Velocity S-Wave (m/s)	Atten. Surface	Atten. P-Wave (db/m-kHz)	Atten. S-Wave
001	Seafloor	02	0.094	70	70	1.000	1500	1500	-	0.022	-	-
020	Base Quaternary	02	0.240	192	121	1.698	1601	1663	401	-	0.078	1.235
045	Base mid Miocene	02	0.316	260	67	1.838	1647	1786	461	-	0.036	0.259
070	Base Tertiary	04	0.377	317	56	1.940	1686	1876	514	-	0.161	0.746
080	Base Campanian	04	0.610	562	245	2.131	1860	2111	687	-	0.158	0.341
090	Base Coniacian	04	0.886	898	336	2.253	2055	2430	933	-	0.015	0.017
105	Base Aptian	04	1.022	1085	186	2.358	2160	2749	1182	-	0.010	0.008
190	Base Aalenian	12	2.621	4462	3376	2.632	3563	4223	2331	-	0.010	0.003

Latitude (degrees): 40.666667
Longitude (degrees): -71.000000

Layer No.	Surface (Age)	Sed. Type	Travel Time (sec)	Depth (m)	Thick-ness (m)	Density (gm/cc)	Velocity RMS (m/s)	Velocity P-Wave (m/s)	Velocity S-Wave (m/s)	Atten. Surface	Atten. P-Wave (db/m-kHz)	Atten. S-Wave
001	Seafloor	02	0.084	63	63	1.000	1500	1500	-		-	-
020	Base Quaternary	02	0.242	195	132	1.717	1619	1680	409	0.020	0.052	0.727
045	Base mid Miocene	02	0.300	247	51	1.834	1652	1783	459	-	0.110	0.797
070	Base Tertiary	04	0.343	287	40	1.926	1680	1864	506	-	0.029	0.144
080	Base Campanian	04	0.559	514	226	2.127	1854	2100	678	-	0.082	0.182
090	Base Coniacian	04	0.796	798	284	2.239	2030	2393	904	-	0.087	0.105
105	Base Aptian	04	0.916	957	159	2.330	2122	2659	1112	-	0.010	0.008
190	Base Aalenian	12	2.274	3710	2753	2.618	3410	4053	2199	-	0.010	0.003

Latitude (degrees): 40.750000
Longitude (degrees): -71.000000

Layer No.	Surface (Age)	Sed. Type	Travel Time (sec)	Depth (m)	Thick-ness (m)	Density (gm/cc)	Velocity RMS (m/s)	Velocity P-Wave (m/s)	Velocity S-Wave (m/s)	Atten. Surface	Atten. P-Wave (db/m-kHz)	Atten. S-Wave
001	Seafloor	02	0.075	56	56	1.000	1500	1500	-	0.021	-	-
020	Base Quaternary	02	0.234	190	134	1.724	1628	1686	411	-	0.053	0.706
070	Base Tertiary	02	0.318	267	77	1.896	1686	1838	490	-	0.070	0.386
080	Base Campanian	04	0.513	469	201	2.116	1843	2075	657	-	0.068	0.163
090	Base Coniacian	04	0.719	710	241	2.218	1997	2335	860	-	0.092	0.123
105	Base Aptian	04	0.808	823	113	2.295	2065	2553	1030	-	0.012	0.011
190	Base Aalenian	12	1.936	3009	2186	2.599	3246	3876	2061	-	0.010	0.004

Seismic Stratigraphy

The acoustic units incorporated into the geoacoustic database are seismostratigraphic units defined by Poag (1982, 1985a,b, 1987; Schlee and others, 1985; Poag and Valentine, 1988; Poag and Ward, 1993) for the U.S. Atlantic margin. This comprehensive division of stratigraphic units has been developed from a seismic stratigraphic analysis of seismic profiles on our multichannel seismic grid (Figure 1). This seismic stratigraphy has been calibrated with biostratigraphic data from the suite of industry drill wells onshore and offshore (Poag, 1982, 1985b, 1987; Poag and Ward, 1993) plus dredge sample data from canyons that dissect the continental slope (Valentine, 1981) and the Blake Escarpment (Dillon and Popenoe, 1988). The two-way travel times to each reflector (sea surface to reflector to sea surface) were digitized along the length of each seismic-reflection profile, creating a seismic stratigraphic cross section of time depth vs distance. As mentioned above, these reflectors are defined as the base of geologic units. Where reflectors intersect, only the youngest reflector is entered into the database. The reflector numbers used in the database are purely arbitrary and are given here to facilitate labelling of computer plots of seismic stratigraphic cross sections. Ages assigned to the geologic units are based on the geologic timescale of Palmer (1983).

Table 4: U.S. Atlantic Margin Seismic Stratigraphy

Refl.No.*	Geologic Surface	Reflector Name**
1	Base of water column - seafloor	seafloor
20	Base Quaternary	
30	Base Pliocene	
40	Base Upper Miocene	
45	Base Middle Miocene	Mid-Miocene Unconformity
50	Base Lower Miocene	
60	Base Upper Oligocene	Mid-Oligocene Unconformity
70	Base Tertiary	Top Cretaceous
80	Base Campanian/Maastrichtian	Horizon A* in Deep Sea
90	Base Coniacian/Santonian	Late Cenomanian Unconformity
100	Base Cenomanian/Turonian	Mid Cretaceous Unconformity
105	Base Aptian/Albian	
110	Base Barremian	Horizon ß in Deep Sea
120	Base Berriasian/Hauterivian	Top Jurassic
130	Base Tithonian	
140	Base Kimmeridgian	
150	Base Oxfordian	Top Middle Jurassic
170	Base Upper Bathonian/Callovian	
180	Base Bajocian/Lower Bathonian	
190	Base Aalenian	Postrift Unconformity
230	Base synrift sediments	Crystalline basement
300	Base of crust	Moho

* Numbers have no geologic significance and are used only as a tag in the digital database. They correspond to the same geologic horizons throughout the data set.

* * Names more commonly used in literature than those in the geologic surface column.

Sediment Types and Lithologies

Lithologies vary within these units as indicated in the database. The gross lithologies of stratigraphic units have been determined from lithologic logs at drill holes and dredge samples from submarine canyons that cut deep into the continental slope integrated with the analysis of acoustic character on seismic profiles in our multichannel seismic grid (Poag, 1982, 1985b, 1987; Poag and Ward, 1993). This technique is based on the association of distinctive acoustic signatures with specific depositional environments and lithologies (Vail and others, 1977; Poag and Schlee, 1984; Van Wagoner and others, 1988). The resulting estimates of sediment types are very subjective, therefore only a small set of lithologies are incorporated into the database (Table 5). There are few surface samples in deep water seaward of the shelf edge and this region has been assigned a general type of clay (k_0 = 0.045).

Table 5: General Lithologic Types Identified on the U.S. Atlantic Margin

Rock Type	Numerical Code in Database
Silt/Sand	02
Clay/Shale	03/04
Chalk/Limestone	06/08
Dolomite	10
Halite + Anhydrite	12
Halite	14

* Rock types are in approximate increasing grain size or proximity to sediment sources

Surficial sediment types (Table 6) along individual seismic lines and on the database grid were extracted from a digital database of over 40 years of surficial sampling compiled by Hathaway and others (1994). This compilation is based on the original work of Hathaway (1971), Schlee (1973), Hathaway and others (1979) and an updated study by Poppe and others (1989) mapping surficial sediment types on the U.S. Atlantic continental margin. The database of surficial sediment types is based on grain size analyses which are then used to define sediment types by standard definitions of grain size for specific sediment types. These grain sizes have been used to determine the surface attenuation of compressional wave velocities (k_0).

Table 6: Surficial Sediment Types and Surface Attenuation

Sediment Type*	Phi Class	Grain Size (mm)	Surface Attenuation (k_0)**
Coarse Sand	<1	>0.5	0.005
Medium Sand	<2	0.25-0.5	0.010
Fine Sand	<3	0.125-0.25	0.015
Sandy Silt	<4	0.0625-0.125	0.020
Silty Sand	<5	0.0312-0.0625	0.025
Silt	<6	0.0156-0.0312	0.030
Silty Clay	<7	0.0078-0.0156	0.035
Clayey Silt	<8	0.0039-0.0078	0.040
Clay	<9	0.00195-0.0039	0.045

* Sediment types arranged by decreasing grain size

** k_0 values are compressional-wave surface attenuation in dB/m-kHz where $\alpha = k_0 f^m$ based on the Biot-Stoll model and applicable only below 1 kHz (Stoll,1985)

Seismic Velocities

Velocity data for the northern U.S. Atlantic margin (Baltimore Canyon Trough, Long Island Platform, and Georges Bank Basin regions) are derived from the stacking velocities determined for the multichannel seismic-reflection profiles as part of the standard industry processing of seismic-reflection data. The velocity data for our grid of seismic profiles were calibrated with velocity data at a suite of industry wells along composite seismic profiles connecting industry wells in Georges Bank Basin (Composite CDP Line G1-G2, Figure 6) and Baltimore Canyon Trough (USGS CDP line 14, Figure 7; USGS CDP Line 15, Figure 8). These calibrated sections of seismic profiles were linked to three standard reference section dip lines (one for each area) and one strike line (Figure 1) as a first step towards developing a consistent velocity structure for the entire region. One dip-line transect crosses Georges Bank Basin (USGS CDP Line 19, Figure 9), one crosses the central Baltimore Canyon Trough (USGS CDP Line 25, Figure 10), and a third goes through a Navy test area south of Long Island (USGS CDP Line 22, Figure 11). USGS CDP Line 12 is the strike line on the shelf that links these velocity calibration sites and dip lines with the rest of the seismic grid. Seismic line 13 links the seaward end of all of the dip lines, but the velscan data on this line are too erratic for it to serve as a calibration tie line.

RMS Velocities

Primary acoustic velocity information for this project is RMS velocity vs two-way travel time data derived from multichannel seismic data velocity analyses. Velocity analyses (velscans) of normal-moveout (NMO) corrections for stacking velocities of multichannel data are used to generate semblance curves (coherence) of RMS compressional-wave velocity (V_{rms}) as a function of two-way travel times at a coarse spacing (velscan points approximately every 5 km) along each multichannel line. The objective of this standard processing is to identify the velocity vs depth functions that would maximize the coherence of stacked data from multiple shots and multiple receivers. Examples of the results from these analyses are shown in Figures 12 and 13. The RMS velocity functions within different travel time intervals (δt = 0.1 sec), which correspond to maximum coherence values of stacked cdp gathers, are indicated by circled symbols in Figure 13a. Only the most reliable of these values have been plotted on Figure 13b. Scatter in these points originate from a variety of sources, including multiple reflections within layers (peg-leg multiples) throughout the section and refracted returns in the uppermost section. Peg-leg multiples create maximum coherence velocity functions that are slower than the true velocities. In contrast, shallow refracted returns, which spend part of their travel time within higher velocity material beneath a given reflector and violate the assumptions used in this velocity analysis technique, generate velocity functions that are faster than the true velocities. Examples of these high velocity functions can be seen in the upper half second of the plots in Figures 12 and 13. A detailed description of the technique is given in Yilmaz (1987, chapter 3). Note in Figure 13b the small difference between the original velscan function used to process the seismic-reflection data (light line) and the final smoothed function (heavy line) and how this small variation compares with the much larger scatter in the maximum coherence data points (circles). This comparison is representative of the entire data set and suggests that the final, smoothed velocity functions are at least as consistent as the stacking velocity functions with the NMO velocity data.

The initial RMS velocity information used in this study (referred to here as original velscan data) were undertaken as part of the original processing of the seismic-reflection data (1973 to 1976). The resolution of this velocity information decreases with depth and there is only minimal constraint on the velocities of material at a depth greater than about 6 km (twice the receiver length on most of the seismic lines). The manual evaluation techniques of individual velocity scans used in this processing led to significant fluctuations in interval velocity profiles from point to point within geologic units (Figures 14, 15, 16 and 17). The fluctuations in RMS velocity (e.g., Figure 18) had little influence on the quality of the reflection data processing but created unacceptable variations in interval velocities of individual acoustic units. As noted above, however, there is considerable leeway in the choice of velocities curves that are consistent with the maximum coherence data.

Some geologic-based assumptions are introduced here into the data processing to create a final smoothed set of velocity functions that represent as acceptable a fit as the original velscan data to the maximum coherence points (Figure 13b) but for which ±10% is a reasonable estimate of the variability. We have assumed that, in general, sedimentary units do not contain short-wavelength fluctuations (less than 2-3 kilometer) in lithology. For example, clastic material grades gradually into carbonate units over a distance of a few kilometers. The most abrupt lithologic (and velocity) changes occur at ancient carbonate bank shelf/slope breaks where erosional/depositional unconformities create abrupt terminations in a seismic unit. These terminations, because they are bounded by unconformities, usually correspond to a layer boundary and the abrupt velocity change occurs between layers and not within a layer. Thus the assumption of gradual changes in velocity within a layer is valid even at buried paleoshelf breaks. Therefore a procedure was used to create smoother interval velocity and associated RMS velocity functions which are more realistic from a geologic perspective. This procedure builds into the RMS data set the type of consistency which is now obtained in state-of-the-art seismic processing.

As an initial step, the initial RMS velocities are merged with our seismic-reflector database of travel times vs distance to calculate, by interpolation, the RMS velocity to each of these reflectors at the velscan points. Then velocity smoothing was undertaken on individual profiles in the RMS velocity domain by two-dimensional gridding of RMS velocity in the travel time and distance (shot point) domains using the commercial package ISM (Interactive Surface Modeling)[1]. The RMS velocity domain was chosen rather than the interval velocity domain because it provides the best representation of the original velocity data and is not sensitive to mismatches in the seismic stratigraphy between seismic lines. In this manner, a surface was created which is a smooth representation of the RMS velocity vs time function at each velscan point and assures a smoothed variation in this function along the length of the profile. The gridding was at a 0.2 second (two-way travel time) and at 1-km (along track) intervals. This gridding, with a minimum curvature assumption, created a smooth surface of RMS velocities and significantly reduced the variations found in the original velscan data sets (e.g., Figure 18). The comparison of original vs smoothed RMS velocities in Figure 13b is typical of the results of this smoothing and illustrates the equal credibility of either curve to fit the original semblance data.

[1] Trade name for descriptive purposes only; no endorsement implied.

Interval Velocities

Interval velocities were calculated from the ISM smoothed RMS velocities (e.g., Figures 14, 15, 16, and 17) using the technique of Taner and Koehler (1969). Although the resultant interval-velocity functions were considerably smoother than the original velscan functions, there were still significant long-wavelength (~20km) fluctuations in the velocity data within very uniform thickness units (see for example the time-stratigraphic sections shown in Figures 9, 10 and 11). These long-wavelength variations are not associated with variations in unit thicknesses (in two-way travel time), changes in overburden or distinct changes in acoustic character within a unit that might signify a change in lithology. These observations and the obvious pattern of similar fluctuations in multiple layers (see Figures 15a, 16a and 17a) indicate that these long-wavelength variations are not real. The pattern of higher velocities for several layers at one velscan location and much lower velocities for the same layers at adjacent velscan locations are caused by only small changes in the slope of velocity curves which have been fit to the RMS semblance data. These changes in slope, however, are not significant because of the steep slope of these curves and the poor velocity resolution at depths significantly greater than the length of the receiver. Therefore, additional hand smoothing of long-wavelength fluctuations was required in the deep sea sections of most profiles. This final smoothed interval velocity (e.g., Figures 15b, 16b and 17b) was used to recalculate the RMS velocity functions (see example shown in Figure 18). Comparison of the ISM smoothed and final hand-smoothed velocity functions with the original RMS velocity functions selected for stacking velocities (Figure 18) demonstrates the minor differences between these three functions. As can be seen in Figure 13b, any of these velocity functions could be selected as a valid representation of the velocity curves fitting the maximum coherence points at individual velscans. The final smoothed V_{rms} is the parameter used to calculate other parameters in the geoacoustic data set.

The interval velocity (V_i) for the unit above each reflector is calculated directly from the difference in RMS velocity to the bounding reflectors of the unit as indicated in Table 1 (Taner and Koehler, 1969). The interval velocity is one of the geoacoustic parameters which has significant geologic relevance; it is the estimate of the compressional-wave velocity for the unit. Geologic parameters derived from this velocity are useful for acoustic studies, gravity modeling studies and thermal subsidence and loading studies. The final interval velocity functions, based on the ISM and hand smoothed velocity data, have a very low variability built into them, based on the assumptions outlined above. These interval velocities for the different layers are displayed in Figures 9, 10, and 11 for the three standard margin cross sections. Note the lack of information below Cretaceous units near the shelf break, where acoustic scattering by a carbonate bank complex masks structures below it.

We outline below the velocity calibration studies on different parts of the margin. The velocity information from the studies at wells is tied into the database by incorporating their velocity vs depth profiles into the multichannel seismic velocity functions where they intersect. Each of the seismic lines was analyzed separately using the ISM smoothing technique outlined above. The ISM smoothed RMS and interval velocities were evaluated at each line crossing (Appendix 1) and adjusted in the final hand-smoothed functions to be both consistent between lines as well as removing the long-wavelength fluctuations (~20 km) which we have determined to be artifacts of the manual velscan interpretations.

Velocity Calibration and Analyses

Geoacoustic calibration for this study comes from direct velocity observations at the COST B-2, B-3, G-1, and G-2 wells (Taylor and others, 1977; Taylor and Anderson, 1980, 1982), other industry wells in the Baltimore Canyon Trough, a shallow seismic-refraction study on Georges Bank undertaken by McGinnis and Otis (1979), and the two acoustic test areas of Brocher and Ewing (1986) south of Long Island and in Buzzards Bay. Correlation of the RMS velocity and interval velocity vs depth from our smoothed velocity analysis with the checkshots and sonic logs at drill holes provides the only reliable means for evaluating these data (Taylor and others, 1977; Taylor and Anderson, 1980, 1982). Sonic logs from industry wells (Appendices 2 and 3) provide a direct measurement of interval velocity vs depth in a borehole. The technique used in this measurement results in considerable variability in velocities because the sample area of acoustic properties on the periphery of the borehole is very small and errors are readily introduced from imperfections in the borehole. Checkshots at the well site, with an acoustic source outside the well on the sea floor and a receiver on a logging tool within the hole provide the best approximation of well velocity data to functions derived from NMO velocity studies. Seismic refraction velocity values at refraction stations near multichannel lines (Figure 3) were always consistent with the MCS interval velocity data. However, the small number of layers identified in these refraction studies (Sheridan and others, 1979, 1988) made these velocities incompatible with the MCS data for representing interval velocities within the larger number of units mapped within this study.

Georges Bank Basin

Velocity calibration in Georges Bank Basin was carried out at the COST G-1 and COST G-2 wells (Amato and Bebout, 1980; Amato and Simonis, 1980; Scholle and Wenkam, 1982). These two COST (Continental Offshore Stratigraphic Test) wells are linked by the composite of multichannel seismic lines USGS CDP Line 77-1, USGS CDP Line 12, USGS CDP Line 1, and USGS CDP Line 77-2, referred to here as Composite CDP Line G1-G2 (Figure 1). This composite line is located in the center of Georges Bank Basin and its stratigraphy (Figure 6a) and interval velocity (Figures 6b and 14) profiles are characteristic of the basin. The final smoothed interval velocities on Composite CDP Line G1-G2 (Figure 6b) are representative of the low variability built into the digital database by the smoothing process outlined above. A comparison of sonic log and checkshot seismic velocity vs depth data with our digital database interval-velocity functions at COST G-1 (Figure 19a) and at COST G-2 (Figure 20a) illustrates the close fit between these three data sets. A comparison of the sonic log data and our digital database interval-velocity functions vs travel time at these wells (Figures 19b and 20b) shows a similarly close fit. There is a scatter of about ±250 m/sec of the sonic and checkshot velocity data with respect to the database velocity functions at well depths shallower than 3000m. The increased variability in the sonic and checkshot velocity data below 3000m is probably real, caused by the fluctuation between lithologies such as dolomite, anhydride, and clastic sands in the synrift and early postrift environments. Our database velocity functions in these regions are only an approximate average of these fluctuations. The comparison of our final velocity profile in the RMS velocity domain with the original velocity scan data from the NMO velocity analyses (Figure 12) and the original velscan interval-velocity functions with

our final smoothed velocity functions (Figure 14) provide checks that our smoothing process has created a velocity vs depth function which is still compatible with the original input data.

The velocity functions along seismic lines 19 and 18 (Figures 9 and 15) are typical of the data in the Georges Bank region. A complete set of final interval velocity functions on all seismic lines is presented in a companion report (Klitgord and others, 1994). Interval velocities in all units increase seaward across the margin to the shelf edge. This increase in velocity is associated primarily with an increasing depth of burial, but there may be a small component of increase caused by increasing carbonate to clastic ratios in the pre-mid Cretaceous units approaching a buried carbonate bank near the shelf edge. This carbonate bank complex effectively masks acoustic information from Jurassic rocks, resulting in a narrow zone on all profiles where the velocity data becomes chaotic and unusable (e.g., near shot point 4000 on line 19 (Figure 9) and shot point 3800 on line 18 (Figure 15)). The rapid decrease in velocities at this zone displayed on most of the original velscan functions is an artifact of the poorly constrained semblance data in this zone. Seaward of the shelf edge, beneath the continental rise, velocities within units and unit thicknesses are reasonably constant, despite the increasing water depth. Velocities decrease again to the east within deep sea sections where the entire sedimentary section thins and overburden of all units gradually decreases. The variations between interval velocity functions in deep water on line 18 (Figure 15) are the largest in the data set. This variability is caused by poorly processed initial data, as reflected in the abnormally low water column velocities (significantly less than 1400m/sec). The final hand-smoothed interval velocities are in agreement with the velocities on adjacent profiles linked to line 18 along lines 38 and 13.

Baltimore Canyon Trough

Velocity calibration in the Baltimore Canyon Trough incorporates velocity data from industry wells along USGS CDP Line 14 (Figure 7), USGS CDP Line 15 (Figure 8), and USGS CDP Line 25 (Figure 10)(Scholle, 1977; Libby-French, 1981; Poag, 1987, 1992; Grow and others, 1988) and from a suite of special wide-angle seismic studies (LASE - Large Aperture Seismic Experiments) (Keen and others, 1986) along USGS CDP Line 25 (Figures 10 and 21). There are additional calibration points on seismic lines 2, 6, and 10, as noted in Appendices 1, 2 and 3. Lines 14 and 15 (Figures 7 and 8) are strike lines crossing the main northern depocenter of the Baltimore Canyon Trough and just landward of the carbonate bank complex which forms its seaward edge. COST B-2 and SHELL 273-1 wells (Appendix 3) are located on line 14 and penetrated about half of the postrift sedimentary section. Five wells (TENNECO 495-1, MOBIL 17-2, GULF 857-1, EXXON 684-2 and TEXACO 598-2; Appendix 3) are located on line 15 and provide the best calibration of velocity variations along a profile. The close fit between our digital database velocity functions and the sonic and checkshot velocity profiles on these various industry lines is clearly displayed on all of these velocity vs time plots. Three shelf wells are located near Line 2 (MOBIL 544-1, COST B-2, and EXXON 684-2) and their checkshot velocity data (Appendix 3) display the same close correlation with our database velocity functions as seen on Lines 14 and 15. The buried Mesozoic carbonate bank shelf edge complex (Poag, 1987, 1991) was penetrated by three wells in deeper water. The checkshot data at SHELL 586-1 and SHELL 587-1 along Line 6 (Poag, 1991, Fig. 18) and SHELL 93-1 on Line 10 (Poag, 1991, Fig. 22) display velocity functions with very good agreement with our

database velocities and provide the only calibration of our velocity database seaward of the shelf edge. For each of these wells, it is the checkshot data which are matched the best by our database velocities. At all of the wells, the variability of ±10% noted in the COST G-1 and COST G-2 wells is a reasonable estimate of the uncertainty in these velocity functions. The differences with the sonic log profiles are primarily a result of initial travel times used in the industry well logs, based on assumed velocities in the upper sedimentary sections not logged. Comparison between the original NMO velocity data and our final RMS velocity functions on these seismic lines shows an agreement similar to that displayed on line 25 (Figure 18).

Velocity data on line 25 was calibrated with both industry well velocity data and wide-angle reflection and refraction data (LASE) (FIgure 10). The MOBIL 17-2 well is located near the intersections of lines 25 and 15a and our database velocity functions represent a best fit between the sonic and checkshot velocity data. Seismic velocity vs depth profiles derived from the LASE studies provide constraints on seismic velocities below the depth of penetration of the industry drill wells. The velocity vs depth functions for these LASE profiles, which were shot perpendicular to USGS CDP Line 25, are shown in Figure 21. The wide-angle technique incorporates refraction velocity information into the data set, which probably accounts for the slightly higher velocity in the LASE data over our database velocity functions at some depths. We interpret this slightly higher velocity on the LASE profiles to be caused by high-velocity carbonate stringers (thin layers) within the sedimentary column. This difference can be seen in the higher velocities on the LASE ESP lines 1, 2 and 3 in the 2-3 sec. two-way travel times depth range on the shelf, which are inconsistent with the checkshot velocities at the MOBIL 17-2 well. We have chosen to use the slightly lower velocities found in the checkshot data for the database calibration. In general, however, there is close agreement between the LASE velocity data and our digital database velocities. An uncertainty of ±10% in our velocity database would enclose the differences with the LASE data.

There are no industry wells in the southern part of the Baltimore Canyon Trough. Therefore our velocity data in this region are based entirely on the extrapolation of velocity data southward along tie lines 37, 12, 13, and 202, using the velscan data on these lines and the crossing dip lines.

Long Island Platform

There are no industry boreholes on Long Island Platform, therefore, our velocity calibration is restricted to seismic line ties to the Georges Bank and Baltimore Canyon Trough well calibration sites and to a comparison of refraction velocities with our database velocity functions. There are three good shelf strike lines (Lines 36, 12, and 204) linking the dip lines to George Bank and Baltimore Canyon regions, therefore the resultant velocity functions are nearly as reliable as in the calibration sites. The standard refraction-velocity data (Figure 22) summarized in Sheridan and others (1988) were inadequate for calibrating velocity data at the resolution being incorporated into our database.

In an attempt to obtain higher resolution refraction data, we created a series of mini-refraction stations from the multichannel seismic data on USGS CDP Line 22 (Figure 23). The multichannel seismic-reflection data, recorded with 2 to 3-km long streamers, includes refraction arrivals for the upper sedimentary layers. This refraction information is removed (muted) during standard data processing of seismic reflection data but can be examined by

reprocessing the data. The seismic data were reassembled into shot gathers (instead of the standard common depth point (CDP) gathers used for seismic-reflection processing). This regrouping of data associates the seismic arrivals at all of the receivers in a multichannel streamer (up to 96 on some seismic lines) with a single shot (outgoing signal from an acoustic source array). The refraction velocities for up to four acoustic units were determined from this technique (Figure 23). On USGS CDP Line 22 (Figure 24) these refracted arrivals were from basement, base of the Tertiary section (reflector 70) and base of the Plio/Pleistocene on the landward end of the line, where the sedimentary column was thinnest. In the middle shelf region, basement refractors were no longer recorded and an Upper Cretaceous surface (reflector 80) is the deepest refractor. Near the shelf edge, a mid-Tertiary unit is the deepest refractor. The shift in deepest refractor is merely a consequence of the finite length of the receiver and the geometric limitation on the depth from which refractors could be received. The refractors do correspond to distinctive reflectors mapped for this database and their velocities are consistent with the velocities obtained from our smoothing procedures on NMO velocity data. However, these refraction data still were not of adequate resolution or depth of coverage to incorporate into the digital data base. Brocher and Ewing (1986) studied the Long Island Platform region using the same type of wide-angle reflection and refraction information from the multichannel seismic data to better constrain the V_p information in the upper sedimentary section. Error estimates of the velocity data derived from this refraction technique are over 20% (Brocher and Ewing, 1986). A similar analysis of multichannel seismic-reflection data was carried out by McGinnis and Otis (1979) over parts of the Long Island Platform and Georges Bank Basin. They identified two distinctive refractors and mapped their areal distribution as well as constructing vertical sections of isovelocity contours. This study suggested that there was a change in velocity patterns over broad regions associated with variations in overburden, but there was an inadequate stratigraphic database tied to these refraction velocity functions to draw any more detailed conclusions. The utility of velocity data from this refraction technique could be enhanced by incorporating seismic-stratigraphic units into the analysis procedure and developing a multilayered refraction-velocity model comparable with the model developed in our database.

Acoustic Attenuation

The attenuation of sound through sediments is an important component of geoacoustic models, but there is no information on these properties in the seismic data sets used in this study. Studies by Hamilton (1976a,b), Stoll (1980, 1985) and Mitchell and Focke (1980) on attenuation (α) have shown that it is frequency (f) dependent, $\alpha = k \cdot f^m$, but their results have differed by over an order of magnitude in estimating k or m. The values for attenuation expressed as k in dB/m-kHz, used in this data base are those used by the Naval Oceanographic Office based on the work of Stoll (1985) and Mitchell and Focke (1980). Inputs are the surficial compressional attenuation (k_0) for the sediment wedge at a point, tops and bottoms of layers beneath this point, and p-wave velocities for each of these layers. The values of k_0 are determined by the surficial sediment type and are listed in Table 6. The shear-wave attenuation is based on the empirical work of Hamilton (1976a,b) and Castagna and others (1985) and has been calculated using the Naval Oceanographic Office's computer program KDTRMN. The formulae used in these calculations are given in Table 1.

Summary

A database of seismic velocity data and associated acoustic parameters has been constructed for the northern U.S. Atlantic continental margin using a grid of 47 multichannel seismic reflection profiles. The velocity functions incorporated into this digital database are derived from standard NMO velocity analyses on multichannel seismic-reflection data calibrated with velocity data obtained at a sparse set of industry wells on the margin. The smoothing of RMS velocity data, based on the assumption that geologically realistic units do not contain abrupt velocity variations over short horizontal distances (less than 2-3 km), creates a data set that is consistent with the original NMO velocity data. There may be a lithologic control on lateral changes in interval velocities within geologic units, but the primary factor on velocity changes is probably changes in overburden. Calibration of this final, smoothed velocity data with velocity profiles at industry wells (Appendix 3) demonstrates the reliability of these velocity functions at well crossings and indicates that a reasonable estimate of variability in these velocity functions is ±10%. Standard refraction data were determined to contain inadequate velocity structure for incorporation into the digital database, but "mini" refraction stations, based on shot gather geometries of standard multichannel lines, do represent potentially valuable sources of velocity information in the upper 1500m of the crust.

Acknowledgements

This project was supported by the U.S. Naval Oceanographic Office. We gratefully acknowledge discussions and collaboration with Dr. Rudi Markl, the Naval Oceanographic Office's project manager during most of this work and P. Schexnayder, program manager during the early stages of the project, and thank Dr. M. Head, R. Hecht, and G. Michel, all of the Naval Oceanographic Office, for their support and technical assistance. Numerous discussions and detailed reviews by R. Markl, D. Hutchinson, L. North, W. Poag and P. Popenoe have led to significant improvements in this study. D. Hutchinson provided the shot-gather refraction data along seismic line 22. Technical support from L. Morse, J. Taylor, K. Delorey, D. Senske, S. Harrison and E. Wright, all of the U.S. Geological Survey, is gratefully acknowledged.

REFERENCES

Amato, R.V., and Bebout, J.W., eds., 1980, Geologic and operational summary, COST No. G-1 well, Georges Bank area, North Atlantic OCS: U.S. Geological Survey Open File Report 80-268, 117p.

Amato, R.V., and Simonis, E.K., eds., 1980, Geologic and operational summary, COST No. G-2 well, Georges Bank area, North Atlantic OCS: U.S. Geological Survey Open File Report 80-269, 120p.

Brocher, T.M., and Ewing, J.I., 1986, A comparison of high-resolution seismic methods for determining seabed velocities in shallow water: Journal of the Acoustical Society of America: v. 79, no. 2, p. 286-298.

Castagna, J.P., Batzle, M.L., and Eastwood, R.L., 1985, Relationships between compressional-wave and shear-wave velocities in clastic silicate rocks: Geophysics, v.50, p. 571-581.

Dillon, W.P., and Popenoe, P., 1988, The Blake Plateau Basin and Carolina Trough, *in* Sheridan, R.S., and Grow, J.A., eds.: The Atlantic Continental Margin, U.S., The Geology of North America, v. I-2, Geological Society of America, p. 291-328.

Grow, J.A., Klitgord, K.D., and Schlee, J.S., 1988, Structural and evolution of the Baltimore Canyon Trough, *in* Sheridan, R.S. and Grow, J.A., eds., The Atlantic Continental Margin, U.S., The Geology of North America, v. I-2, Geological Society of America, p. 269-290.

Hamilton, E.L., 1976a, Sound attenuation as a function of depth in the sea floor: Journal of the Acoustical Society of America, v. 59, no. 3, p. 528-535.

Hamilton, E.L., 1976b, Attenuation of shear waves in marine sediments: Journal of the Acoustical Society of America, v. 60, no. 2, p. 334-338.

Hamilton, E.L., 1978, Sound velocity-density relations in sea-floor sediments and rocks: Journal of the Acoustical Society of America: v. 63, no. 2, p. 366-377.

Hamilton, E.L., 1979, V_p/V_s and Poisson's ratios in marine sediments and rocks: Journal of the Acoustical Society of America, v. 66, no. 4, p. 1093-1101.

Hamilton, E.L., 1980, Geoacoustic modeling of the sea floor: Journal of the Acoustical Society of America, v. 68, no. 5, p. 1313-1340.

Hamilton, E.L., and Bachman, R.T., 1982, Sound velocity and related properties of marine sediments: Journal of the Acoustical Society of America, v. 72, no. 6, p. 1891-1904.

Hathaway, J.C., 1971, Data file - continental margin program Atlantic coast of the United States Vol. 2 - Sample collection and analytical data: Woods Hole Oceanographic Institution Ref. No. 71-15, 496 p.

Hathaway, J.C., Poag, C.W., Valentine, P.C., Miller, R.E., Schultz, D.M., Manheim, F.T., Kohout, F.A., Bothner, M.H., and Sangrey, D.A., 1979, U.S. Geological Survey core drilling on the Atlantic shelf: Sciences, v. 206, p. 515-527.

Hathaway, J.C., and others, 1994, Digital data base of surficial sediments on U.S. Atlantic Margin, USGS Open File Report, in review.

Houtz, R.E., 1983a, Seismic velocity structure, *in* Uchupi, E., and Shor, A.N., eds., Eastern North American Continental Margin and adjacent ocean floor, 39°N to 46°N and 64°W to 74°W: Ocean Margin Drilling Program, Regional Atlas Series 3, sheet 6.

Houtz, R.E., 1983b, Seismic velocity structure, *in* Shor, A.N., and Uchupi, E. eds., Eastern North American Continental Margin and adjacent ocean floor, 34°N to 41°N and 68°W to 78°W: Ocean Margin Drilling Program, Regional Atlas Series 4, sheet 6.

Keen, C., and others, 1986, Deep structure of the US East Coast passive margin from large aperture seismic experiments (LASE): Marine and Petroleum Geology, v. 3, p. 234-242.

Klitgord, K.D., Hutchinson, D.R., and Schouten, H., 1988, U.S. Atlantic continental margin; Structural and tectonic framework, *in* Sheridan, R.S., and Grow, J.A., eds., The Atlantic Continental Margin, U.S., The Geology of North America, v. I-2, Geological Society of America, p. 19-55.

Klitgord, K.D., Poag, C.W., Schneider, C., and North, L., 1994, Geophysical database of the East Coast of the United States: Northern Atlantic margin: Georges Bank Basin, Long Island Platform, and Baltimore Canyon Trough: U.S. Geological Survey Open File Report OF94-637, 189 pp.

Libby-French, J., 1981, Lithostratigraphy of Shell 272-1 and 273-1 wells: Implications as to depositional history of Baltimore Canyon Trough, mid-Atlantic OCS: American Association of Petroleum Geologists Bulletin, v. 65, p. 1476-1484.

McGinnis, L.D., and Otis, R.M., 1979, Compressional velocities from multichannel refraction arrivals on Georges Bank - northwest Atlantic Ocean: Geophysics, v. 44, p. 1022-1033.

Mitchell, S.K., and Focke, K.C., 1980, New measurements of compressional wave attenuation in deep ocean sediments, Journal of Acoustic Society of America, v. 67, no. 5, p. 1582-1589.

Palmer, A.W., 1983, The Decade of North American Geology 1983 geologic timescale: Geology,

v. 11, p. 503-504.
Poag, C.W., 1982, Stratigraphic reference section for the Georges Bank Basin: depositional model for New England passive margin: American Association of Petroleum Geologists Bulletin, v. 66, p. 1021-1041.
Poag, C.W., ed., 1985a, Geologic Evolution of the United States Atlantic Margin: New York, Van Nostrand Reinhold Company, 385 p.
Poag, C.W., 1985b, Depositional history and stratigraphic reference section for central Baltimore Canyon Trough, in Poag, C.W.,ed., Geologic Evolution of the United States Atlantic Margin: p. 217-263.
Poag, C.W., and Schlee, J.S., 1984, Depositional sequences and stratigraphy gaps on submerged United States Atlantic margin, in Schlee, J.S., ed., Interregional Unconformities and Hydrocarbon Accumulation, The American Association of Petroleum Geologists Memoir 36, p. 165-182.
Poag, C.W., 1987, The New Jersey Transect: Stratigraphic framework and depositional history of a sediment-rich passive margin, *in* Poag, C.W., Watts, A.B., and others, eds., Initial Reports of the Deep Sea Drilling Project, Volume 95: Washington, D.C., U.S. Government Printing Office, p. 763-817.
Poag, C.W., and Valentine, P., 1988, Mesozoic and Cenozoic stratigraphy of the United States Atlantic continental shelf and slope, *in* Sheridan, R.S. and Grow, J.A., eds., The Atlantic Continental Margin, U.S., The Geology of North America, Vol. I-2, Geological Society of America, p. 67-85.
Poag, C.W., 1991, Rise and demise of the Bahama-Grand Banks gigaplatform, northern margin of the Jurassic proto-Atlantic seaway: Marine Geology, v. 102, p. 63-130.
Poag, C.W., 1992, U.S. middle Atlantic continental rise: provenance, dispersal, and deposition of Jurassic to Quaternary sediments: *in* Poag, C.W., and de Graciansky, P.C., eds., Geological Evolution of Atlantic Continental Rises: Van Nostrand Reinhold, New York, p. 100-156.
Poag, C.W., and Ward, L.W., 1993, Allostratigraphy of the U.S. Middle Atlantic Continental Margin -- characteristics, distribution and depositional history of principal unconformity bounded Upper Cretaceous and Cenozoic sedimentary units: U.S. Geological Survey Professional Paper 1542, 81pp.
Poppe, L., Schlee, J.S., Butman, B., and Lane, C., 1989, Map showing distribution of surficial sediment, Gulf of Maine and Georges Bank: U.S. Geological Survey, MI Map I-1986-A.
Sheridan, R.A., Grow, J.A., Behrendt, J.C., and Bayer, K.C., 1979, Seismic refraction study of the continental edge off the eastern United States: Tectonophysics, v. 59, p. 1-26.
Sheridan, R.A., and Grow, J.A., 1988, The Atlantic Continental Margin, U.S.: The Geology of North America, Vol. I-2, Geological Society of America, 610p.
Sheridan, R.A., Grow, J.A., and Klitgord, K.D., 1988, Geophysical data, *in* Sheridan, R.S., and Grow, J.A., eds., The Atlantic Continental Margin, U.S., The Geology of North America, v. I-2, Geological Society of America, p. 177-196.
Schlee, J., 1973, Atlantic Continental Shelf and Slope of the United States -- Sediment Texture of the Northeastern Part, USGS Professional Paper 529-L.
Schlee, J.S., ed., 1984, Interregional Unconformities and Hydrocarbon Accumulation, American Association of Petroleum Geologists Memoir 36.
Schlee, J., Poag, C.W., and Hinz, C., 1985, Seismic stratigraphy of the continental slope and rise seaward of Georges Bank, in Poag, C.W., ed., Geologic Evolution of the United States Atlantic Margin: New York, Van Nostrand Reinhold Company, p. 265-292.
Scholle, P.A., ed., 1977, Geological studies on the COST No. B-2 well, U.S. mid-Atlantic outer

continental shelf area: U.S. Geological Survey Circular 750.
Scholle, P.A., and Wenkam, C.R., eds., 1982, Geological studies of the COST Nos. G-1 and G-2 wells, United States North Atlantic outer continental shelf: U.S. Geological Survey Circular 861, 193p.
Stoll, R.D., 1980, Theoretical aspects of sound transmission in sediments: Journal of Acoustic Society of America, v. 68, p. 1341-1350.
Stoll, R.D., 1985, Acoustic waves in ocean sediments: Geophysics, v. 42, p. 715-725.
Taner, M.T., and Koehler, F., 1969, Velocity spectra, digital computer derivatives and applications of velocity functions: Geophysics, v. 34, p. 859-881.
Taylor, D.J., Mattick, R.E., and Bayer, K.C., 1977, Geophysical studies, *in* Geological studies on the COST No. B-2 Well, U.S. Mid-Atlantic Outer Continental Shelf area: U.S. Geological Survey Circular 750, p. 63-67.
Taylor, D.J., and Anderson, R.C., 1980, Geophysical studies, *in* Geological studies of the COST No. B-3 Well, United States Mid-Atlantic Continental Slope area: U.S. Geological Survey Circular 833, p. 105-110.
Taylor, D.J., and Anderson, R.C., 1982, Geophysical studies of the COST Nos. G-1 and G-2 Wells, *in* Geological studies of the COST Nos. G-1 and G-2 Wells, United States North Atlantic Outer Continental Shelf: U.S. Geological Survey Circular 861, p. 153-159.
Vail, P.R, Mitchum, R.M., Jr., Todd, R.G., Widmier, J.M., Thompson III, S., Sangree, J.B., Bubb, J. N., and Hatlelid, W.G., 1977. Seismic stratigraphy and global changes of sea level, *in* Payton, C.E., ed., Seismic stratigraphy; Applications to hydrocarbon exploration: American Association of Petroleum Geologists Memoir 26, p. 49-212.
Valentine, P.C., 1981, Continental margin stratigraphy along the U.S. Geological Survey Seismic line 5 -- Long Island Platform and western Georges Bank Basin: U.S. Geological Survey Miscellaneous Field Studies Map MF-857, 2 sheets.
Van Wagoner, J.C., Posamentier, H.W., Mitchum, R.M., Vail, P.R., Sarg, J.D., Loutit, T.S., and Hardenbol, J., 1988, An overview of the fundamentals of sequence stratigraphy and key definitions, *in* Wilgus, C.K., and others, eds., Sea-level changes: An integrated approach: Society of Economic Paleontologists and Mineralogists Special Publication 42, p. 39-45.
Yilmaz, O., 1987, Seismic velocity processing: Investigations in Geophysics No. 2, Society of Exploration Geophysicists, Tulsa OK, 526p.

Figure Captions

Figure 1: Multichannel seismic reflection profile grid used in the construction of this geoacoustic database superimposed on bathymetric contour map of the northern U.S. Atlantic Continental Margin. Heavier weight lines indicate seismic-reflection profiles used as primary stratigraphic and velocity calibration lines for this study (USGS CDP Lines 12, 14, 15, 19, 22, and 25). G-1 and G-2 refer to the ends of the composite seismic line connecting the COST G-1 and COST G-2 wells.

Figure 2: Industry drill wells on the U.S. margin with velocity data (sonic logs or velocity checkshots) used to calibrate the velocity vs depth functions in the digital database. See Appendix 2 for well identification labels and Appendix 3 for velocity profiles at these wells.

Figure 3: Selected refraction profile locations on the U.S. Atlantic margin. Locations of LASE wide-angle refraction lines, suite of refraction stations along USGS Line 22, and refraction transect A (Georges Bank) and transect B (Baltimore Canyon Trough) of Sheridan and others (1988) and shown in Figure 22 are indicated. Summary tables and reference lists for these seismic-refraction data sets are given in Houtz (1983a,b) and Sheridan and others (1988).

Figure 4: Diagrammatic representation of the geometry of geologic features in the geoacoustic database. Parameters *X(n)* in Table 1 refer to either properties of the unit directly above reflector n or properties of the entire section between the sea surface (z=0) and the reflector n. A.) Time section. B.) Depth section.

Figure 5: Diagram portraying the nomenclature for acoustic reflectors used in this geoacoustic database based on the tags using the base of units. Note for example that the top of the Maastrichtian unit is reflector 70, then reflector 60 and then again reflector 70 whereas reflector 60 is always the base of the Upper Oligocene.

Figure 6: Composite CDP seismic line G1-G2 in Georges Bank Basin used to calibrate seismic-reflection profiles with COST Wells G-1 and G-2. A.) Time depth of acoustic reflectors in digital database (in seconds two-way travel time) vs distance (shot points). B.) Interval velocities (m/s) of units just above acoustic reflectors in Figure 6A vs distance (shot points). Shot point spacing is 100m. See Figure 1 for location. Well locations and crossing points of other seismic lines are indicated across the top of the profile. Faults, boundaries of diapirs, and reflectors beneath the postrift unconformity are shown but not numbered or included in the velocity database. Reflector numbers from Table 4 are at ends of the lines and at other points.

Figure 7: USGS Line 14 in the northern Baltimore Canyon Trough used to calibrate seismic-reflection profiles with industry wells Shell 273-1 and Cost B-2. See Appendix 3 for velocity profiles at wells. Locations of other wells and seismic line crossings used in stratigraphic correlations are indicated. Line is composite of Line 14a and Line 14b with shot points at top for each line. A.) Time depth of acoustic reflectors vs distance. B.) Interval velocities of units above reflectors in Figure 7A vs distance. Shot point spacing is 50m. See Figure 1 for location and Figure 6 for explanation.

Figure 8: USGS CDP Line 15 in the northern Baltimore Canyon Trough used to calibrate seismic-reflection profiles with industry wells Tenneco 495-1, Mobil 17-2, Gulf 857-1, Exxon 684-2, and Texaco 598-2. See Appendix 3 for velocity profiles at wells. Line is composite of Line 15a and Line 15b with shot points at top for each line. A.) Time depth of acoustic reflectors vs distance. B.) Interval velocities of units above acoustic reflectors in Figure 8A vs distance. Shot point spacing is 50m. See Figure 1 for location and Figure 6 for explanation.

Figure 9: USGS Line 19 in Georges Bank Basin used as primary dip line for calibration of seismic stratigraphy and velocities. A.) Time depth of acoustic reflectors vs distance. B.) Interval velocities of units above acoustic reflectors in Figure 9A vs distance. Shot point spacing is 50m. See Figure 1 for location and Figure 6 for explanation.

Figure 10: USGS Line 25 in northern Baltimore Canyon Trough used as primary dip line for calibration of seismic stratigraphy and velocities. A.) Time depth of acoustic reflectors vs distance. B.) Interval velocities of units above acoustic reflectors in Figure 10A vs distance. Shot point spacing is 50m. See Figure 1 for location and Figure 6 for explanation.

Figure 11: USGS Line 22 across Long Island Platform used as primary dip line for calibration of seismic stratigraphy and velocities. A.) time depth of acoustic reflectors vs distance. B.) Interval velocities of units above acoustic reflectors in Figure 11A vs distance. Shot point spacing is 50m. See Figure 1 for location and Figure 6 for explanation.

Figure 12: RMS velocity functions vs time depth (two-way travel time in sec.). Contours of coherence (relative values only) of different RMS velocity functions vs time depth are shown. Final smoothed database velocity functions are shown as heavy line. A.) Velscan at shot point 111 on USGS Line 77-1 near Cost G-1 well. B.) Velscan at shot point 98 on USGS Line 77-2 near COST G-2 well.

Figure 13: RMS velocity functions vs time depth (two-way travel time in sec.) at shot point 3062 on USGS Line 22. A.) Example of original velscan data displays. At left is series of cdp gather panels for velocity functions V1 to V7 and then cdp stacks for the same velocity functions. At right is the RMS velocity vs time panel. Plots of the 7 velocity functions used in the left and central panels are shown (curves dipping to right). Relative values of coherence of stacked data for moving windows of RMS velocity (δv ~25 m/s) and time (δt = 0.1 sec.) are shown as scattered points representing various values of coherence (+, Δ, . in decreasing level. Maximum coherence values within each 0.1 sec. time depth interval are circled. B.) RMS velocity vs time functions for original analysis used to stack data (light line), final smoothed function (heavy line) and maximum coherence points from Figure 13a.

Figure 14: Comparison of interval velocity profiles at different analysis stages on Composite CDP Line G1-G2. A.) Original velscan vs ISM smoothed data. B.) ISM smoothed vs final hand-smoothed data. Plus symbols indicate spacing of velscans.

Figure 15: Comparison of interval velocity profiles at different analysis stages on USGS Line 18 just east of Line 19. A.) Original velscan vs ISM smoothed data. B.) ISM smoothed vs final hand-smoothed data.

Figure 16: Comparison of interval velocity profiles at different analysis stages on USGS Line 25. A.) Original velscan vs ISM smoothed data. B.) ISM smoothed vs final hand-smoothed data.

Figure 17: Comparison of interval velocity profiles at different analysis stages on USGS Line 22. A.) Original velscan vs ISM smoothed data. B.) ISM smoothed vs final hand-smoothed data.

Figure 18: Comparison of RMS velocity profiles for original velscan data and final hand smoothed data profiles. A.) USGS Line 25. B.) USGS Line 22.

Figure 19a: Interval velocities (m/s) vs depth (m) at well COST G-1 for sonic log, checkshots, and digital database at shot point 100 on USGS Line 77-1.

Figure 19b: Interval velocities (m/s) vs time depth (sec. two-way travel time) at well COST G-1 for sonic log and digital database at shot point 100 on USGS Line 77-1.

Figure 20a: Interval velocities (m/s) vs depth (m) at well COST G-2 for sonic log, checkshots, and digital database at shot point 110 on USGS Line 77-2.

Figure 20b: Interval velocities (m/s) vs time depth (sec. two-way travel time) at well COST G-2 for sonic log and digital database at shot point 110 on USGS Line 77-2.

Figure 21: Interval velocities (m/s) vs time depth (sec. two-way travel time) for the 5 expanding spread profiles (ESP) on the large aperture seismic experiment (LASE) lines (Keen and others, 1986) along USGS Line 25. LASE ESP numbers and shot point locations on USGS Line 25 (Figure 10) are indicated on each profile.

Figure 22: Cross sections of the continental margin based on seismic refraction profiles from Sheridan and others (1988). A.) Georges Bank transect. B.) Baltimore Canyon Trough transect. See Figure 3 for locations.

Figure 23: A "mini" seismic-refraction station constructed from a single shot gather on USGS Line 22. The refraction velocity for 4 clearly defined refractors are indicated.

Figure 24: Refraction velocities (m/s) derived from shot-gather processing of seismic data on USGS Line 22 plotted vs depth (m) and distance along line (shot points). Refraction velocity values are superimposed on depth vs distance plot of acoustic reflectors in digital database. Note the highest refraction velocities (over 4.5 km/s) correspond to crystalline basement on the left hand (landward) half of the profile. On the seaward part of the profile, only sedimentary units were penetrated by the shot-gather processed data set. These data were not processed using the stratigraphic data to control inflection points in the refraction travel time vs distance analysis, but the data do show a consistent correlation of refractors with specific reflectors.

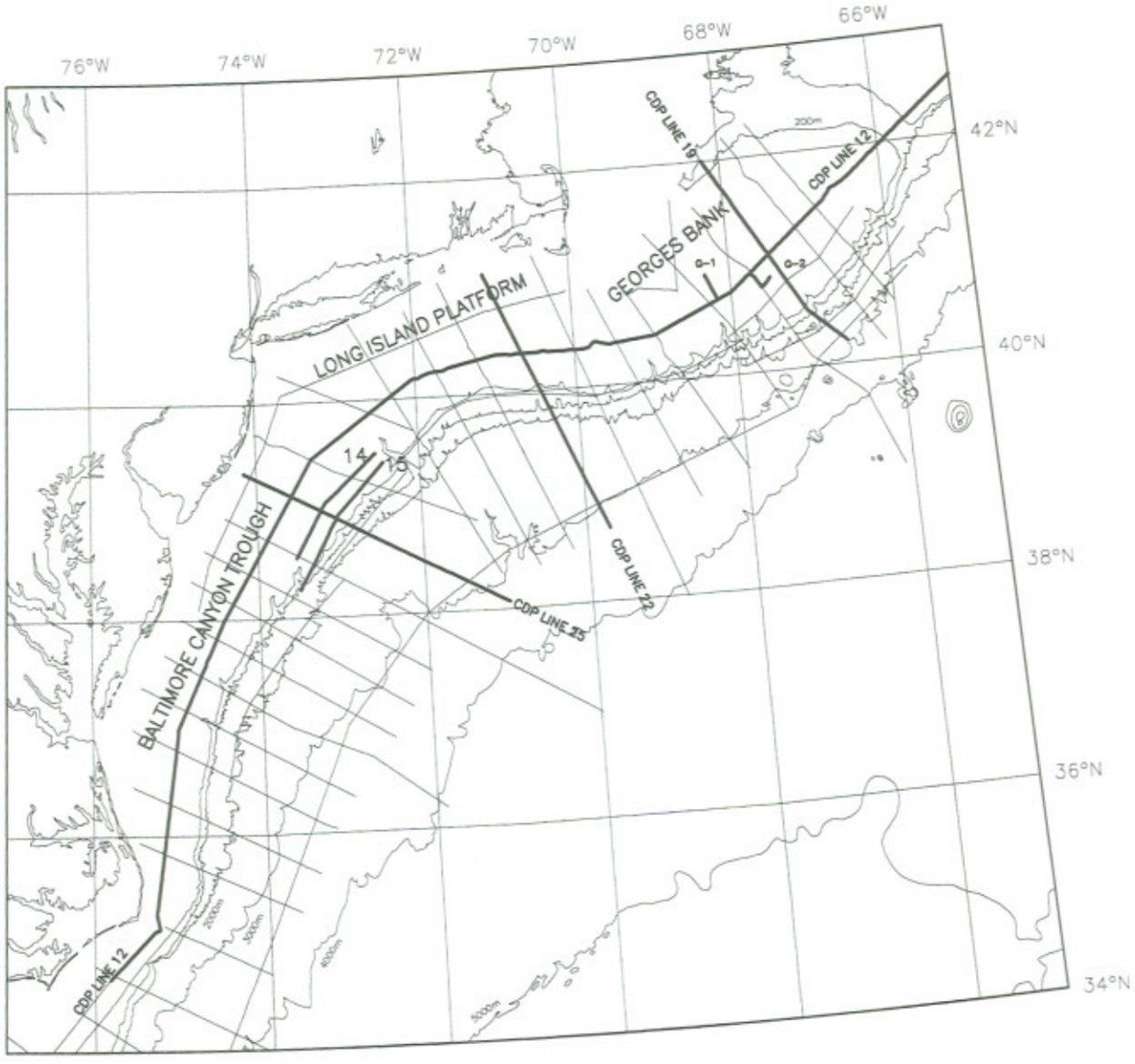
76°W
74°W
72°W
70°W
68°W
66°W
42°N
40°N
38°N
36°N
34°N
CDP LINE 19
CDP LINE 12
GEORGES BANK
LONG ISLAND PLATFORM
14
15
CDP LINE 22
CDP LINE 25
BALTIMORE CANYON TROUGH
CDP LINE 12
200m
2000m
3000m
4000m
5000m

Figure 1

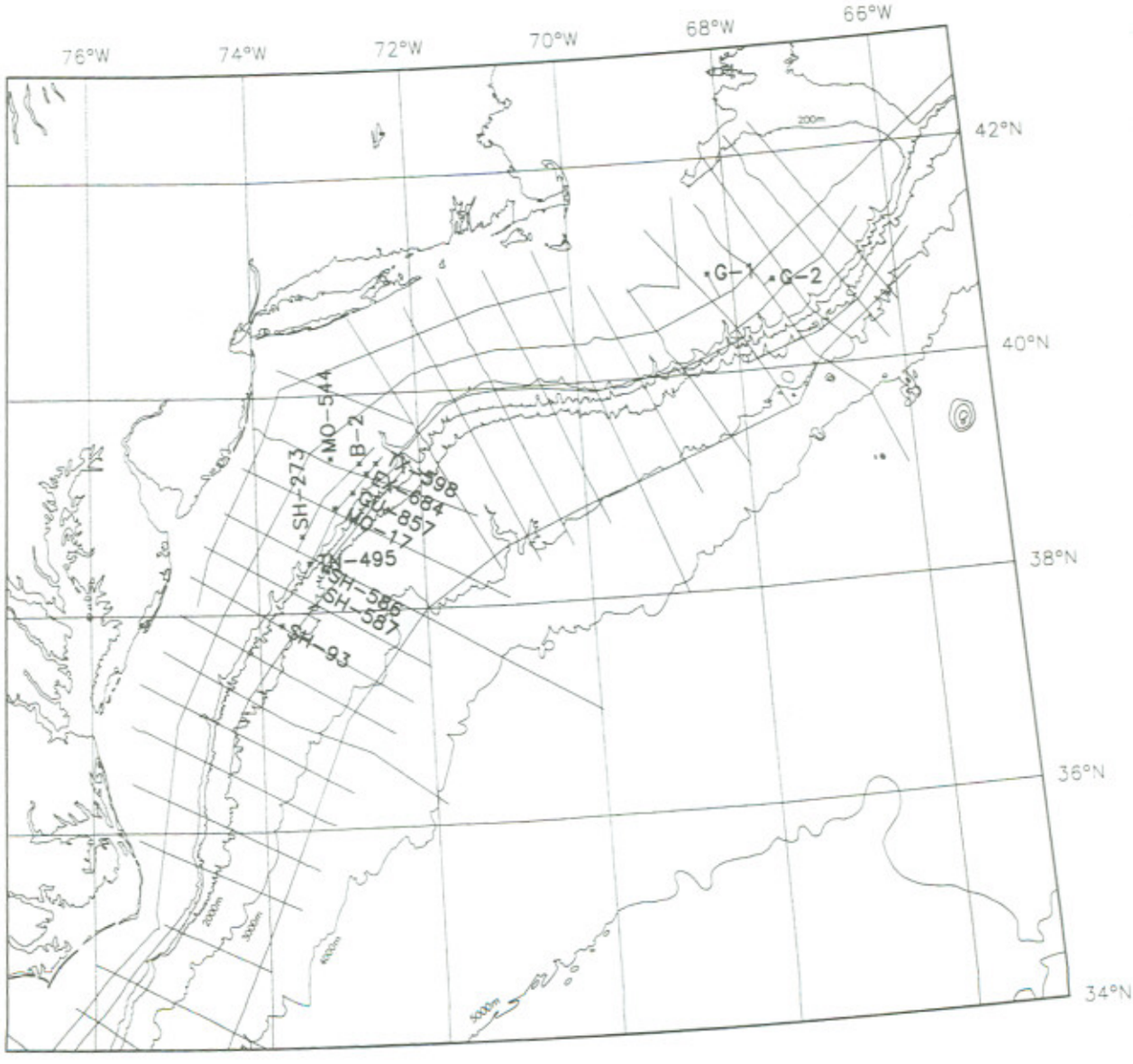
76°W
74°W
72°W
70°W
68°W
66°W
42°N
40°N
38°N
36°N
34°N
200m
G-1
G-2
MO-544
B-2
SH-273
TY-398
EX-684
GU-857
MO-17
SH-495
SH-586
SH-587
SH-93
2000m
3000m
4000m
5000m

Figure 2

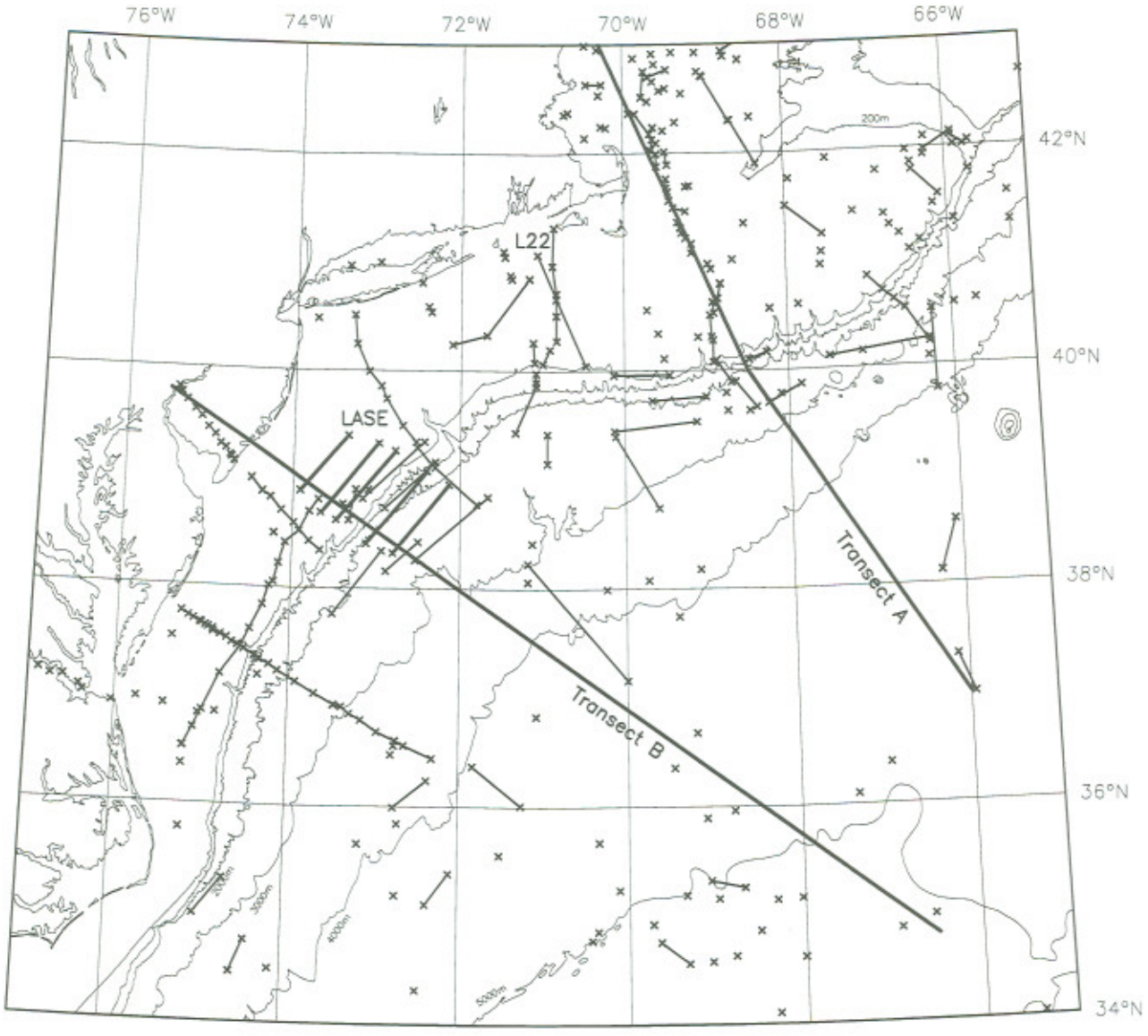
76°W
74°W
72°W
70°W
68°W
66°W
42°N
40°N
38°N
36°N
34°N
200m
L22
LASE
Transect A
Transect B
3000m
4000m
5000m

Figure 3

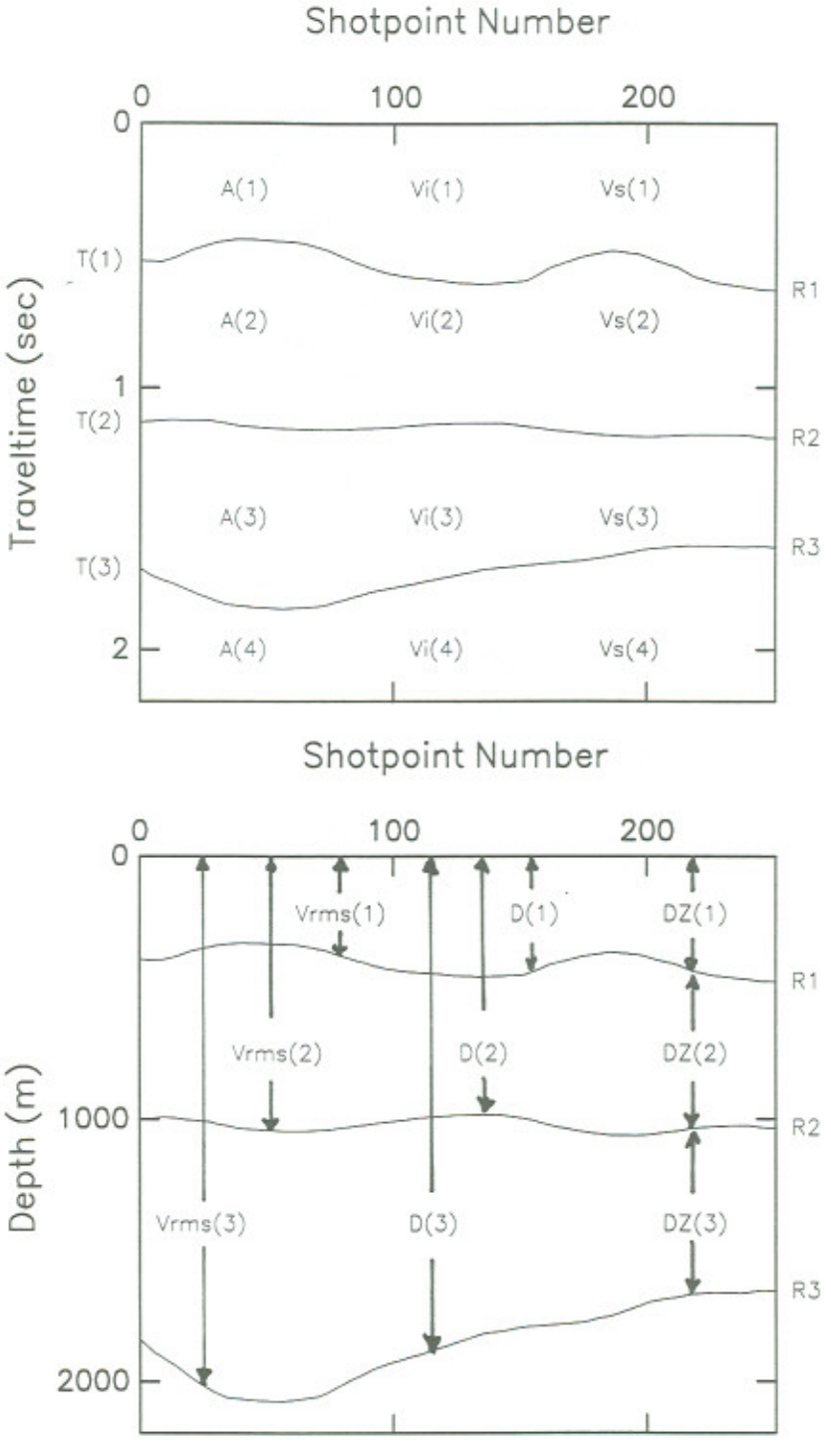
Shotpoint Number
0
100
200
0
A(1)
Vi(1)
Vs(1)
T(1)
R1
A(2)
Vi(2)
Vs(2)
1
T(2)
R2
A(3)
Vi(3)
Vs(3)
R3
T(3)
2
A(4)
Vi(4)
Vs(4)
Traveltime (sec)
Shotpoint Number
0
100
200
0
Vrms(1)
D(1)
DZ(1)
R1
Vrms(2)
D(2)
DZ(2)
1000
R2
Vrms(3)
D(3)
DZ(3)
R3
2000
Depth (m)

Figure 4

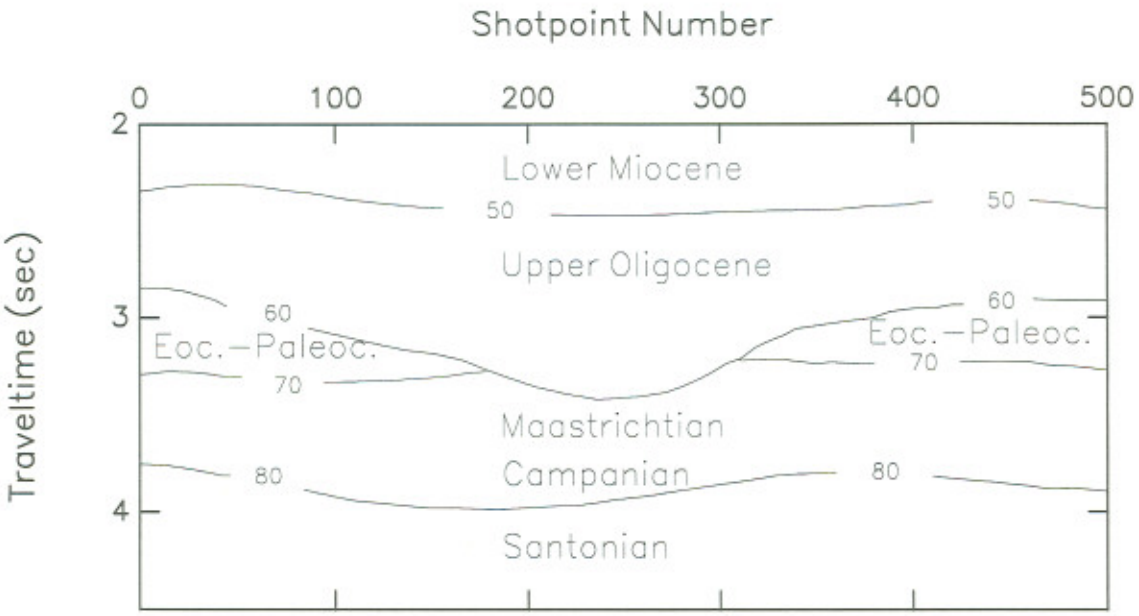
Shotpoint Number
0
100
200
300
400
500
2
3
4
Traveltime (sec)
Lower Miocene
50
50
Upper Oligocene
60
60
Eoc.–Paleoc.
Eoc.–Paleoc.
70
70
Maastrichtian
Campanian
80
80
Santonian

Figure 5

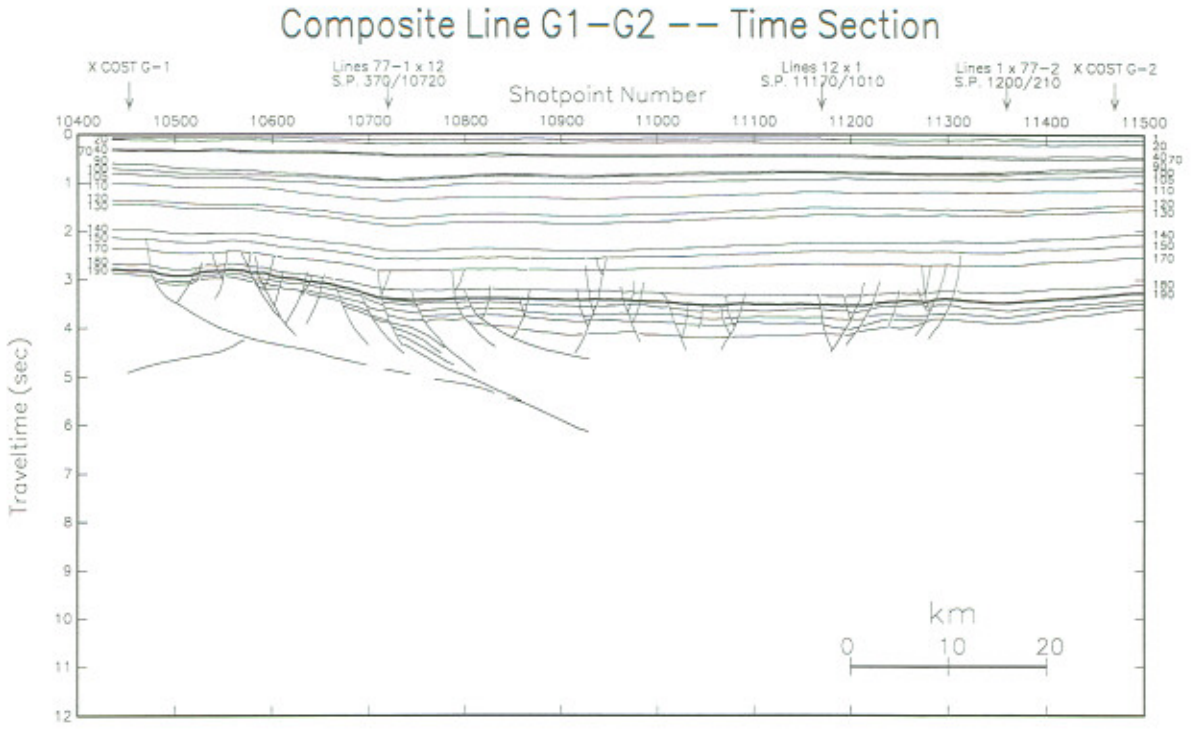
Composite Line G1–G2 -- Time Section
X COST G-1
Lines 77-1 x 12
S.P. 370/10720
Lines 12 x 1
S.P. 11170/1010
Lines 1 x 77-2
S.P. 1200/210
X COST G-2
Shotpoint Number
10400
10500
10600
10700
10800
10900
11000
11100
11200
11300
11400
11500
Traveltime (sec)
km
0
10
20

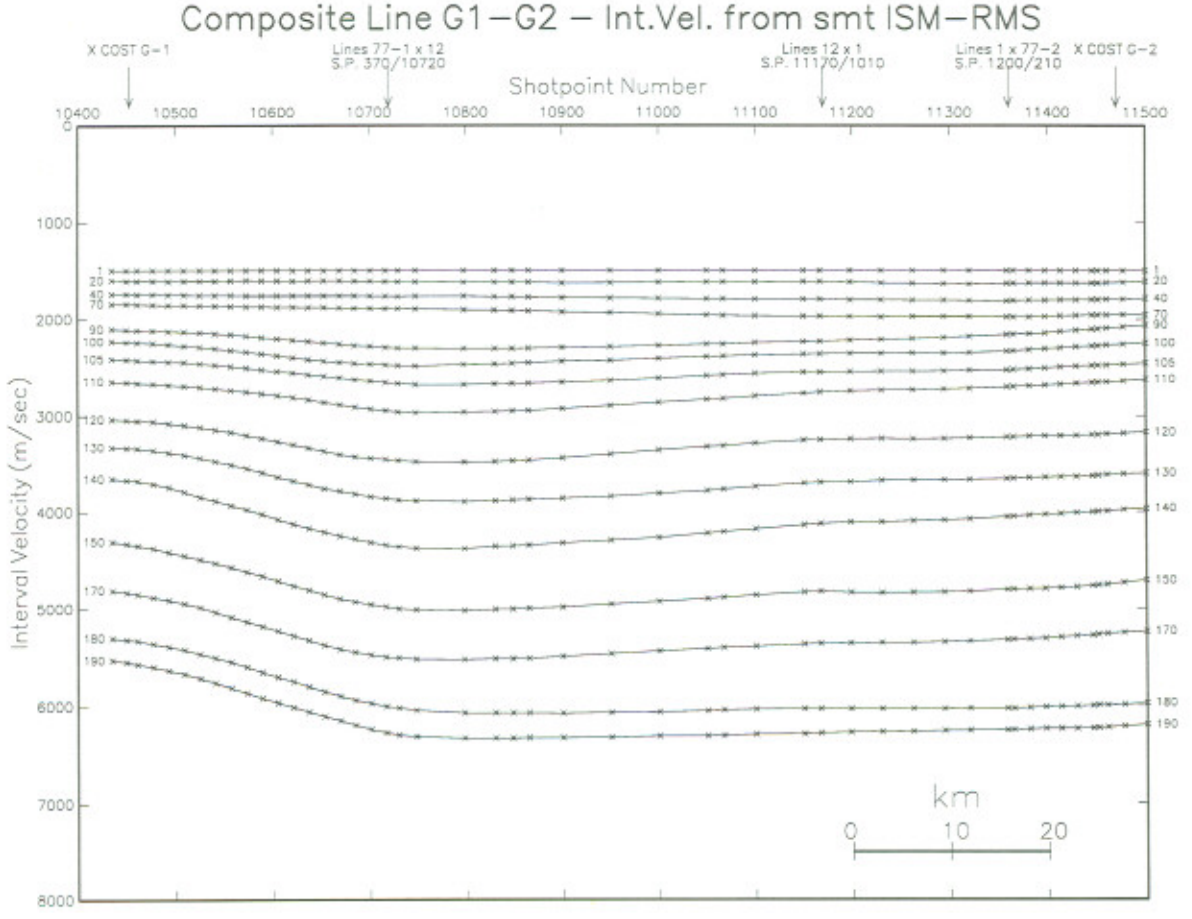
Composite Line G1–G2 – Int.Vel. from smt ISM–RMS
X COST G-1
Lines 77-1 x 12
S.P. 370/10720
Lines 12 x 1
S.P. 11170/1010
Lines 1 x 77-2
S.P. 1200/210
X COST G-2
Shotpoint Number
10400
10500
10600
10700
10800
10900
11000
11100
11200
11300
11400
11500
Interval Velocity (m/sec)
1000
2000
3000
4000
5000
6000
7000
8000
km
0
10
20

Figure 6

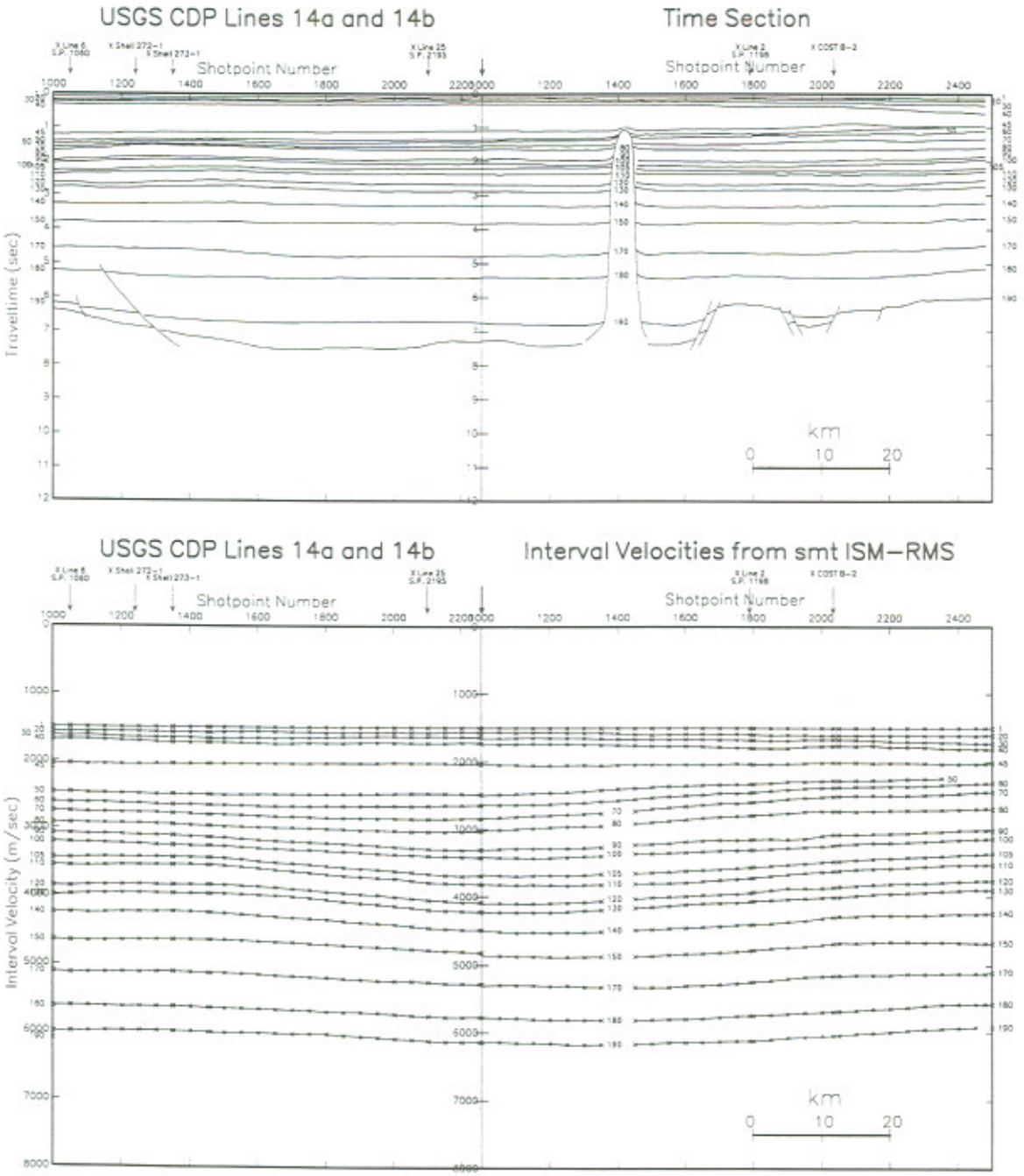
USGS CDP Lines 14a and 14b
Time Section
Shotpoint Number
Traveltime (sec)
km
0
10
20
USGS CDP Lines 14a and 14b
Interval Velocities from smt ISM–RMS
Shotpoint Number
Interval Velocity (m/sec)
km
0
10
20

Figure 7

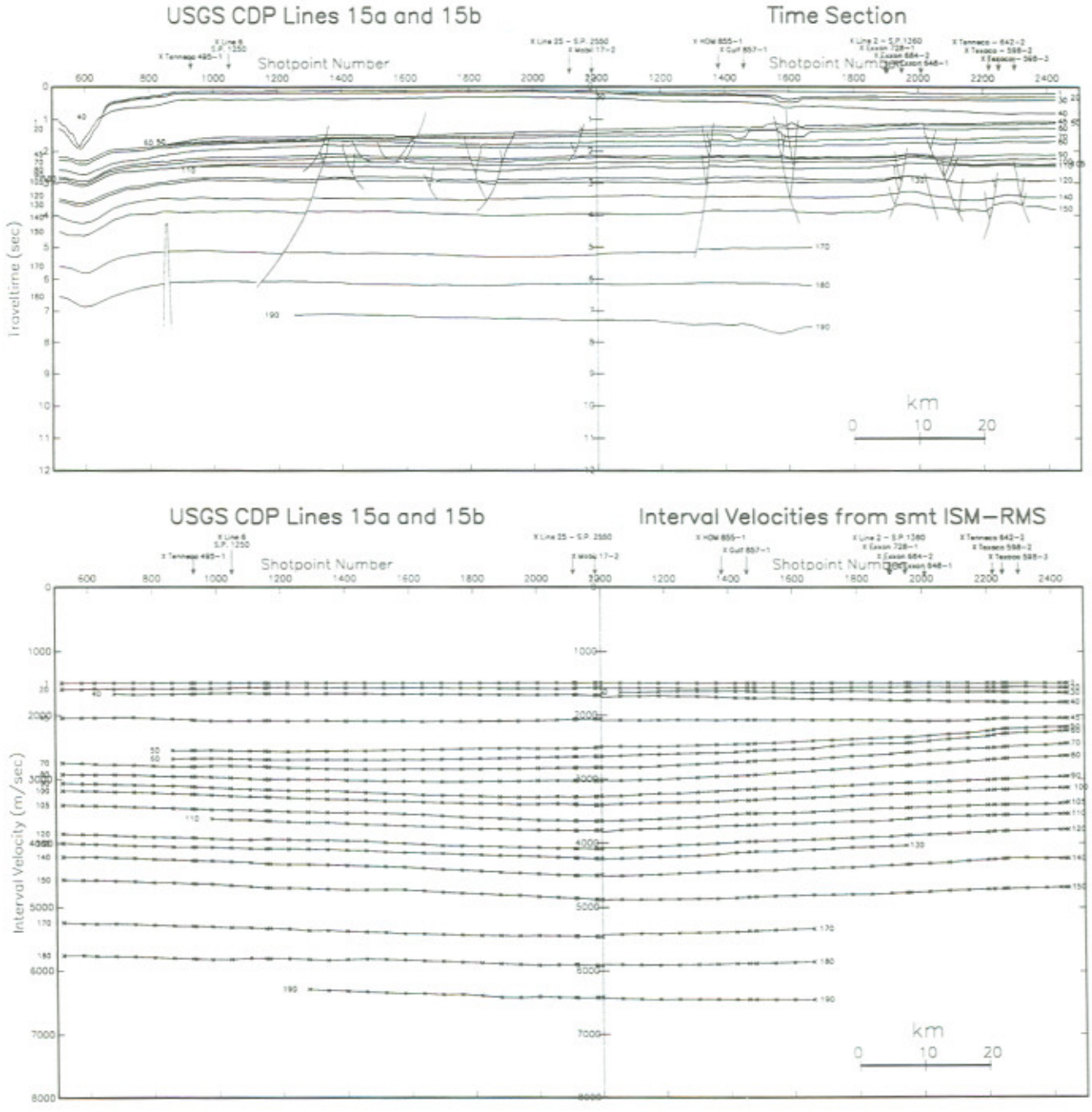
USGS CDP Lines 15a and 15b
Time Section
Shotpoint Number
Traveltime (sec)
km
0 10 20
USGS CDP Lines 15a and 15b
Interval Velocities from smt ISM–RMS
Shotpoint Number
Interval Velocity (m/sec)
km
0 10 20

Figure 8

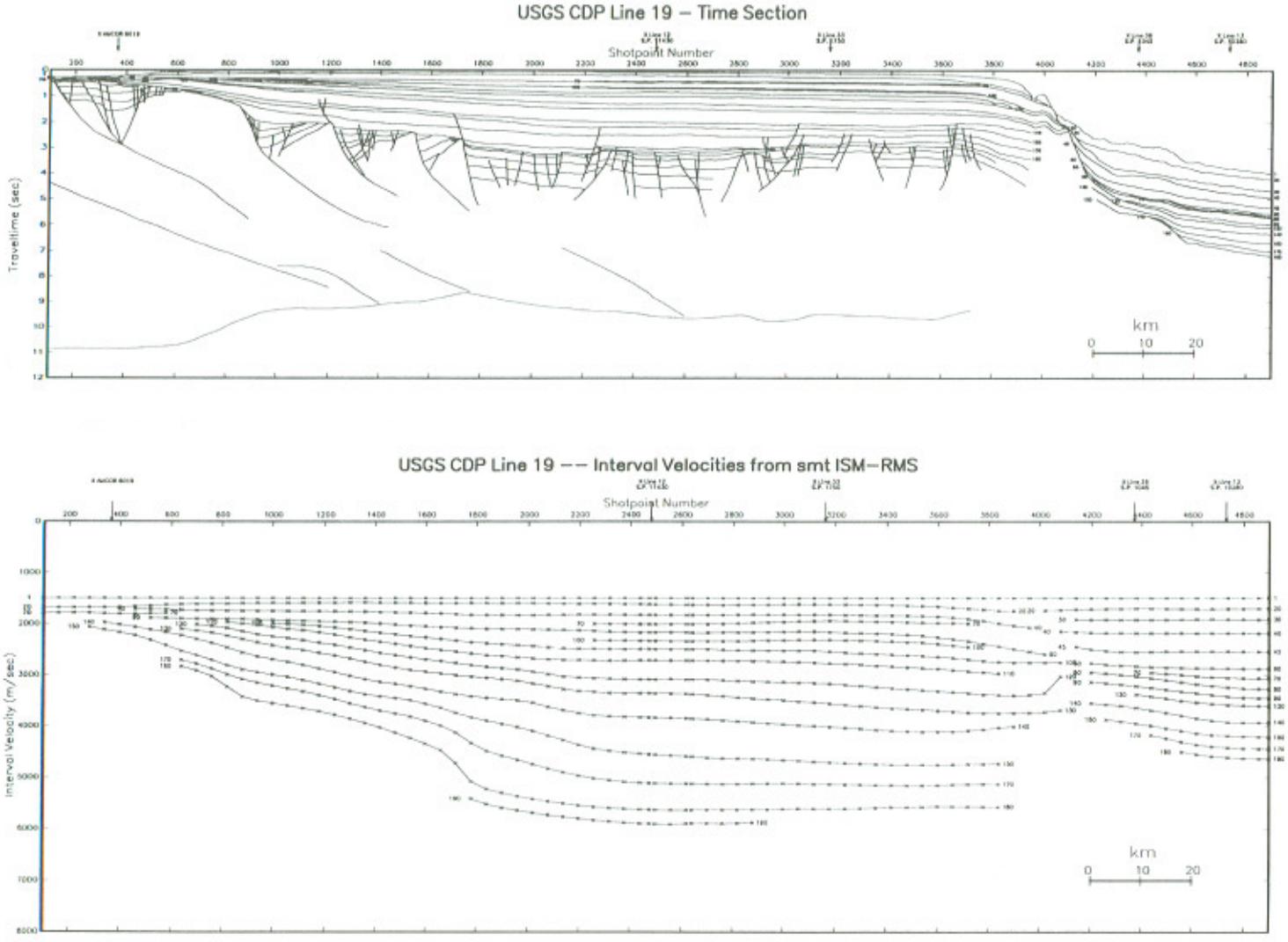
USGS CDP Line 19 – Time Section
Shotpoint Number
Traveltime (sec)
km
0
10
20
USGS CDP Line 19 -- Interval Velocities from smt ISM-RMS
Shotpoint Number
Interval Velocity (m/sec)
km
0
10
20

Figure 9

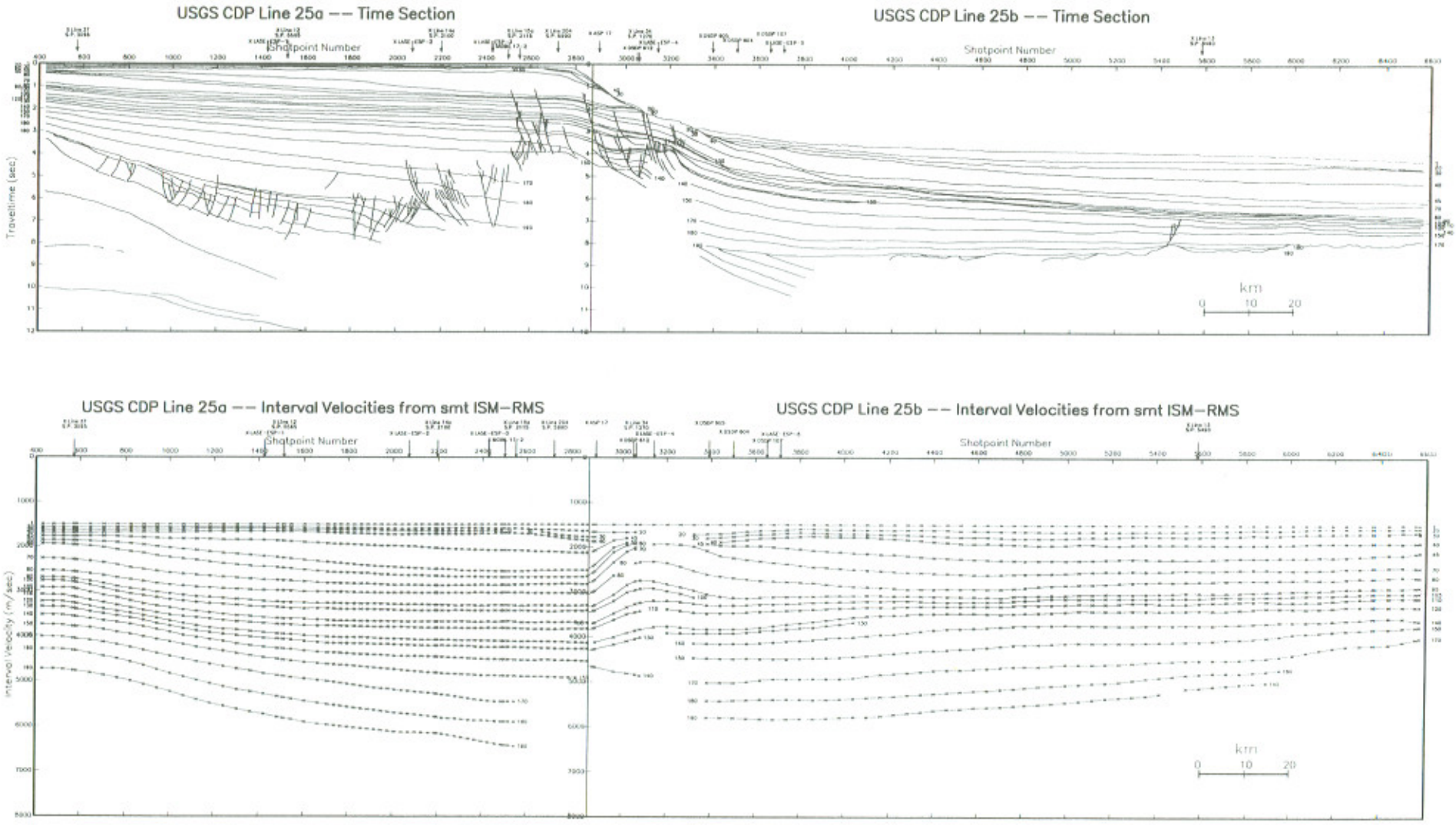
USGS CDP Line 25a -- Time Section
USGS CDP Line 25b -- Time Section
Shotpoint Number
Traveltime (sec)
km
0
10
20
USGS CDP Line 25a -- Interval Velocities from smt ISM-RMS
USGS CDP Line 25b -- Interval Velocities from smt ISM-RMS
Interval Velocity (m/sec)

Figure 10

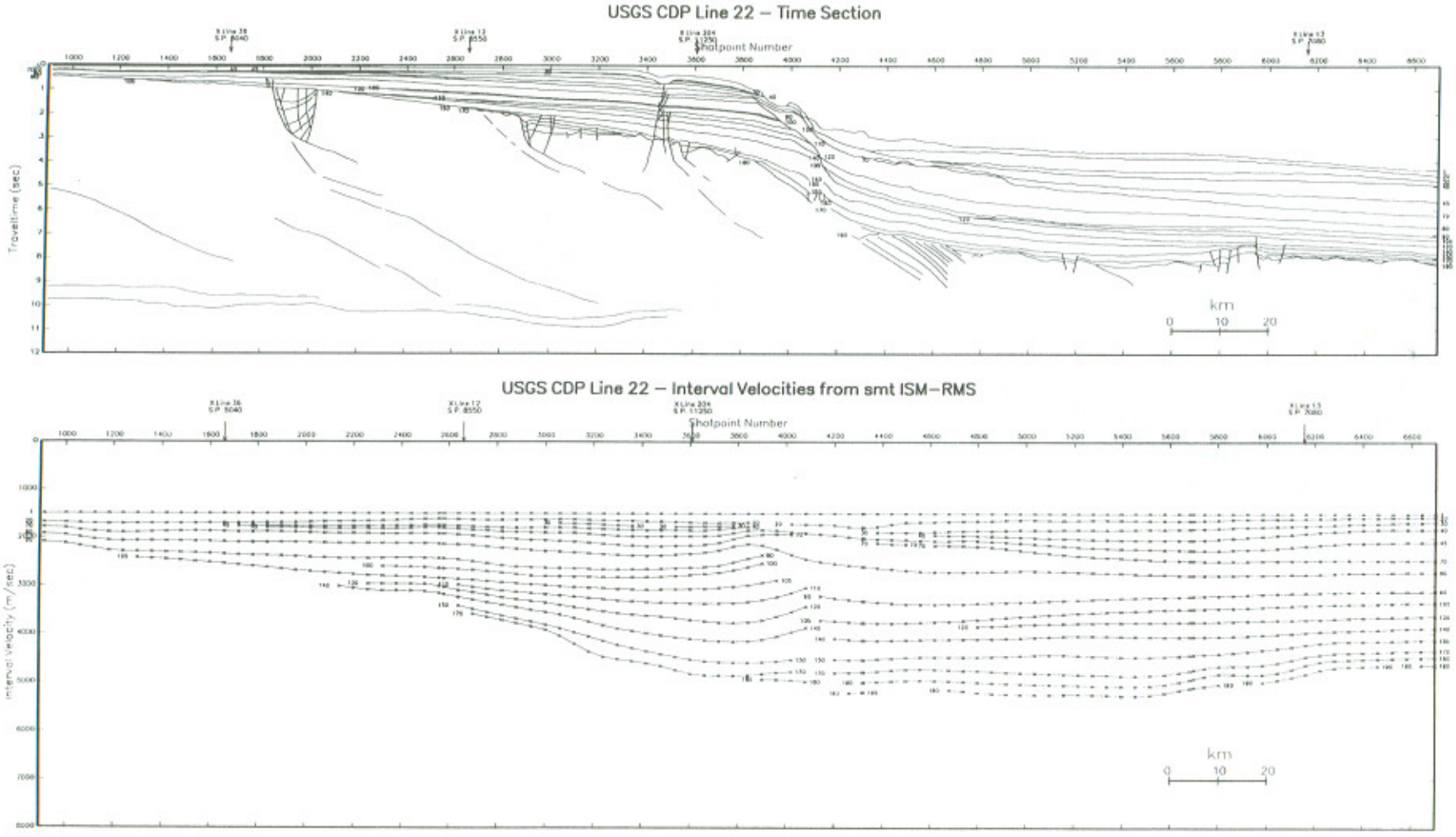
USGS CDP Line 22 – Time Section
Shotpoint Number
Traveltime (sec)
km
0
10
20
USGS CDP Line 22 – Interval Velocities from smt ISM–RMS
Shotpoint Number
Interval Velocity (m/sec)
km
0
10
20

Figure 11

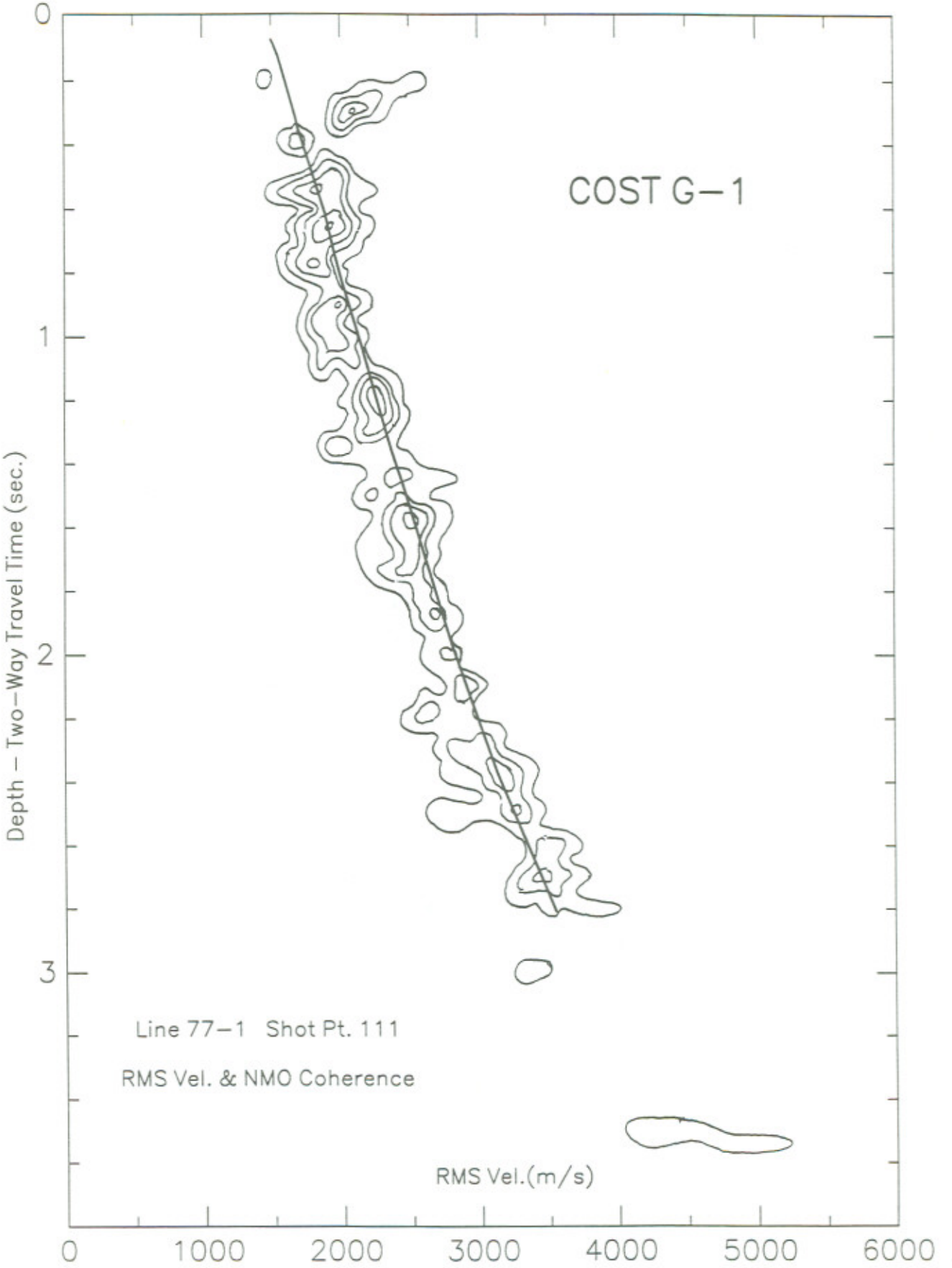
COST G-1
Depth - Two-Way Travel Time (sec.)
0
1
2
3
Line 77-1 Shot Pt. 111
RMS Vel. & NMO Coherence
RMS Vel.(m/s)
0
1000
2000
3000
4000
5000
6000

Figure 12a

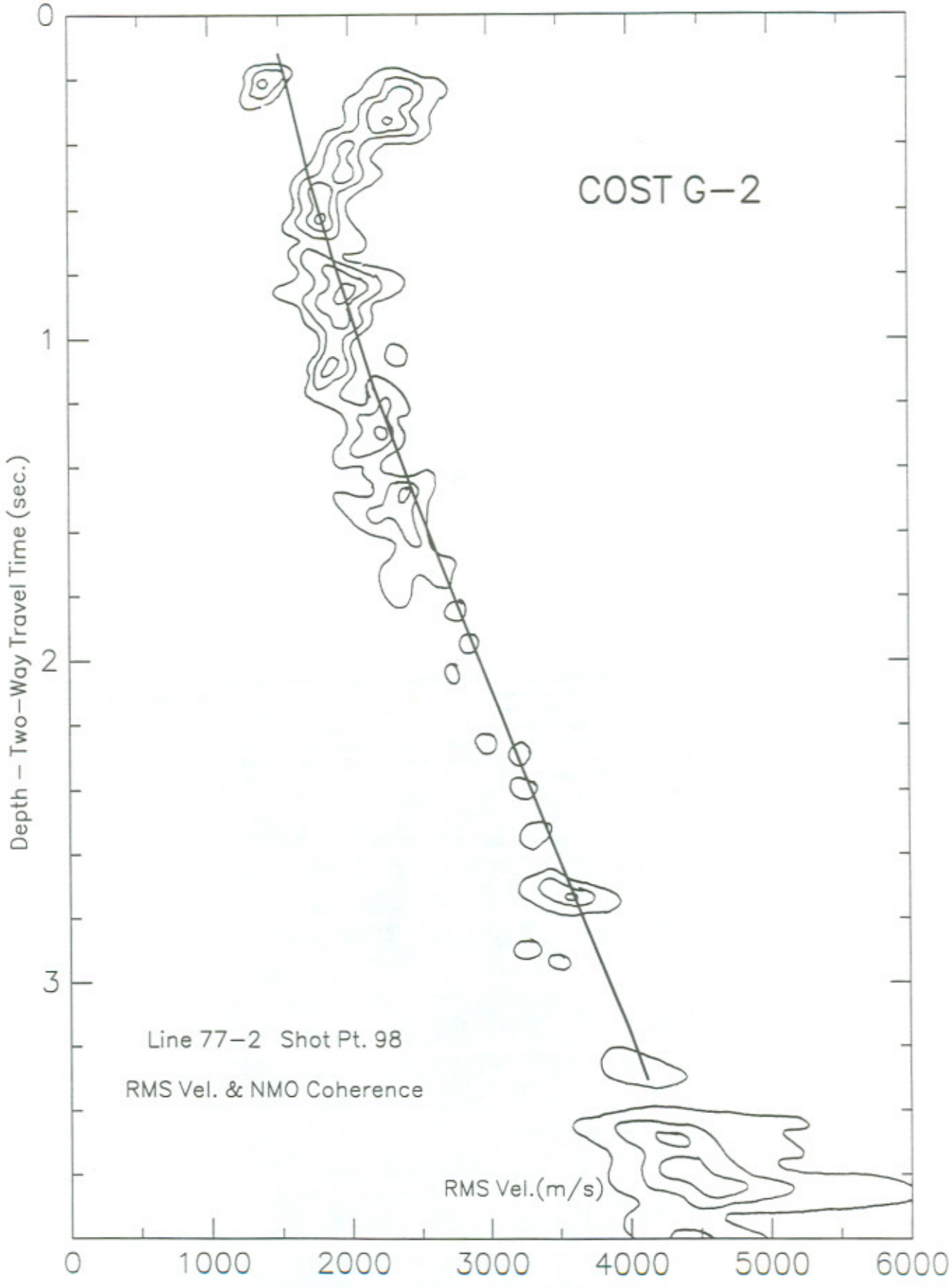
COST G-2
Depth - Two-Way Travel Time (sec.)
0
1
2
3
Line 77-2 Shot Pt. 98
RMS Vel. & NMO Coherence
RMS Vel.(m/s)
0
1000
2000
3000
4000
5000
6000

Figure 12b

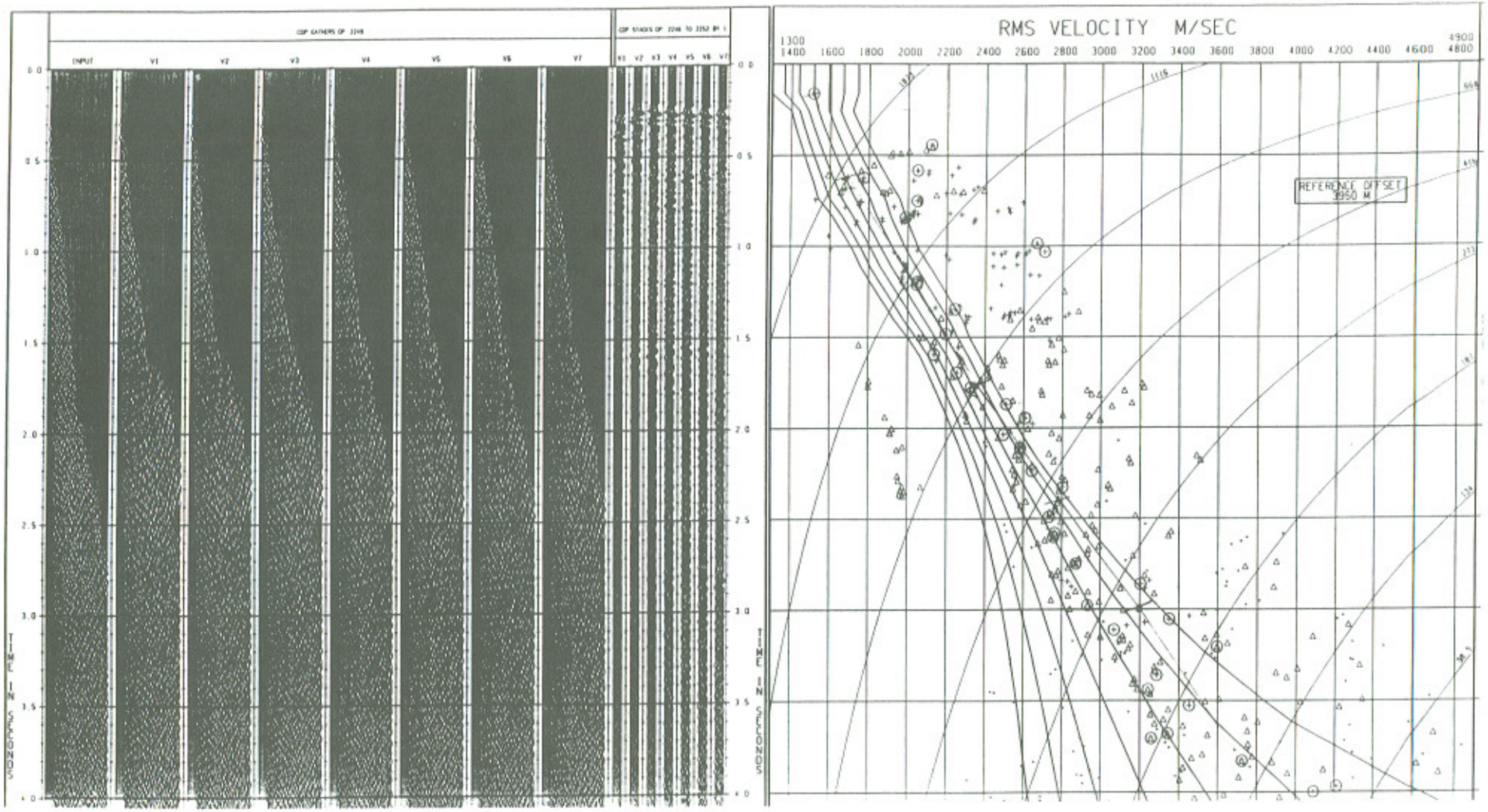
RMS VELOCITY M/SEC
1300
1400
1600
1800
2000
2200
2400
2600
2800
3000
3200
3400
3600
3800
4000
4200
4400
4600
4800
4900
REFERENCE OFFSET
2950 M
INPUT
V1
V2
V3
V4
V5
V6
V7
TIME IN SECONDS
0.0
0.5
1.0
1.5
2.0
2.5
3.0
3.5
4.0

Figure 13a

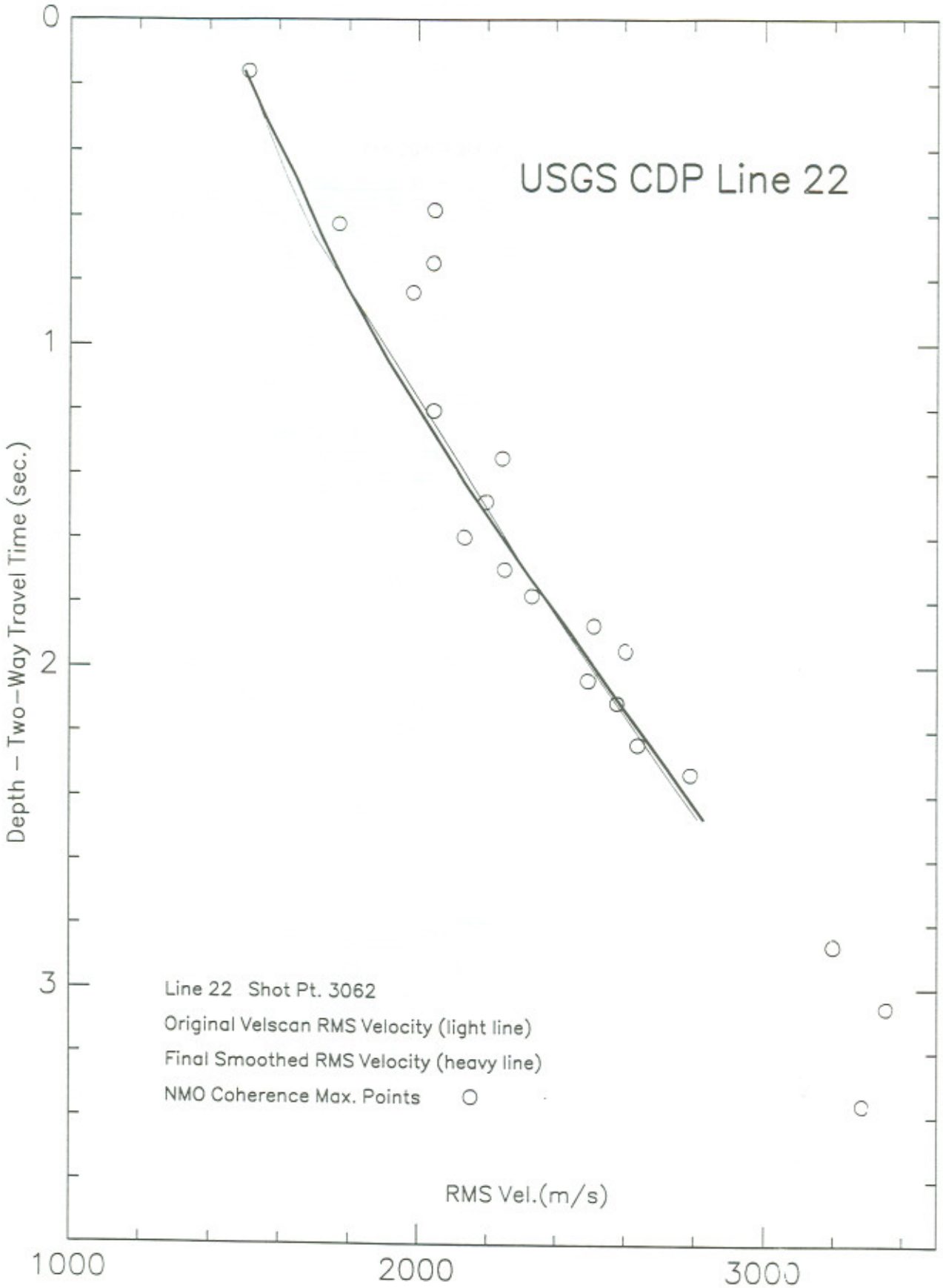
USGS CDP Line 22
Depth – Two–Way Travel Time (sec.)
0
1
2
3
1000
2000
3000
RMS Vel.(m/s)
Line 22 Shot Pt. 3062
Original Velscan RMS Velocity (light line)
Final Smoothed RMS Velocity (heavy line)
NMO Coherence Max. Points

Figure 13b

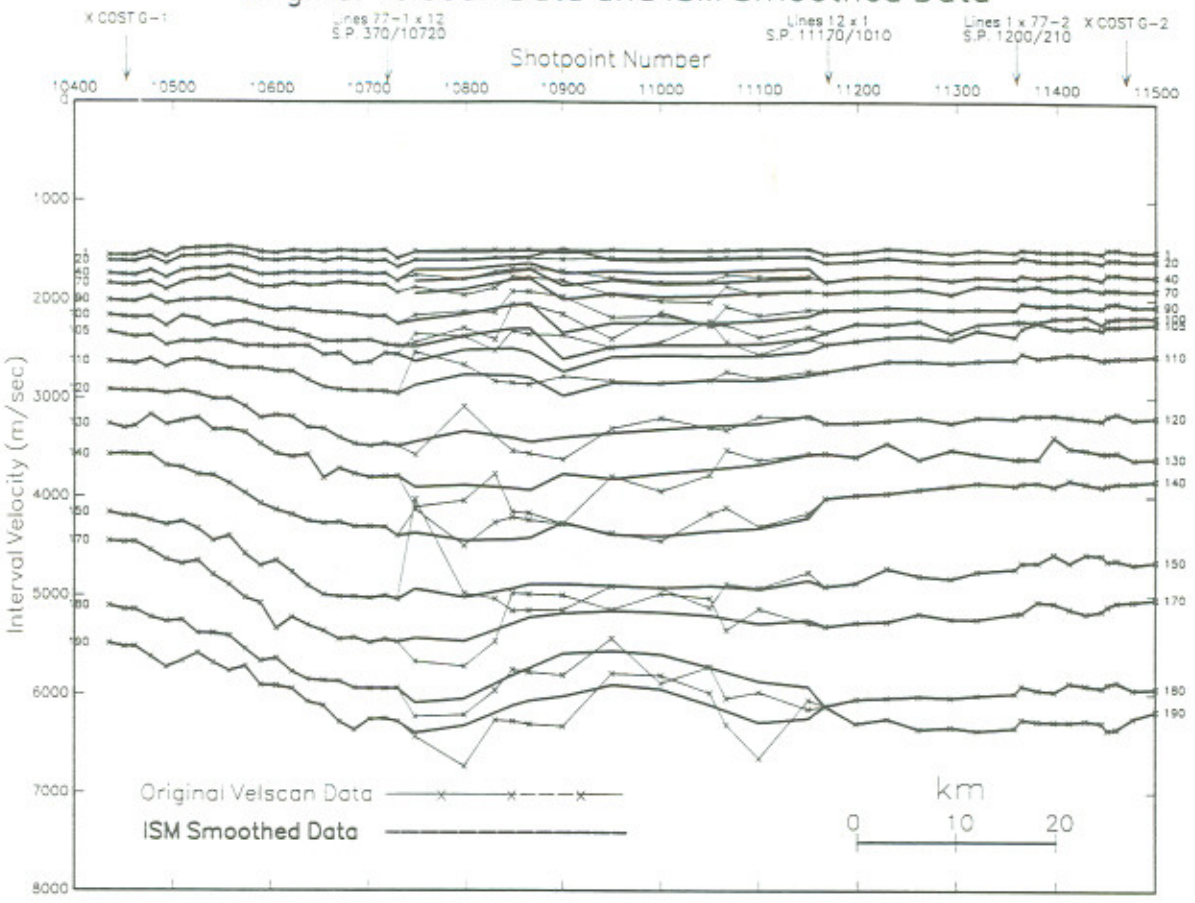
Composite Line G1–G2 -- Interval Velocities
Original Velscan Data and ISM Smoothed Data
X COST G-1
Lines 77-1 x 12
S.P. 370/10720
Lines 12 x 1
S.P. 11170/1010
Lines 1 x 77-2
S.P. 1200/210
X COST G-2
Shotpoint Number
10400
10500
10600
10700
10800
10900
11000
11100
11200
11300
11400
11500
Interval Velocity (m/sec)
1000
2000
3000
4000
5000
6000
7000
8000
Original Velscan Data
ISM Smoothed Data
km
0
10
20

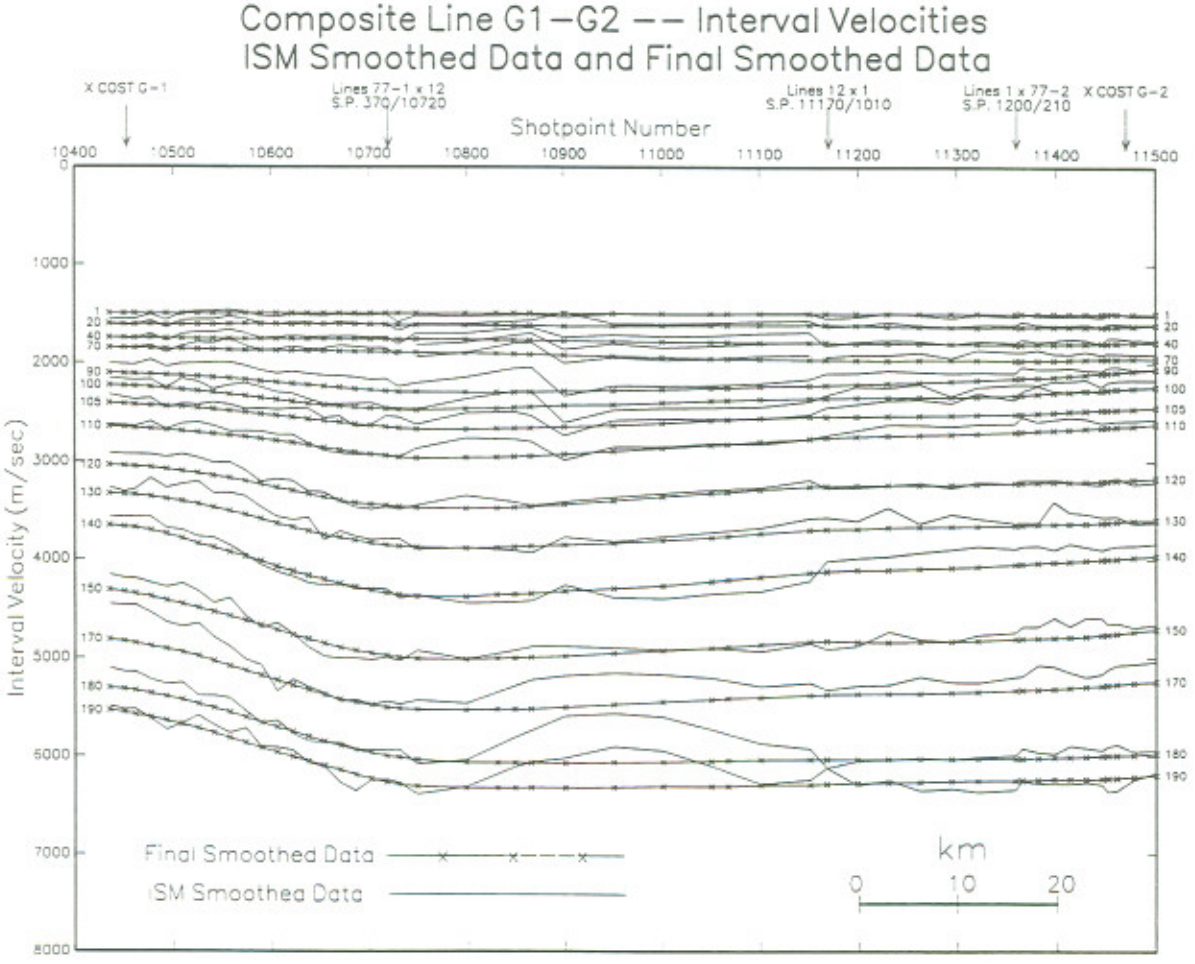
Composite Line G1–G2 -- Interval Velocities
ISM Smoothed Data and Final Smoothed Data
X COST G-1
Lines 77-1 x 12
S.P. 370/10720
Lines 12 x 1
S.P. 11170/1010
Lines 1 x 77-2
S.P. 1200/210
X COST G-2
Shotpoint Number
10400
10500
10600
10700
10800
10900
11000
11100
11200
11300
11400
11500
Interval Velocity (m/sec)
1000
2000
3000
4000
5000
6000
7000
8000
Final Smoothed Data
ISM Smoothed Data
km
0
10
20

Figure 14

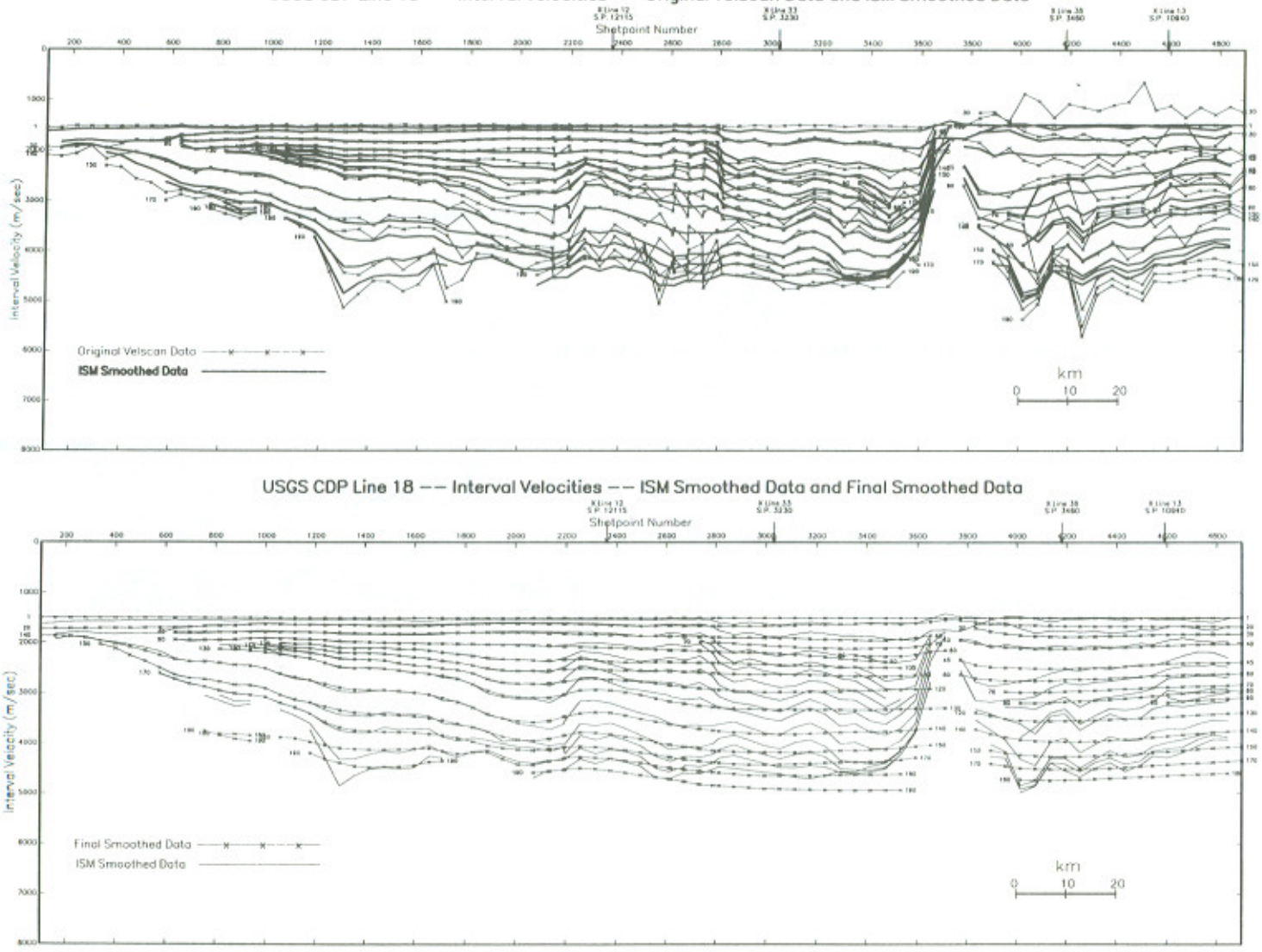
USGS CDP Line 18 -- Interval Velocities -- Original Velscan Data and ISM Smoothed Data
Shotpoint Number
Interval Velocity (m/sec)
Original Velscan Data
ISM Smoothed Data
km
0 10 20
USGS CDP Line 18 -- Interval Velocities -- ISM Smoothed Data and Final Smoothed Data
Shotpoint Number
Interval Velocity (m/sec)
Final Smoothed Data
ISM Smoothed Data
km
0 10 20

Figure 15

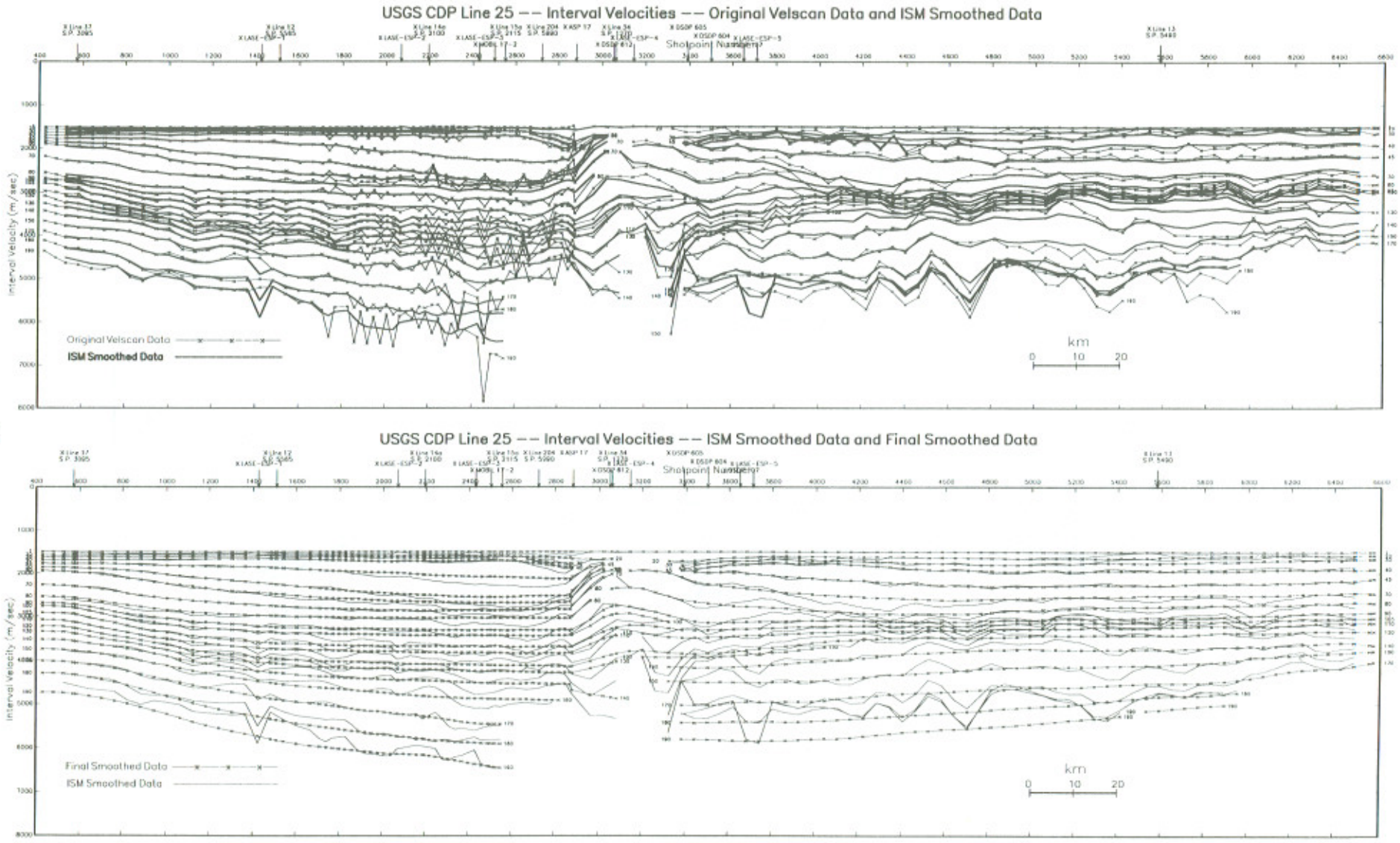
USGS CDP Line 25 -- Interval Velocities -- Original Velscan Data and ISM Smoothed Data
Shotpoint Numbers
Interval Velocity (m/sec)
Original Velscan Data
ISM Smoothed Data
km
0 10 20
USGS CDP Line 25 -- Interval Velocities -- ISM Smoothed Data and Final Smoothed Data
Shotpoint Numbers
Interval Velocity (m/sec)
Final Smoothed Data
ISM Smoothed Data
km
0 10 20

Figure 16

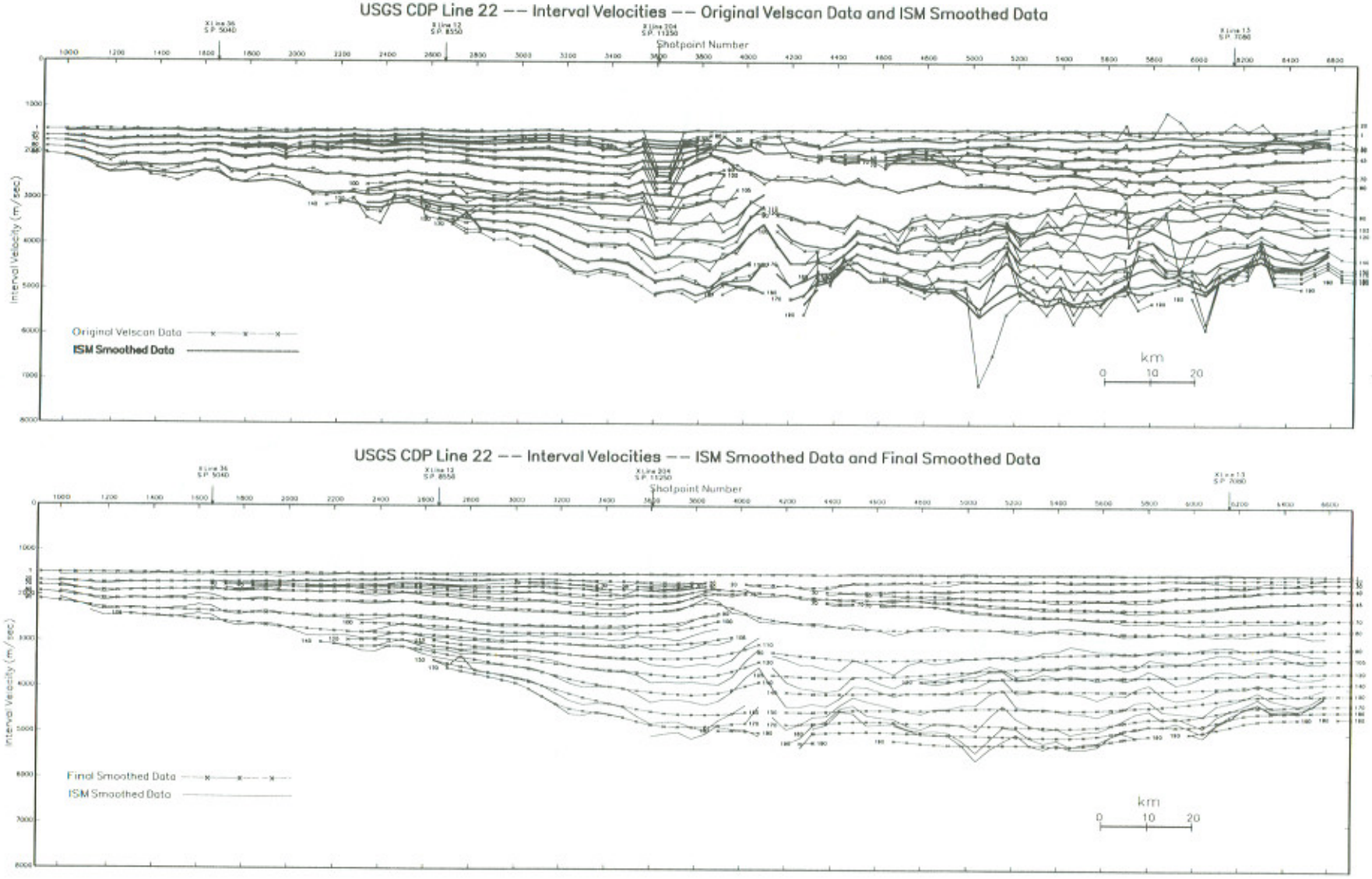
USGS CDP Line 22 -- Interval Velocities -- Original Velscan Data and ISM Smoothed Data
Shotpoint Number
Interval Velocity (m/sec)
Original Velscan Data
ISM Smoothed Data
km
0 10 20
USGS CDP Line 22 -- Interval Velocities -- ISM Smoothed Data and Final Smoothed Data
Shotpoint Number
Interval Velocity (m/sec)
Final Smoothed Data
ISM Smoothed Data
km
0 10 20

Figure 17

USGS CDP Line 25 -- RMS Velocities -- Original Velscan Data and Final Smoothed Data

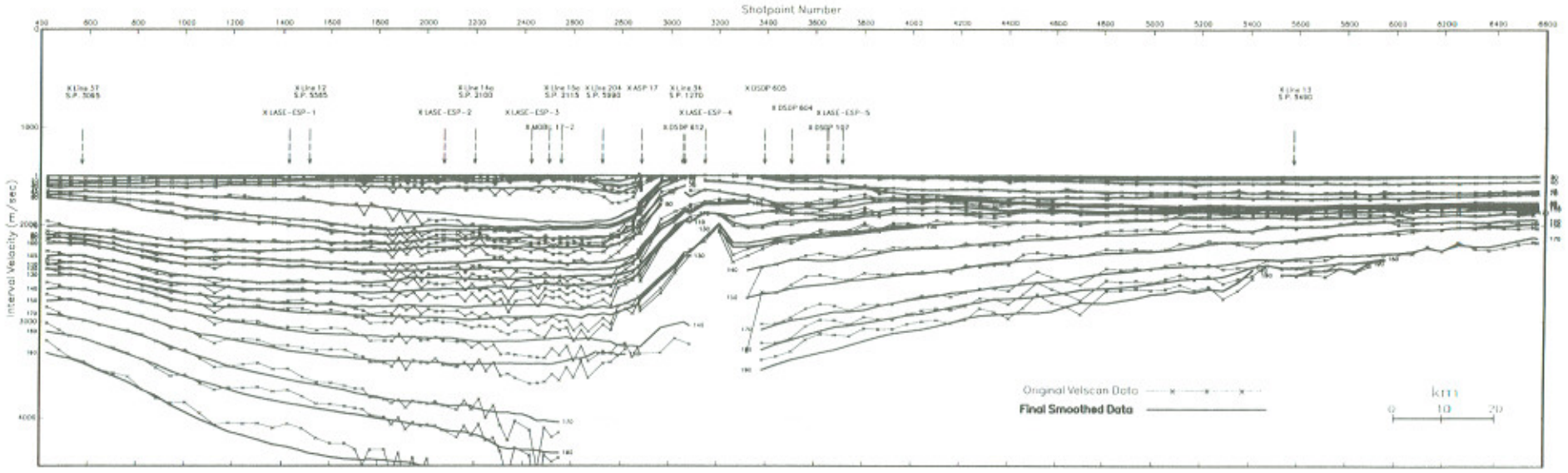

USGS CDP Line 22 -- RMS Velocities -- Original Velscan Data and Final Smoothed Data

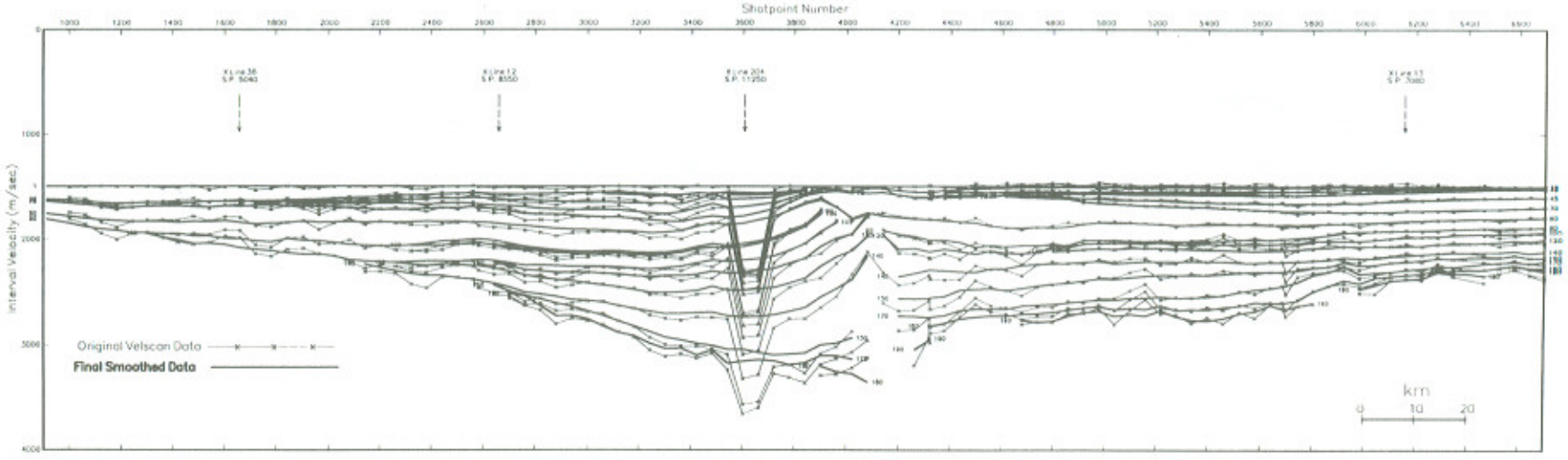

Figure 18

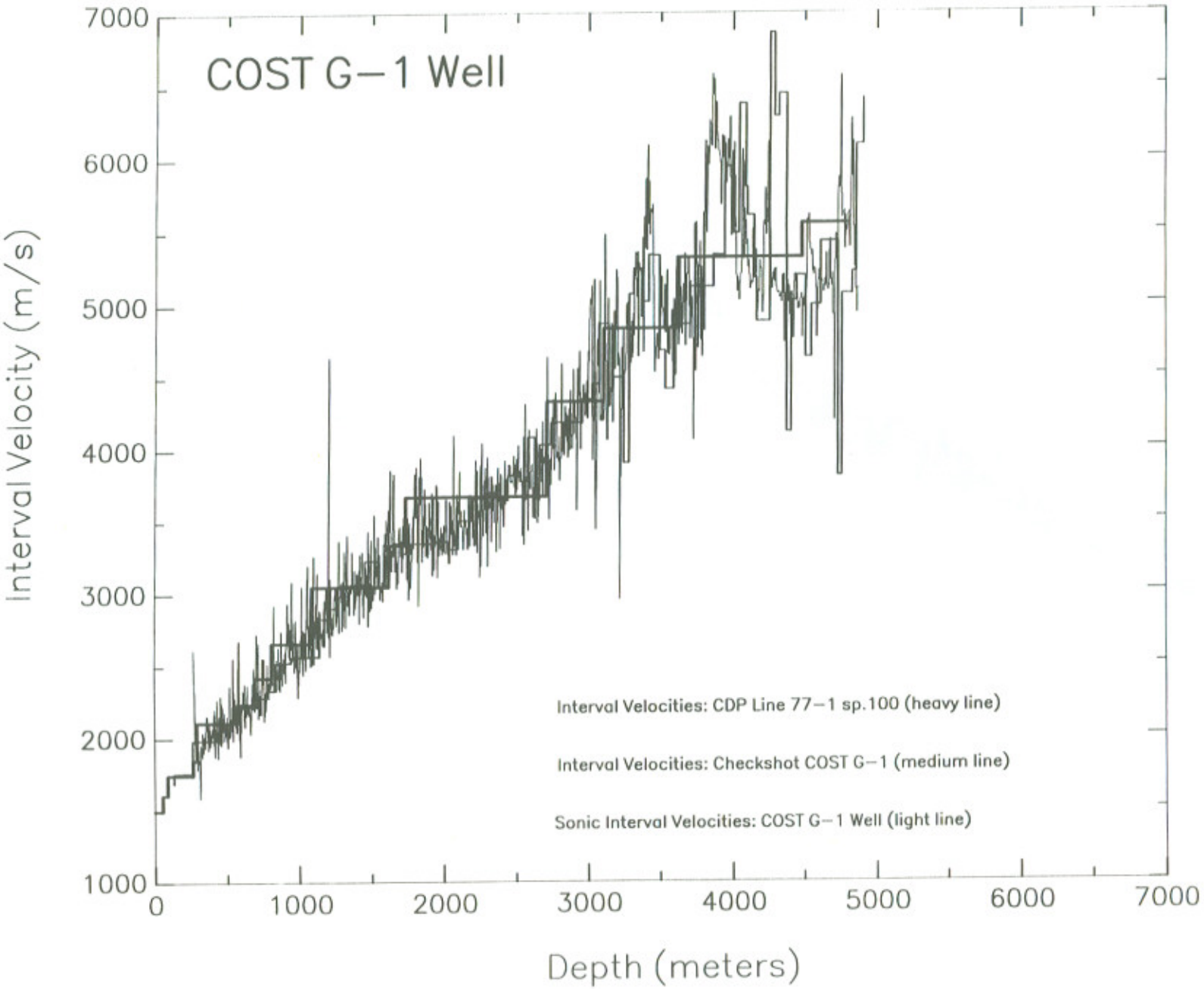
COST G–1 Well
Interval Velocity (m/s)
Depth (meters)
7000
6000
5000
4000
3000
2000
1000
0
1000
2000
3000
4000
5000
6000
7000
Interval Velocities: CDP Line 77–1 sp.100 (heavy line)
Interval Velocities: Checkshot COST G–1 (medium line)
Sonic Interval Velocities: COST G–1 Well (light line)

Figure 19a

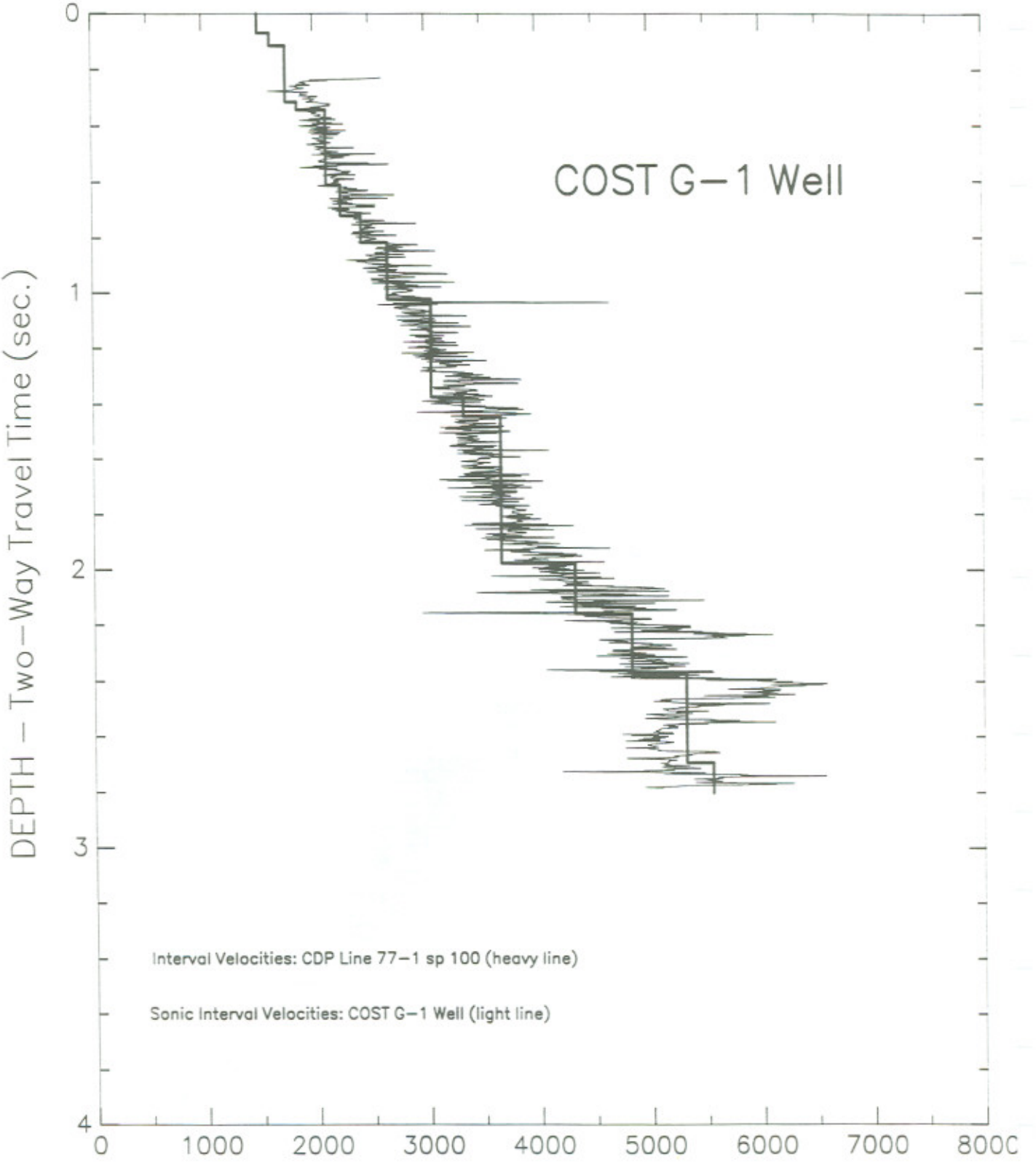
COST G–1 Well
DEPTH – Two–Way Travel Time (sec.)
0
1
2
3
4
0
1000
2000
3000
4000
5000
6000
7000
8000
Interval Velocities: CDP Line 77–1 sp 100 (heavy line)
Sonic Interval Velocities: COST G–1 Well (light line)
INTERVAL VELOCITY (m/s)

Figure 19b

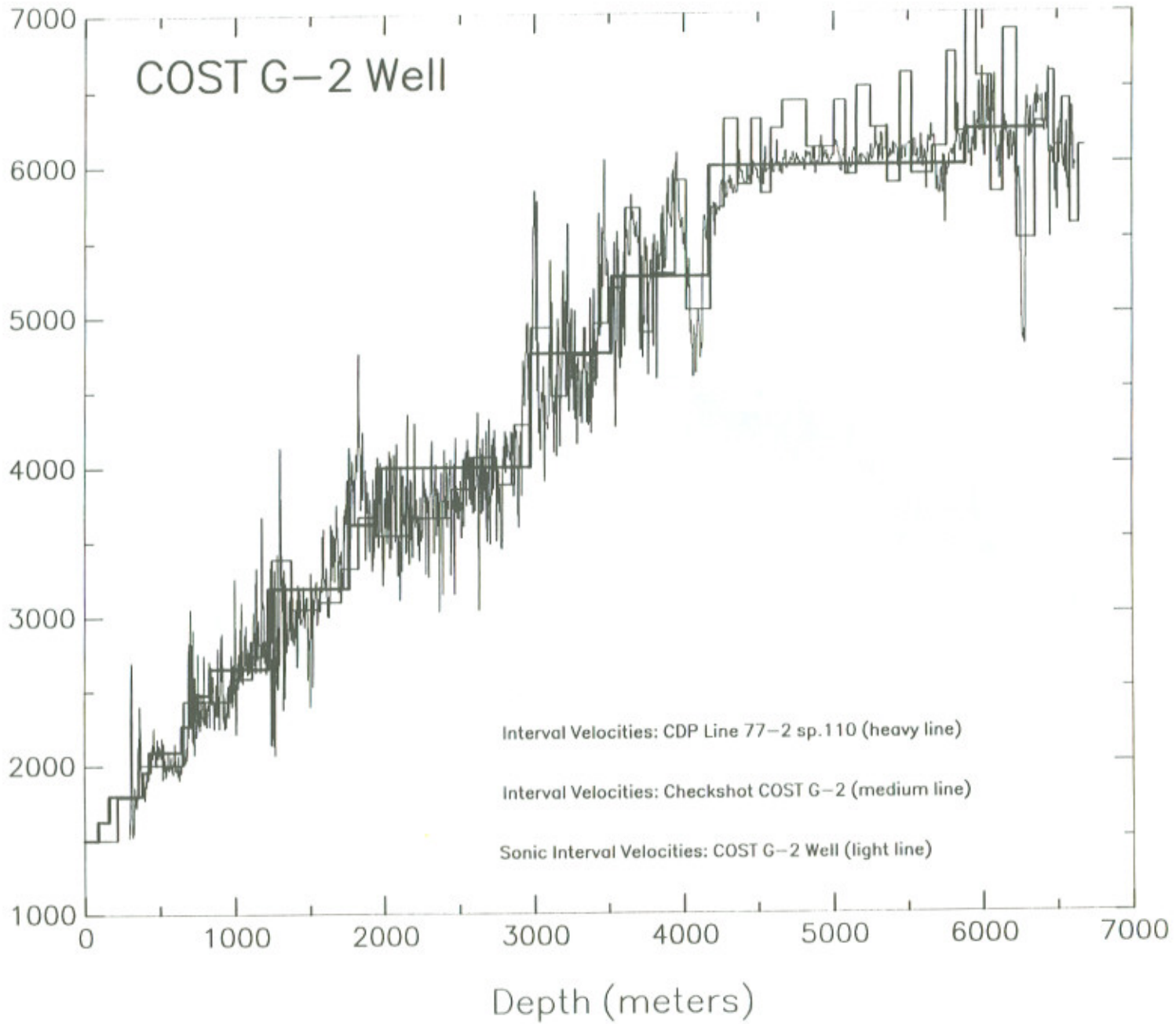
COST G–2 Well
Interval Velocity (m/s)
7000
6000
5000
4000
3000
2000
1000
0
1000
2000
3000
4000
5000
6000
7000
Depth (meters)
Interval Velocities: CDP Line 77–2 sp.110 (heavy line)
Interval Velocities: Checkshot COST G–2 (medium line)
Sonic Interval Velocities: COST G–2 Well (light line)

Figure 20a

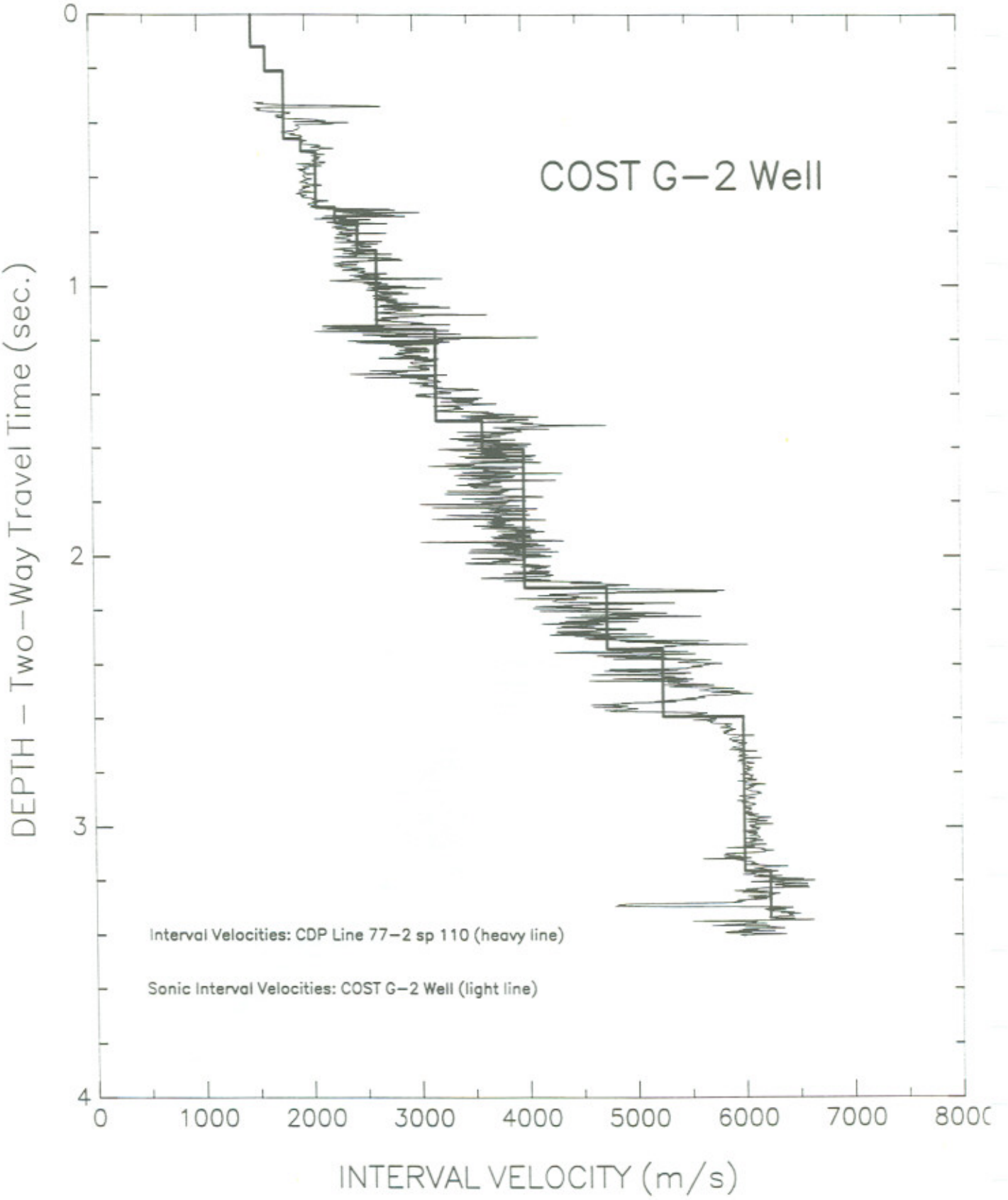
COST G–2 Well
DEPTH – Two–Way Travel Time (sec.)
0
1
2
3
4
0
1000
2000
3000
4000
5000
6000
7000
8000
INTERVAL VELOCITY (m/s)
Interval Velocities: CDP Line 77–2 sp 110 (heavy line)
Sonic Interval Velocities: COST G–2 Well (light line)

Figure 20b

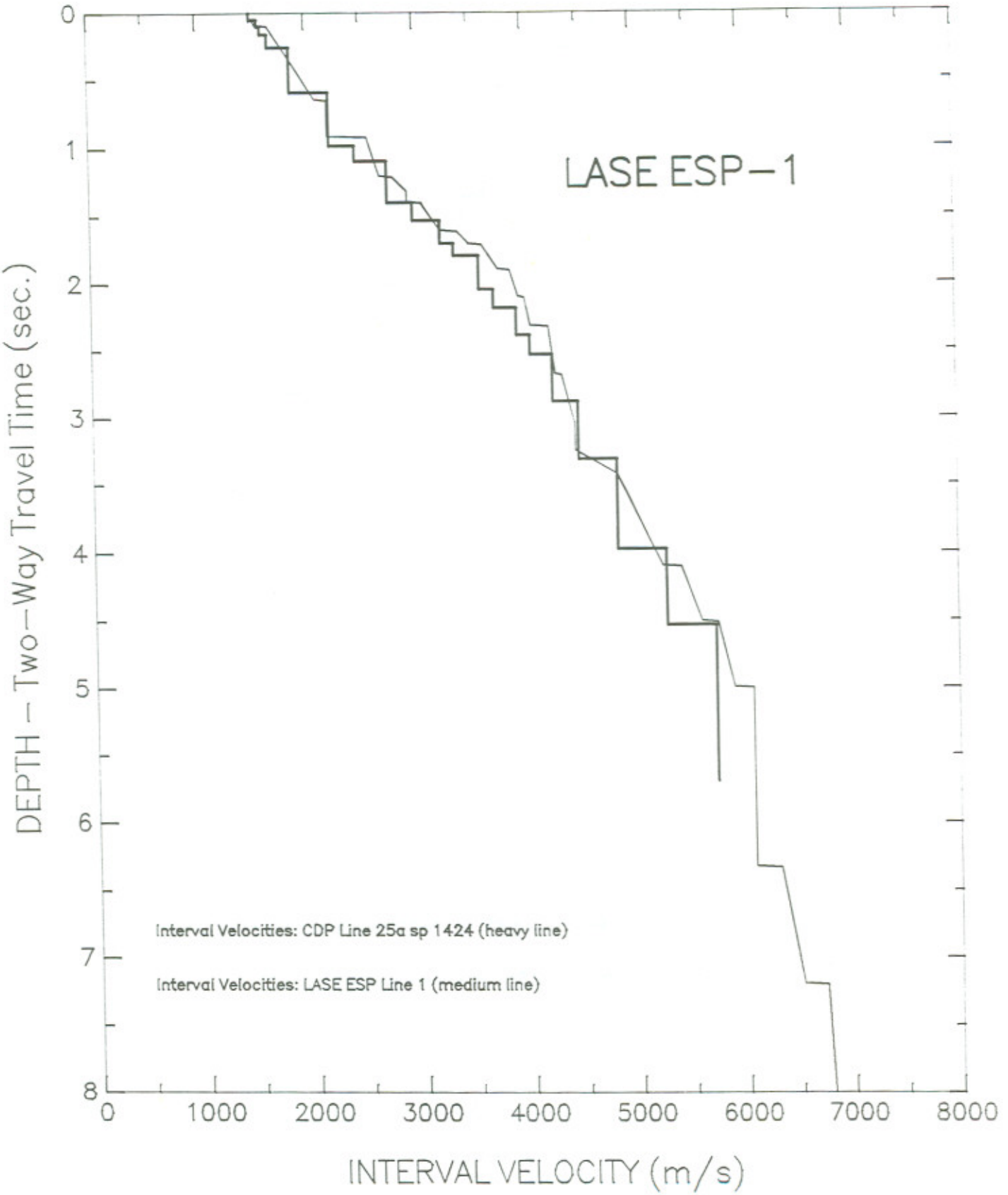
LASE ESP–1
DEPTH – Two–Way Travel Time (sec.)
INTERVAL VELOCITY (m/s)
0
1
2
3
4
5
6
7
8
0
1000
2000
3000
4000
5000
6000
7000
8000
Interval Velocities: CDP Line 25a sp 1424 (heavy line)
Interval Velocities: LASE ESP Line 1 (medium line)

Figure 21a

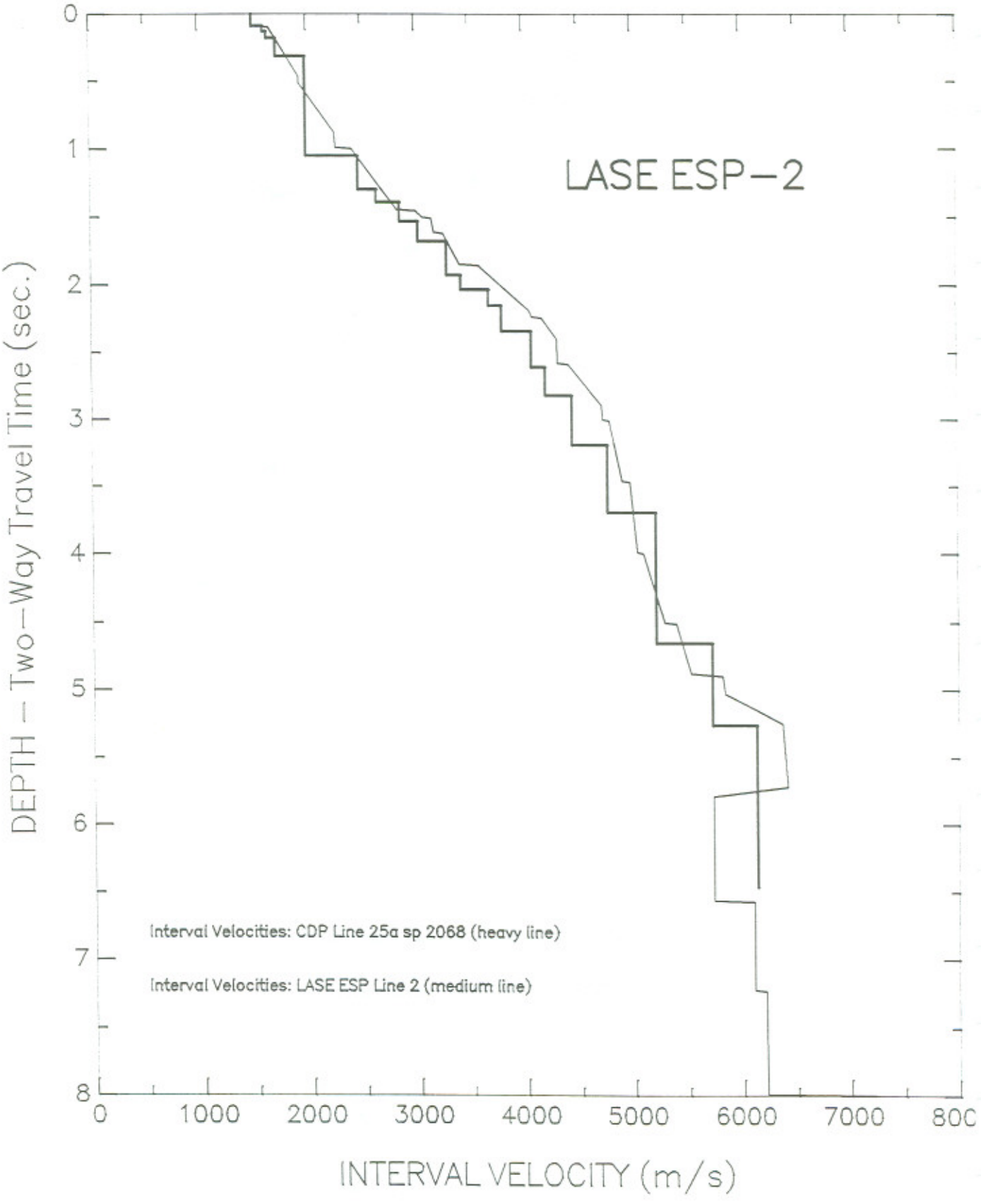
LASE ESP–2
DEPTH – Two–Way Travel Time (sec.)
INTERVAL VELOCITY (m/s)
0
1
2
3
4
5
6
7
8
0
1000
2000
3000
4000
5000
6000
7000
800
Interval Velocities: CDP Line 25a sp 2068 (heavy line)
Interval Velocities: LASE ESP Line 2 (medium line)

Figure 21b

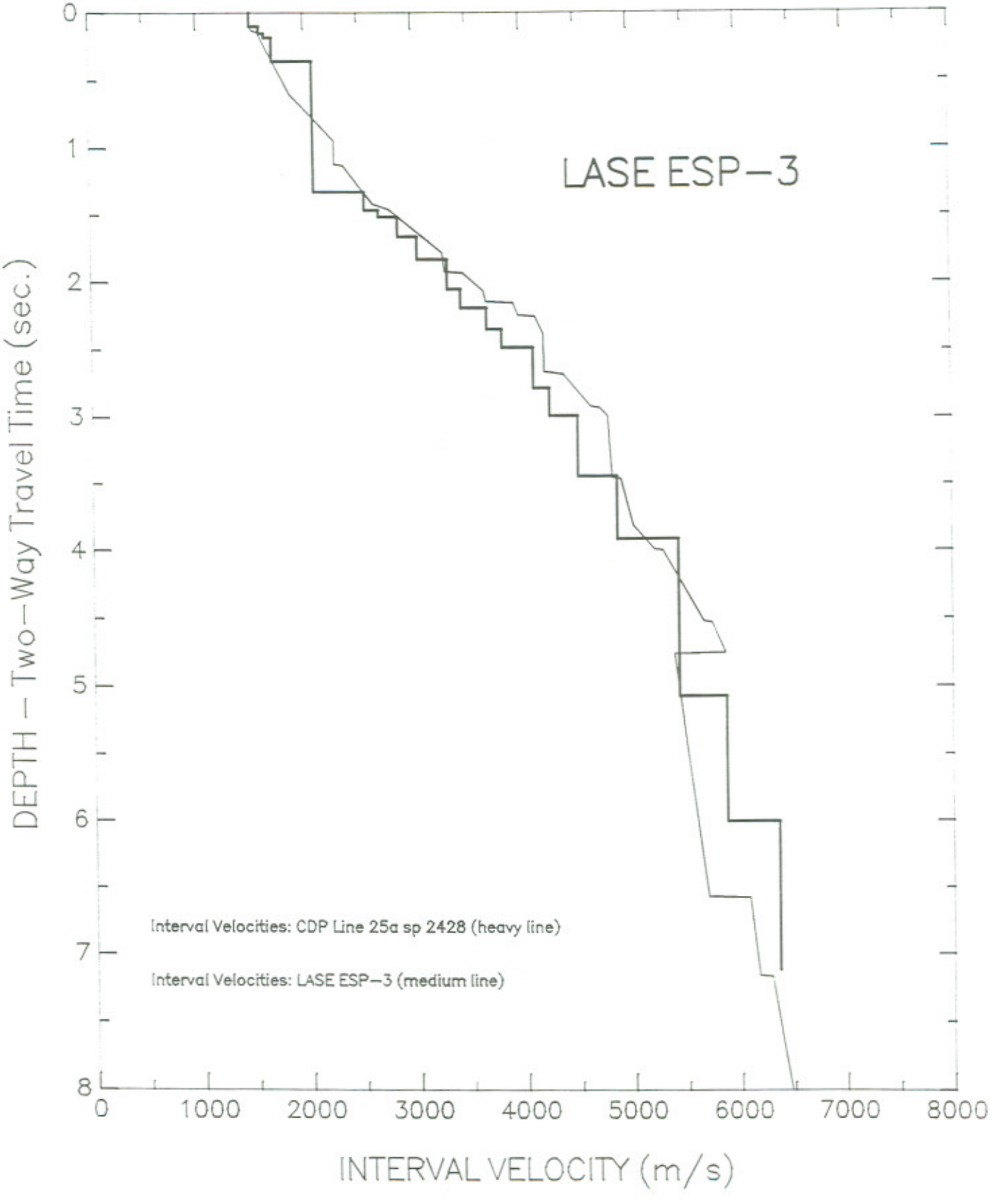
LASE ESP–3
DEPTH – Two–Way Travel Time (sec.)
INTERVAL VELOCITY (m/s)
0
1
2
3
4
5
6
7
8
0
1000
2000
3000
4000
5000
6000
7000
8000
Interval Velocities: CDP Line 25a sp 2428 (heavy line)
Interval Velocities: LASE ESP–3 (medium line)

Figure 21c

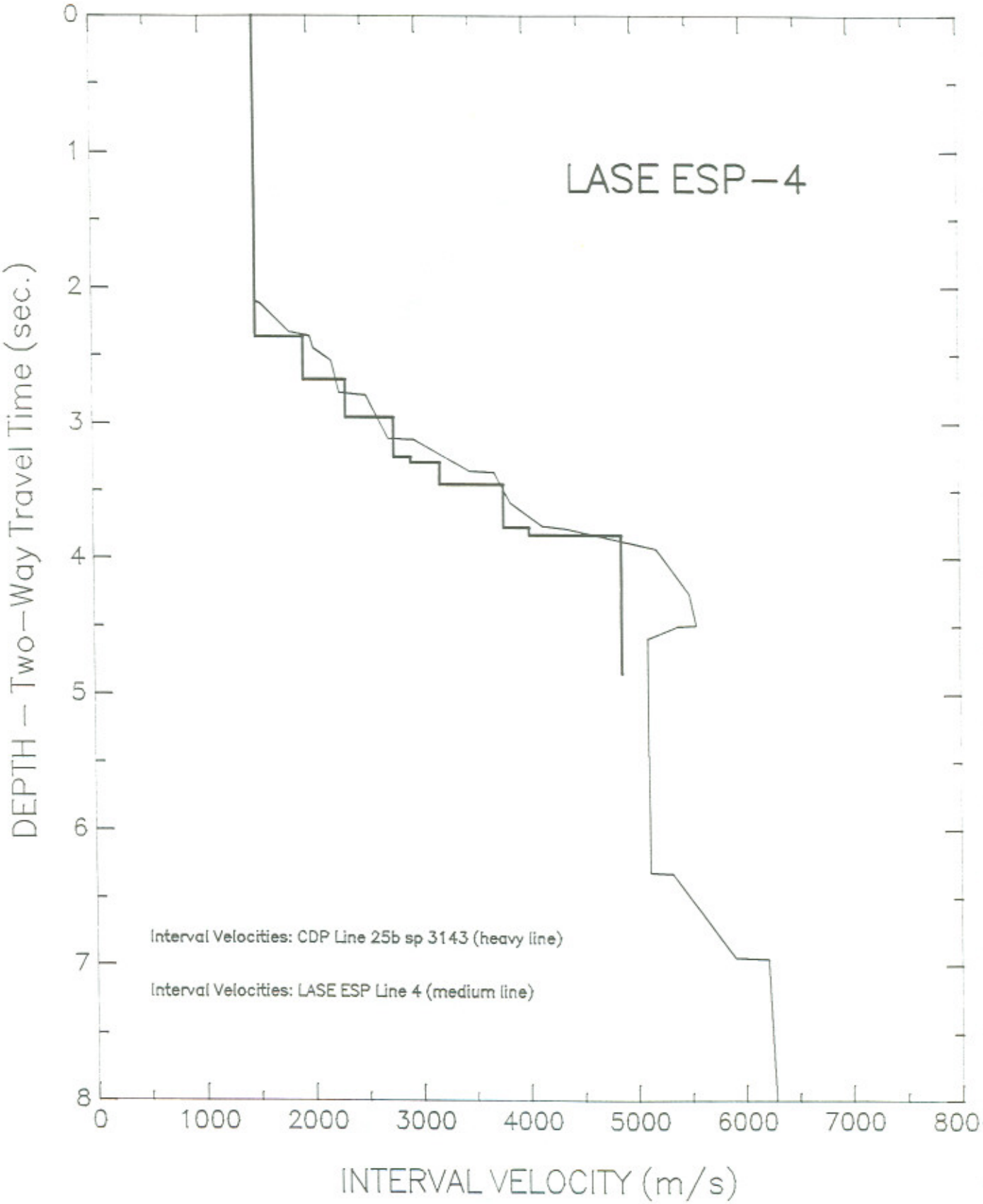
LASE ESP–4
DEPTH – Two–Way Travel Time (sec.)
0
1
2
3
4
5
6
7
8
0
1000
2000
3000
4000
5000
6000
7000
800
INTERVAL VELOCITY (m/s)
Interval Velocities: CDP Line 25b sp 3143 (heavy line)
Interval Velocities: LASE ESP Line 4 (medium line)

Figure 21d

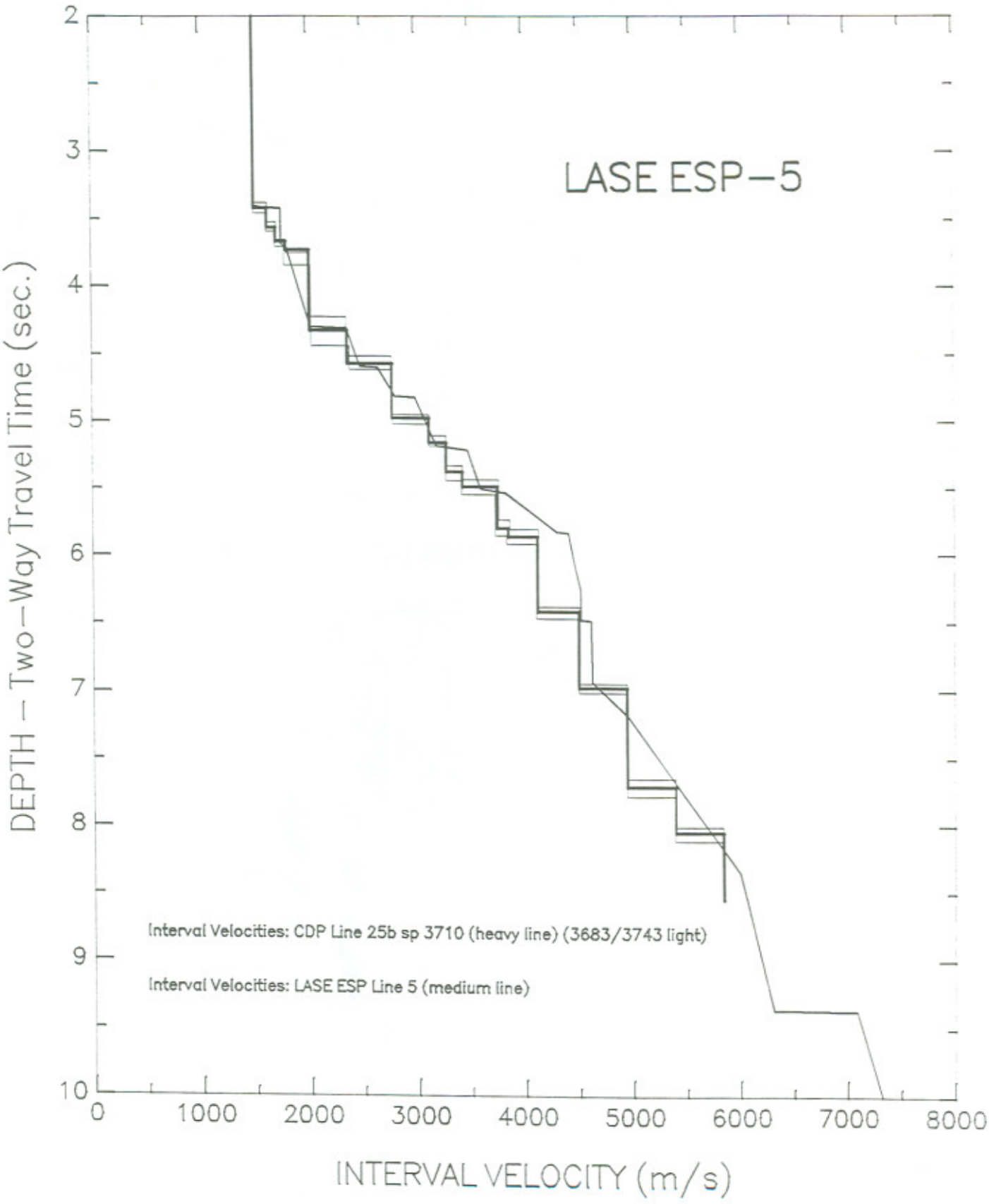
LASE ESP–5
DEPTH – Two–Way Travel Time (sec.)
INTERVAL VELOCITY (m/s)
Interval Velocities: CDP Line 25b sp 3710 (heavy line) (3683/3743 light)
Interval Velocities: LASE ESP Line 5 (medium line)
2
3
4
5
6
7
8
9
10
0
1000
2000
3000
4000
5000
6000
7000
8000

Figure 21e

GEORGES BANK CROSS SECTION

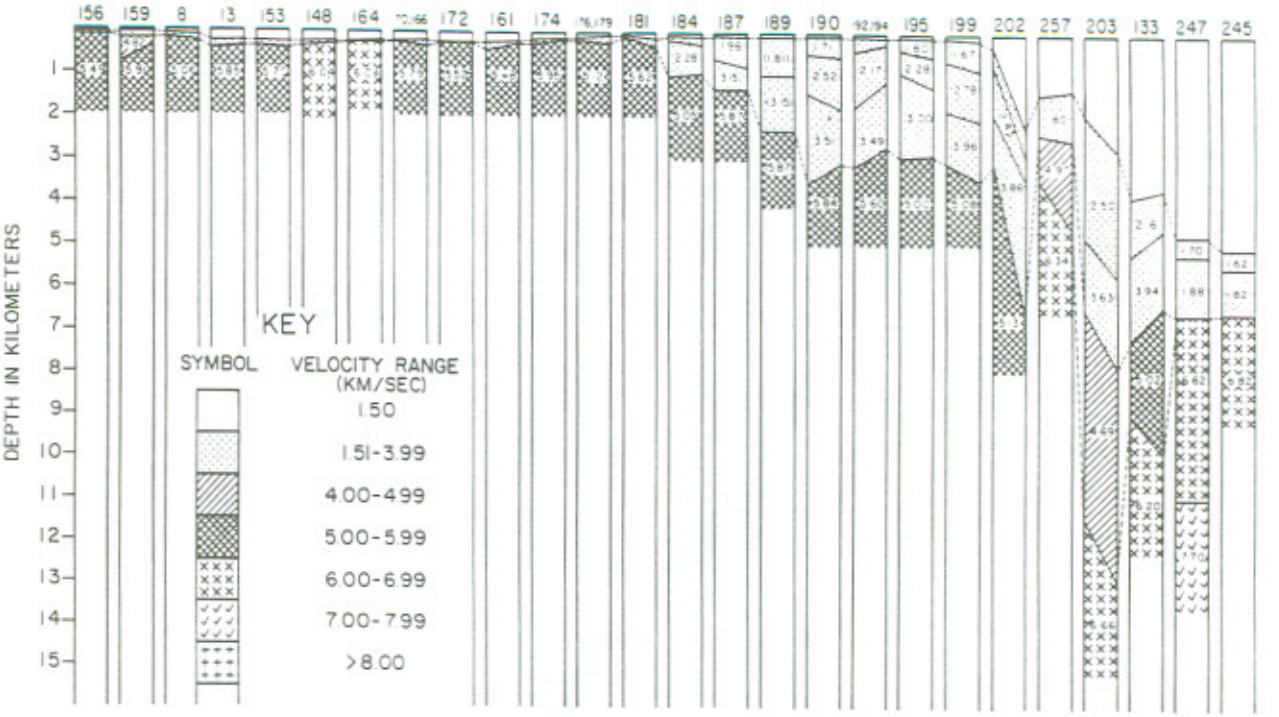

Refraction cross-section summary A—Georges Bank. Insert shows symbols for velocity range.

BALTIMORE CANYON TROUGH CROSS SECTION

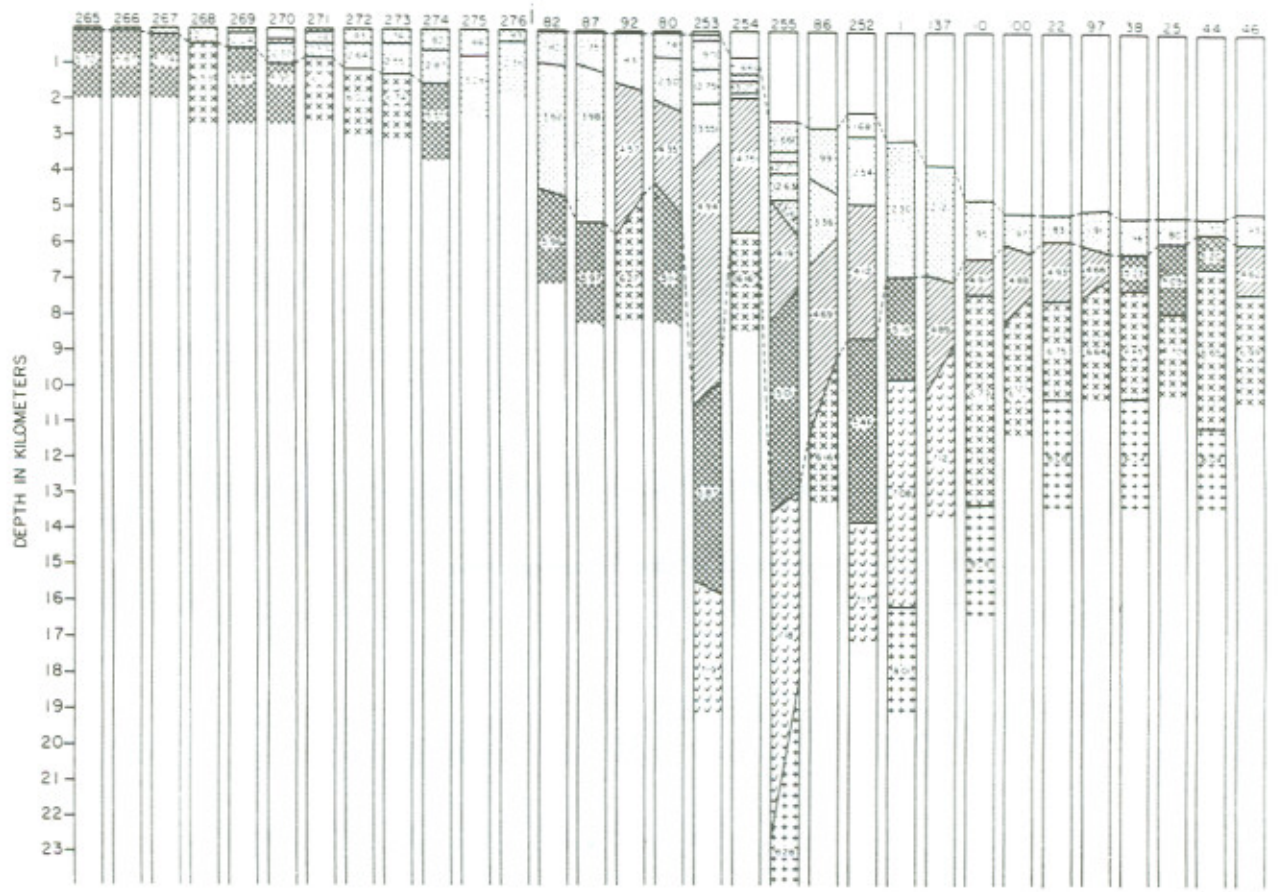

Refraction cross-section summary B—Baltimore Canyon Trough.

Figure 22

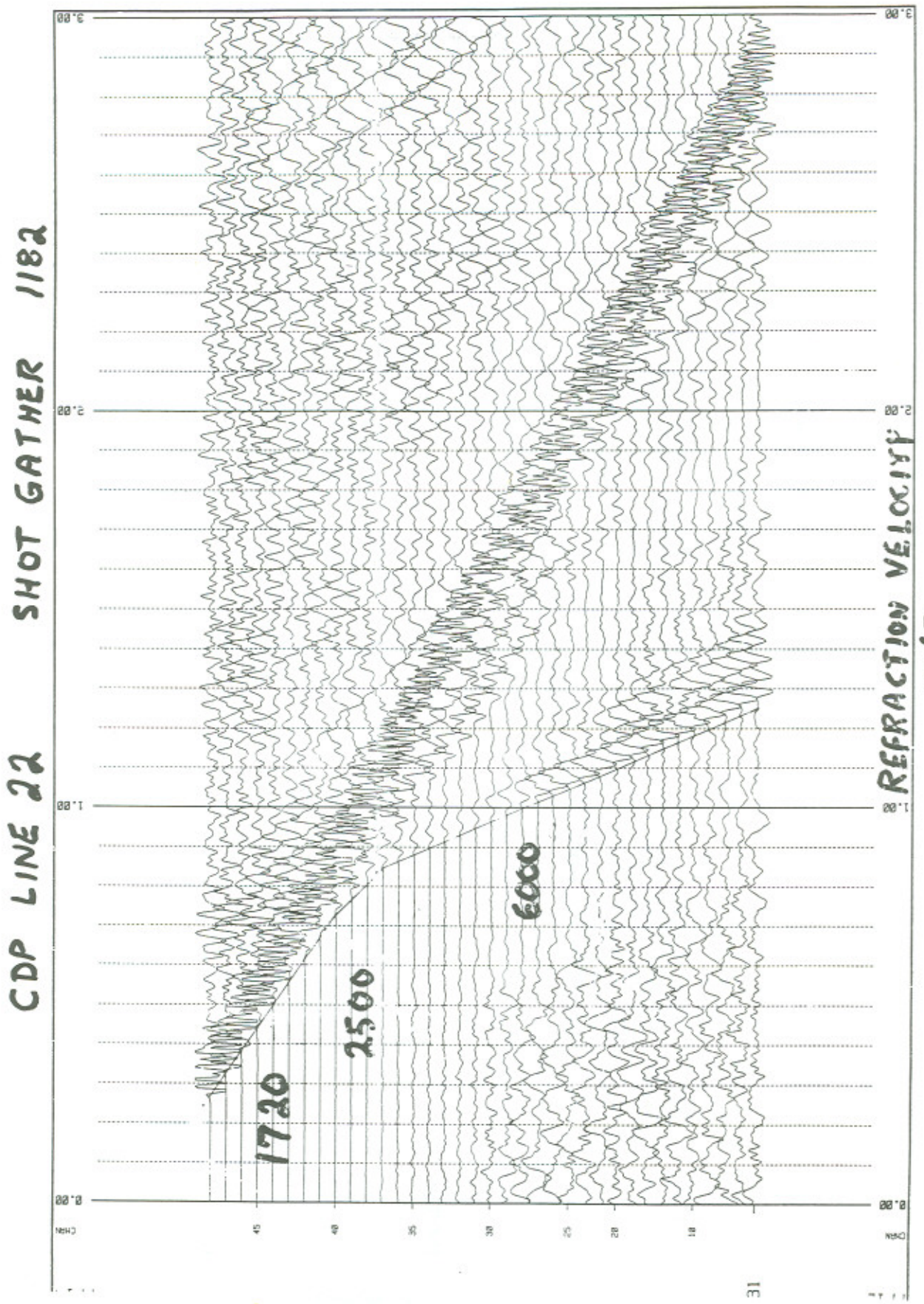
CDP LINE 22
SHOT GATHER 1182
REFRACTION VELOCITY
m/s
1720
2500
6000

Figure 23

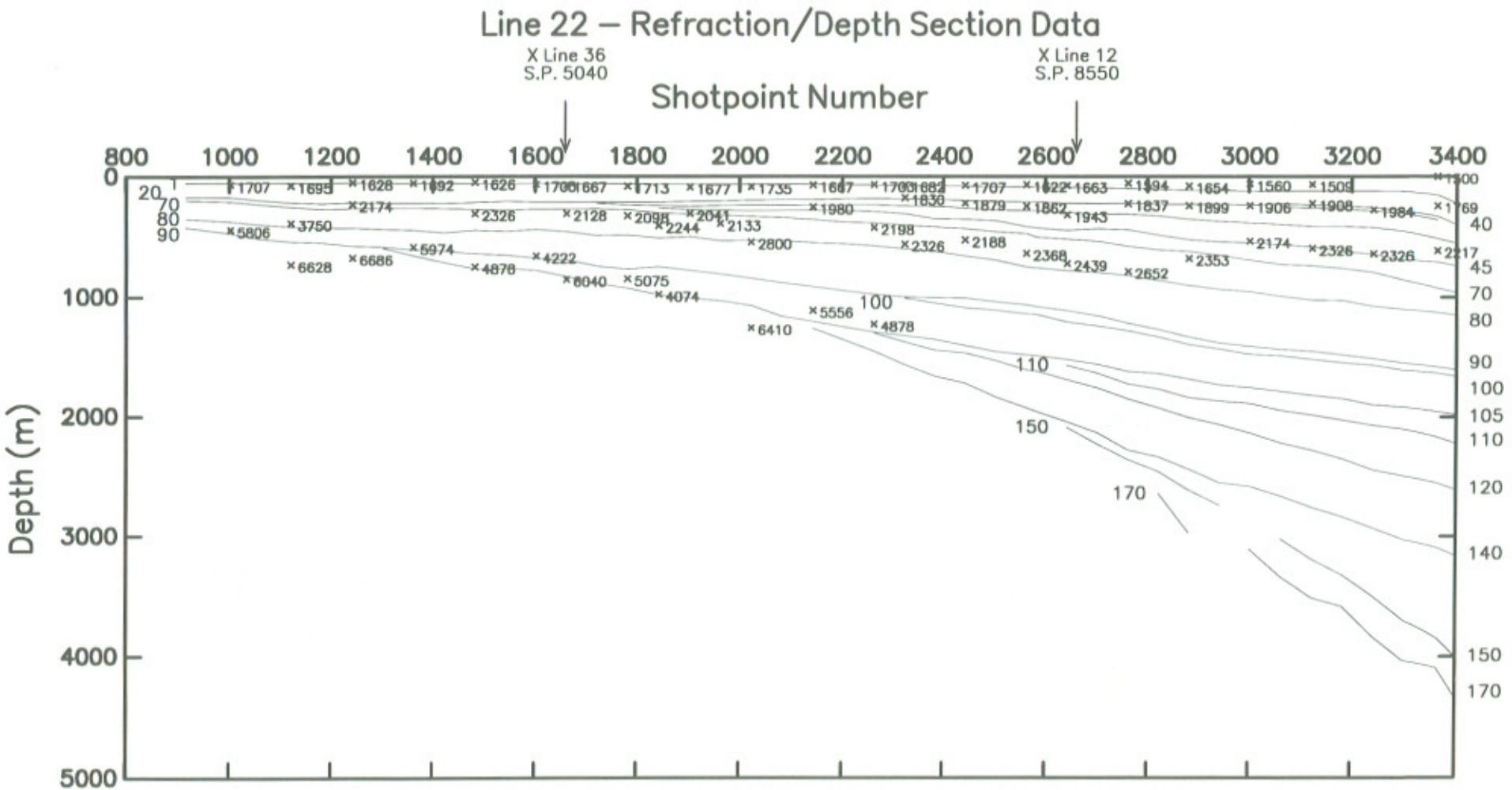
Line 22 – Refraction/Depth Section Data
X Line 36
S.P. 5040
X Line 12
S.P. 8550
Shotpoint Number
800
1000
1200
1400
1600
1800
2000
2200
2400
2600
2800
3000
3200
3400
Depth (m)
0
1000
2000
3000
4000
5000
20
70
80
90
100
110
150
170
40
45
70
80
90
100
105
110
120
140
150
170

Figure 24

APPENDIX 1
U.S. Geological Survey CDP Lines

Seismic Line #	Starting Shot Pt.#	Ending Shot Pt.#	Shot Point Spacing
Composite Line G1-G2	10435	11500	100m
USGS CDP Line 1	100	2920	100m
USGS CDP Line 2	100	2625	100m
USGS CDP Line 3	130	2370	100m
USGS CDP Line 5	100	3410	100m
USGS CDP Line 6	200	3870	100m
USGS CDP Line 7	70	2765	100m
USGS CDP Line 8c	140	2400	100m
USGS CDP Line 9	100	3135	100m
USGS CDP Line 10	120	2780	100m
USGS CDP Line 11	190	2540	100m
USGS CDP Line 12a	100	1620	100m
USGS CDP Line 12bc	1600	4100	100m
USGS CDP Line 12de	4100	7400	100m
USGS CDP Line 12fg	7400	9160	100m
USGS CDP Line 12hi	9120	10720	100m
USGS CDP Line 12j1	10720	12600	100m
USGS CDP Line 13a	90	2000	100m
USGS CDP Line 13b	2000	4000	100m
USGS CDP Line 13cd	4000	6040	100m
USGS CDP Line 13ef	6040	8600	100m
USGS CDP Line 13gh	8580	11270	100m
USGS CDP Line IPOD	100	2170	100m
USGS CDP Line 14a	1000	2260	50m
USGS CDP Line 14b	1000	2480	50m
USGS CDP Line 15a	520	2200	50m
USGS CDP Line 15b	1000	2425	50m
USGS CDP Line 16	1	6200	50m
USGS CDP Line 17	1290	4370	50m
USGS CDP Line 18	100	4900	50m
USGS CDP Line 19	100	4895	50m
USGS CDP Line 20	4870	100	50m
USGS CDP Line 21	210	5035	50m
USGS CDP Line 22	915	6700	50m
USGS CDP Line 23	360	6260	50m
USGS CDP Line 24	490	3560	50m
USGS CDP Line 25a	430	2870	50m
USGS CDP Line 25b	2845	6570	50m
USGS CDP Line 26	100	5470	50m
USGS CDP Line 27	240	5350	50m
USGS CDP Line 28	365	5315	50m
USGS CDP Line 29	640	4940	50m
USGS CDP Line 30	470	3060	50m
USGS CDP Line 33	85	3840	50m
USGS CDP Line 34	100	2820	50m
USGS CDP Line 36	100	6500	50m
USGS CDP Line 37	100	4865	50m
USGS CDP Line 38	100	4600	50m
BGR 79-202	1	4880	50m
BGR 79-204	7500	15650	50m

Line crossing and well crossing shot point numbers

Seismic Line#	Shot Pt. #	Crossing Line# or Well	Shot Pt. #
2	125	AMCOR 6011 (on line)	
2	940	Mobil 544-1 (2 km NE of line)	
2	1060	Conoco 590-1 (3 km NE of line)	
5	1770	ASP 17/18 (10 km NE of line)	
6	1060	Shell 273-1 (5 km SW of line)	
6	1415	Shell 586-1 (5 km SW of line)	
6	1470	Shell 587-1 (5 km SW of line)	
8a	800	20	3900
9	1400	24	3560
9	2450	2	2495
10	1140	Shell 93-1 (on line)	
11	190	USCGLT-CH1-2	
12ab	160	IPOD	320
12ab	900	30	470
12ab	1598	17	1835
12ab	2117	29	1480
12ab	2672	11	680
12c	3095	28	1420
12c	3470	3	565
12c	3900	27	1060
12d	4298	10	603
12d	4650	26	1189
12d	5050	6	704
12d	5565	25	1510
12d	5850	AMCOR 6020 (17 km NW of line)	
12d	6000	2	735
12e	6785	24	2565
12e	7095	9	945
12fg	7620	23	1740
12fg	8060	16	1780
12fg	8550	22	2660
12fg	9110	5	1150
12hi	9570	21	1440
12hi	9965	8	680
12hi	10630	20	2850
12hi	10720	77-1	370
12j1	11170	1	1010
12j1	11430	19	2480
12j1	11815	7	1280
12j1	12115	18	2360
12j1	12410	4	1090
13ad	170	IPOD	1709
13ad	825	30	2800
13ad	1548	17	4370
13ad	2000	29	4410
13ad	2485	11	2300
13ad	2890	28	4700
13ad	3300	3	2200

13ad	3645	27	4360
13ad	4030	10	2325
13ad	4435	26	4700
13ad	4815	6	2540
13ad	5490	25	5580
13ad	5840	9	2980
13eh	6250	23	5690
13eh	6640	16	5580
13eh	7080	22	6155
13eh	7540	5	2705
13eh	8065	21	4250
13eh	8615	8	2040
13eh	9335	20	120
13eh	9930	1	2160
13eh	10280	19	4730
13eh	10620	7	2390
13eh	10940	18	4590
13eh	11260	4	2205
14a	1050	6	1060
14a	1240	Shell 272-1 (8 km NW of line)	
14a	1350	Shell 273-1 (2 km NW of line)	
14a	2100	25	2195
14a	2260	14b	1000
14b	1790	2	1198
14b	2035	COST B-2 (on line)	
15a	930	Tenneco 495-1 (on line)	
15a	1050	6	1250
15a	2115	25	2550
15a	2185	Mobil 17-2 (2 km NW of line)	
15a	2200	15b	1010
15b	1380	HOM 855-1 (5 km NW of line)	
15b	1460	Gulf 857-1 (1 km SE of line)	
15b	1900	2	1360
15b	1905	Exxon 728-1 (1 km SE of line)	
15b	1950	Exxon 684-2 (1 km NW of line)	
15b	2010	Exxon 648-1 (2 km NE of line)	
15b	2220	Tenneco 642-2 (5 km SE of line)	
15b	2250	Texaco 598-2 (NW of line)	
15b	2300	Texaco 598-3 (on line)	
19	365	AMCOR 6019	
20	4150	AMCOR 6016	
25	570	37	3095
25	1424	LASE ESP-1	
25	1510	12d	5565
25	2068	LASE ESP-2	
25	2195	14a	2100
25	2428	LASE ESP-3	
25	2550	15a	2115
25	2720	204	5990

25	2880	ASP-17	
25	3050	DSDP 612 (on line)	
25	3060	34	1270
25	3143	LASE ESP-4	
25	3390	DSDP 605 (on line)	
25	3500	DSDP 604 (on line)	
25	3650	DSDP 107 (on line)	
25	3710	LASE ESP-5	
25	5580	13	5490
26	2340	Shell 586-1 (on line)	
26	2440	Shell 587-1 (on line)	
28	1905	ASP 10	
28	2100	ASP 22	
30	470	USCG-LT DS-1/2	
33	238	20	2082
33	1220	1	1345
33	1750	19	3160
33	2590	7	1680
33	3230	18	3030
33	3845	4	1390
34	190	6	1400
34	1170	ASP 15	
34	1270	25	3060
34	1450	COST B-3 (Proj.)	
34	2325	2	1640
36	640	24	1075
36	2130	9	527
36	3230	23	1000
36	4120	16	910
36	5040	22	1659
36	6130	5	550
37	4871	36	101
37	3900	2	240
37	3095	25	570
37	2105	6	260
37	1300	26	340
37	600	10	250
38	355	20	1328
38	1390	1	1880
38	2045	19	4370
38	2760	7	2250
38	3460	18	4180
38	4090	4	1960

77-1	105	COST G-1	
77-1	370	12	10720
77-2	210	1	1200
77-2	105	COST G-2	
202	0001	11	1320
202	865	28	2560
202	1595	3	1140
202	2445	27	2365
202	3240	10	1327
202	4000	26	2750
202	4880	6	1600
204	0005	11	1020
204	900	28	1920
204	900	ASP 10	
204	1650	3	810
204	2530	27	1675
204	3340	10	990
204	4070	26	2050
204	4900	6	1220
204	5990	25	2720
204	7010	2	1440
204	8350	9	1490
204	9370	23	2600
204	9725	AMCOR 6012	
204	10250	16	2300
204	11250	22	3605
204	12380	5	1685
204	13310	21	2400
204	14230	8	1190
204	15660	20	1840
204	16600	1	1635

Appendix 2

U.S. Atlantic Margin Wells with Velocity Data Used to Calibrate Database.

Basin	Co.	WELL NO.	LATITUDE	LONGITUDE	W.D.	T.D.	Sonic	Ckshot
GBB		COST G-1	40°55.87'N	68°18.32'W	47.9m	4821m	yes	yes
GBB		COST G-2	40°50.26'N	67°30.49'W	81.7m	6554m	yes	yes
BCT		COST B-2	39°22.53'N	72°44.06'W	90.8m	4863m	yes	yes
BCT	SHELL	SH-273-1	38d42.974'N	73d27.341'W	72m	5237m	yes	yes
BCT	SHELL	SH-587-1	38d22.92'N	73d09.85'W	2042m	4420m	no	yes
BCT	SHELL	SH-586-1	38d24.34'N	73d13.05'W	1794m	3076m	no	yes
BCT	SHELL	SH-93-1	37d53.58'N	73d44.16'W	1529m	5407m	yes	yes
BCT	GULF	Gu-857-1	39d06.318'N	72d49.457'W	102m	5527m	no	yes
BCT	TEXACO	TX-598-2	39d22.316'N	72d31.859'W	128m	5244m	no	yes
BCT	MOBIL	MO-17-2	38d58.067'N	73d02.943'W	79m	4160m	yes	yes
BCT	MOBIL	MO-544-1	39d25.47'N	73d04.60'W	66m	2543m	no	yes
BCT	EXXON	EX-684-2	39d16.731'N	72d39.133'W	126m	4969m	yes	yes
BCT	TENNECO	TN-495-1	38d27.981'N	73d22.698'W	108m	5443m	yes	yes

---

Industry wells on the northern U.S. continental margin not used to construct the velocity database. Bio-/lithostratigraphic information from selected wells was incorporated into the stratigraphic analyses as indicated in the reports by Poag (1982, 1985b,1987,1991,1992), Poag and Valentine (1988) and Poag and Wade (1993).

Basin	Co.	WELL NO.	LATITUDE	LONGITUDE	W.D.	T.D.
GBB	EXXON	EX-133-1	40d49.08'N	67d56.046'W	69m	4303m
GBB	EXXON	EX-975-1	41d00.90'N	67d37.35'W	64m	4361m
GBB	SHELL	SH-410-1	40d34.39'N	67d12.54'W	136m	4587m
GBB	MOBIL	MO-312-1	40d39.10'N	67d46.90'W	84m	6096m
GBB	MOBIL	MO-187-1	40d46.25'N	67d23.32'W	94m	5407m
GBB	GULF	GU-145-1	40d50.73'N	67d17.57'W	91m	4302m
GBB	MOBIL	MO-273-1	40d41.08'N	67d30.21'W	98m	4624m
GBB	SHELL	SH-357-1	40d37.57'N	67d44.77'W	82m	5818m
BCT		COST B-3	38°55.10'N	72°46.38'W	819m	3991m
BCT	CONOCO	CO-590-1	39d22.560'N	72d58.040'W	70m	3562m
BCT	SHELL	SH-632-1	39d20.999'N	73d06.320'W	64m	4180m
BCT	TEXACO	TX-598-1	39d22.319'N	72d30.328'W	130m	4423m
BCT	HOUSTON	HO-676-1	39d17.217'N	73d06.383'W	67m	3713m
BCT	EXXON	EX-684-1	39d18.163'N	72d38.499'W	12m	5226m
BCT	MOBIL	MO-17-1	38d58.080'N	73d02.950'W	85m	261m
BCT	HOUSTON	HO-855-1	39d06.347'N	72d54.840'W	89m	5217m
BCT	SHELL	SH-272-1	38d42.070'N	73d32.430'W	66m	4024m
BCT	GULF	GU-718-1	39d15.657'N	73d09.957'W	58m	3825m
BCT	EXXON	EX-902-1	39d04.239'N	72d45.246'W	132m	4713m
BCT	TENNECO	TN-642-2	39d20.597'N	72d29.650'W	139m	5447m
BCT	EXXON	EX-500-1	39d26.920'N	73d06.100'W	62m	3647m
BCT	TEXACO	TX-642-1	39d20.865'N	72d30.878'W	139m	5264m
BCT	MURPHY	MU-106-1	38d51.238'N	72d57.304'W	125m	4908m
BCT	TENNECO	TN-642-3	39d20.262'N	72d31.736'W	137m	4861m
BCT	EXXON	EX-599-1	39d21.88'N	72d29.15'W	135m	5058m
BCT	TEXACO	TX-598-4	39d21.70'N	72d30.35'W	129m	4724m
BCT	EXXON	EX-816-1	39d10.05'N	72d38.10'W	143m	5257m
BCT	EXXON	EX-728-1	39d15.22'N	72d39.15'W	132m	4477m
BCT	SHELL	SH-372-1	38d36.02'N	72d52.23'W	2119m	3545m

Appendix 3

Checkshot and sonic log velocity profiles at industry wells used to calibrate the geoacoustic database. Locations of wells are labeled on seismic lines (Figures 6, 7, 8, 10) and given in Appendices 1 and 2.

Well	Seismic Line Crossings	Shot Point	Figure #
COST G-1	Composite Line G1-G2	10450	Figure 6
COST G-2	Composite Line G1-G2	11480	Figure 6
COST B-2	USGS Line 14b	2035	Figure 7
COST B-2	USGS Line 2	1198	
SHELL 273-1	USGS Line 14a	1240	Figure 7
TENNECO 495-1	USGS Line 15a	930	Figure 8
TENNECO 495-1	USGS Line 6	1250	
MOBIL 17-2	USGS Line 15a	2185	Figure 8
MOBIL 17-2	USGS Line 25	2550	Figure 10
GULF 857-1	USGS Line 15b	1460	Figure 8
EXXON 684-2	USGS Line 15b	1950	Figure 8
EXXON 684-2	USGS Line 2	1360	
TEXACO 598-2	USGS Line 15b	2250	Figure 8
MOBIL 544-1	USGS Line 2	940	
SHELL 586-1	USGS Line 6	1415	
SHELL 587-1	USGS Line 6	1470	
SHELL 93-1	USGS Line 10	1140	

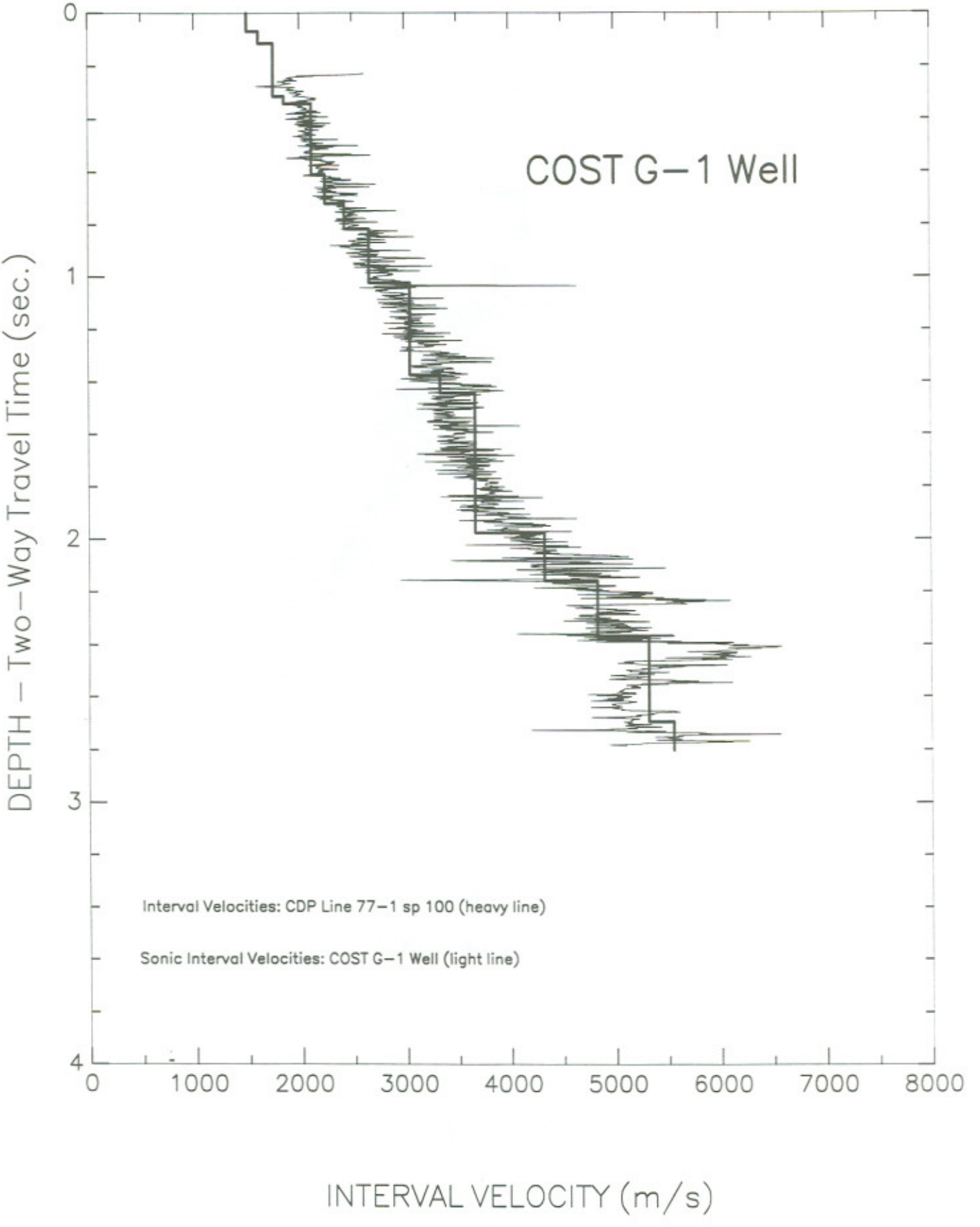
COST G–1 Well
DEPTH – Two–Way Travel Time (sec.)
0
1
2
3
4
0
1000
2000
3000
4000
5000
6000
7000
8000
INTERVAL VELOCITY (m/s)
Interval Velocities: CDP Line 77–1 sp 100 (heavy line)
Sonic Interval Velocities: COST G–1 Well (light line)

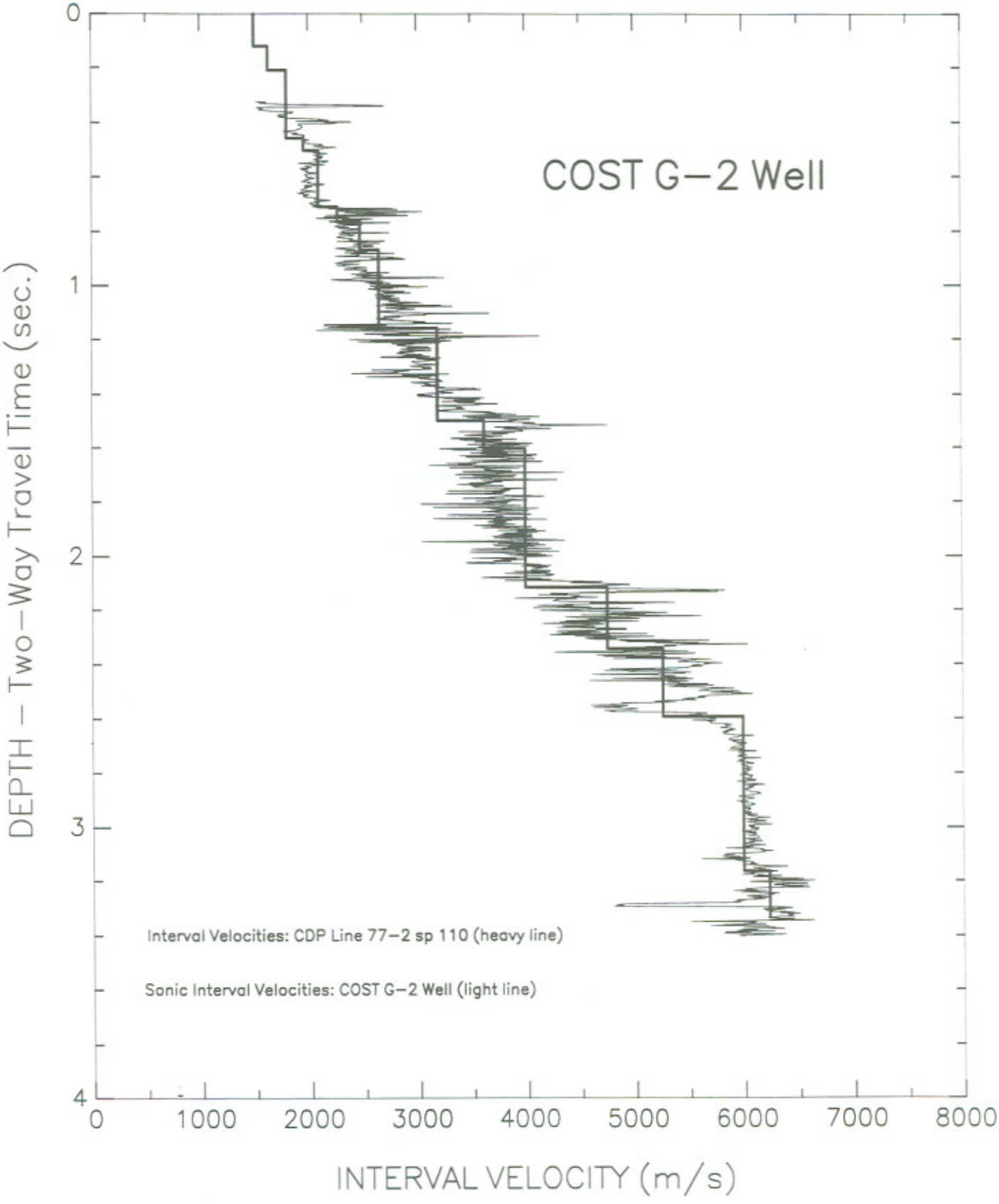
COST G–2 Well
DEPTH – Two–Way Travel Time (sec.)
0
1
2
3
4
0
1000
2000
3000
4000
5000
6000
7000
8000
INTERVAL VELOCITY (m/s)
Interval Velocities: CDP Line 77–2 sp 110 (heavy line)
Sonic Interval Velocities: COST G–2 Well (light line)

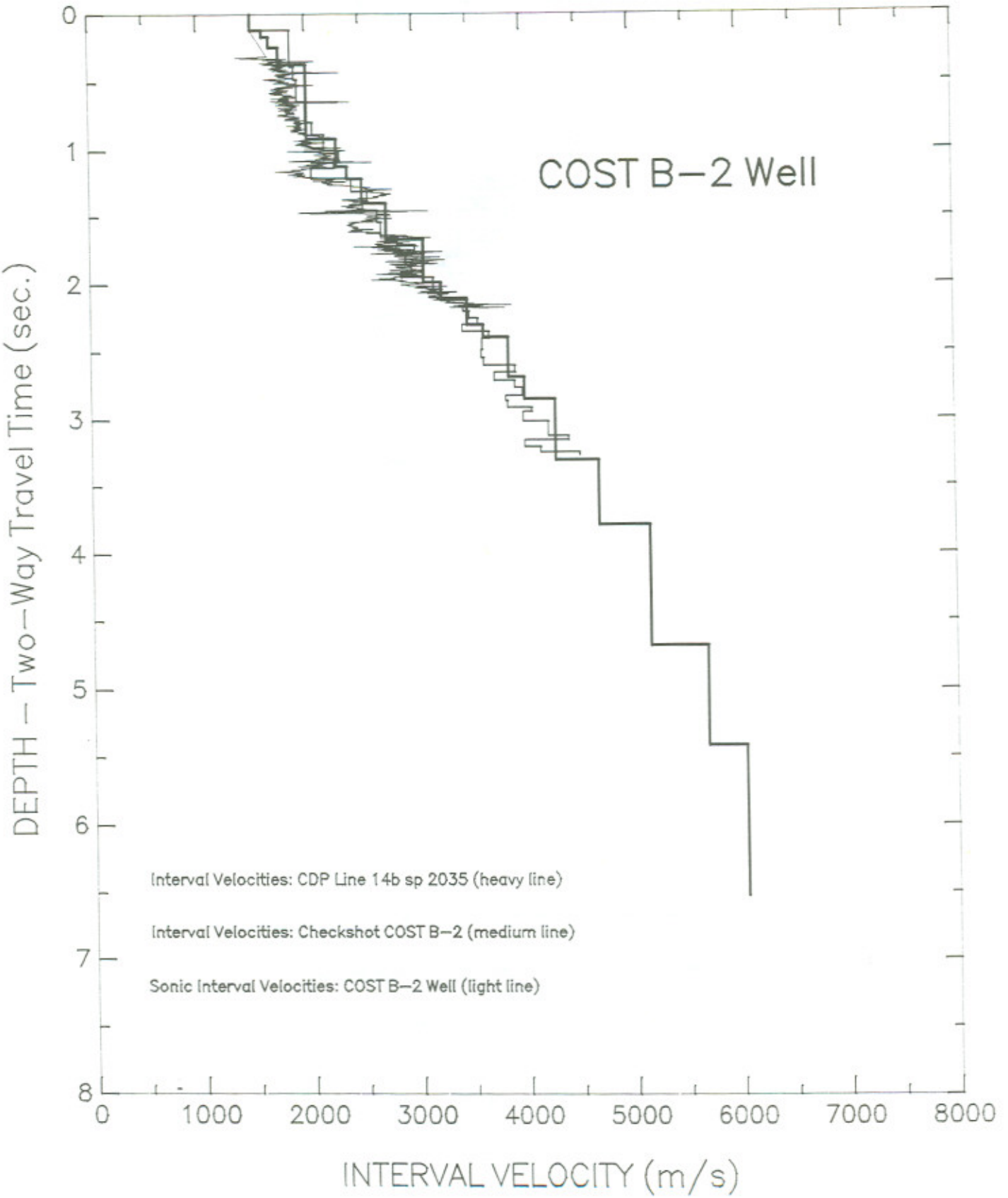
COST B–2 Well
DEPTH – Two–Way Travel Time (sec.)
INTERVAL VELOCITY (m/s)
0
1
2
3
4
5
6
7
8
0
1000
2000
3000
4000
5000
6000
7000
8000
Interval Velocities: CDP Line 14b sp 2035 (heavy line)
Interval Velocities: Checkshot COST B–2 (medium line)
Sonic Interval Velocities: COST B–2 Well (light line)

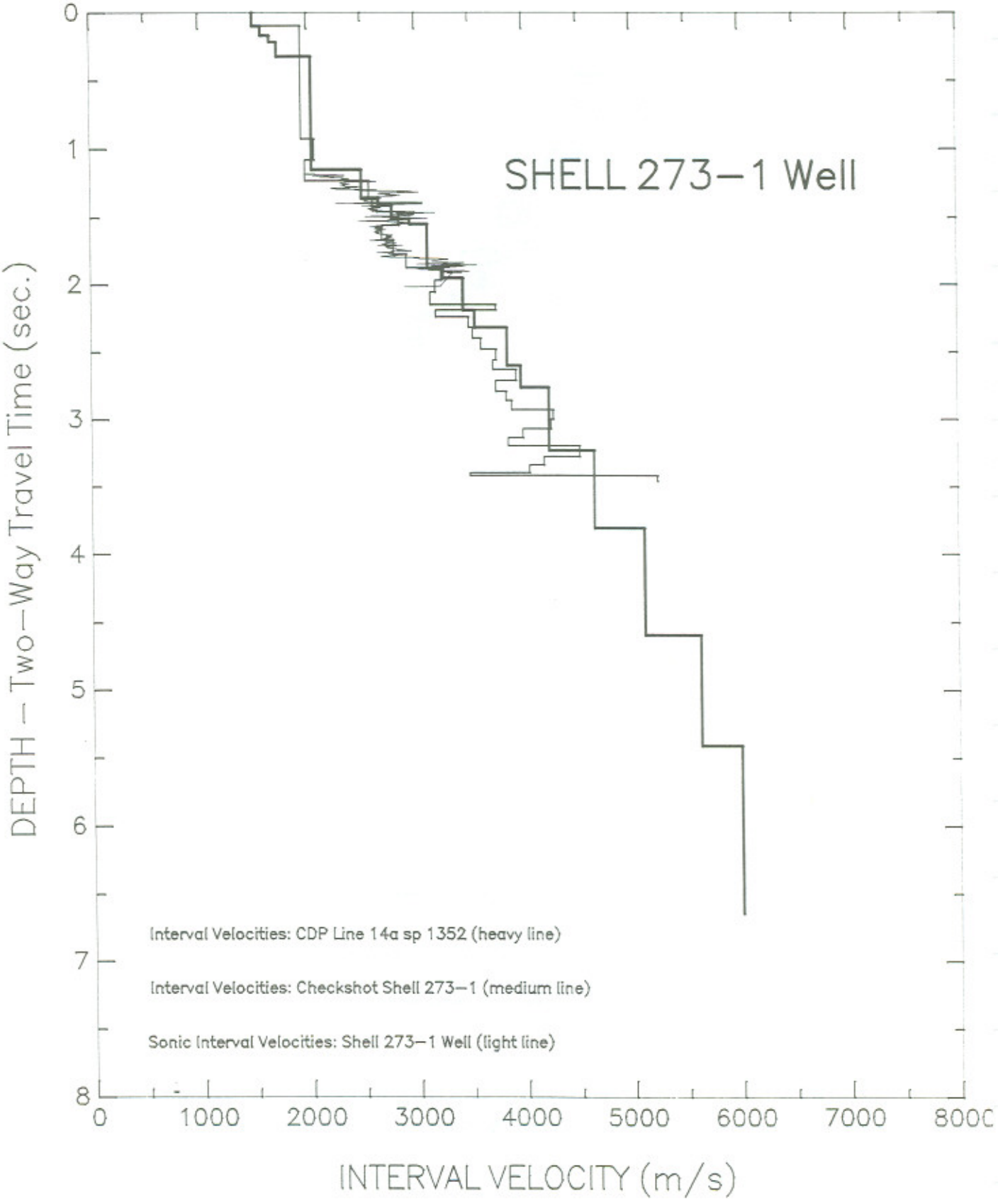
SHELL 273–1 Well
DEPTH – Two–Way Travel Time (sec.)
INTERVAL VELOCITY (m/s)
0
1
2
3
4
5
6
7
8
0
1000
2000
3000
4000
5000
6000
7000
8000
Interval Velocities: CDP Line 14a sp 1352 (heavy line)
Interval Velocities: Checkshot Shell 273–1 (medium line)
Sonic Interval Velocities: Shell 273–1 Well (light line)

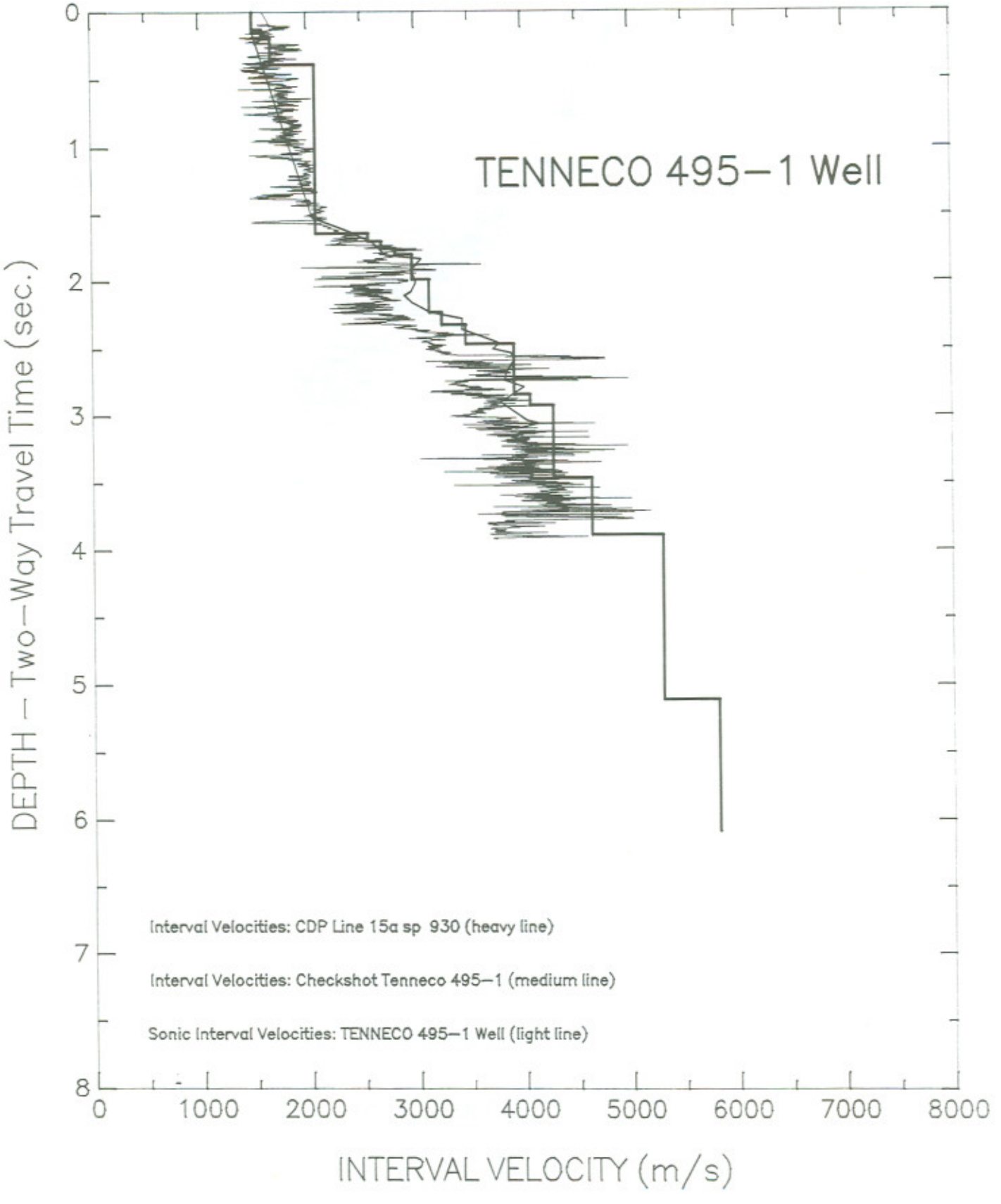
TENNECO 495–1 Well
DEPTH – Two–Way Travel Time (sec.)
0
1
2
3
4
5
6
7
8
0
1000
2000
3000
4000
5000
6000
7000
8000
INTERVAL VELOCITY (m/s)
Interval Velocities: CDP Line 15a sp 930 (heavy line)
Interval Velocities: Checkshot Tenneco 495–1 (medium line)
Sonic Interval Velocities: TENNECO 495–1 Well (light line)

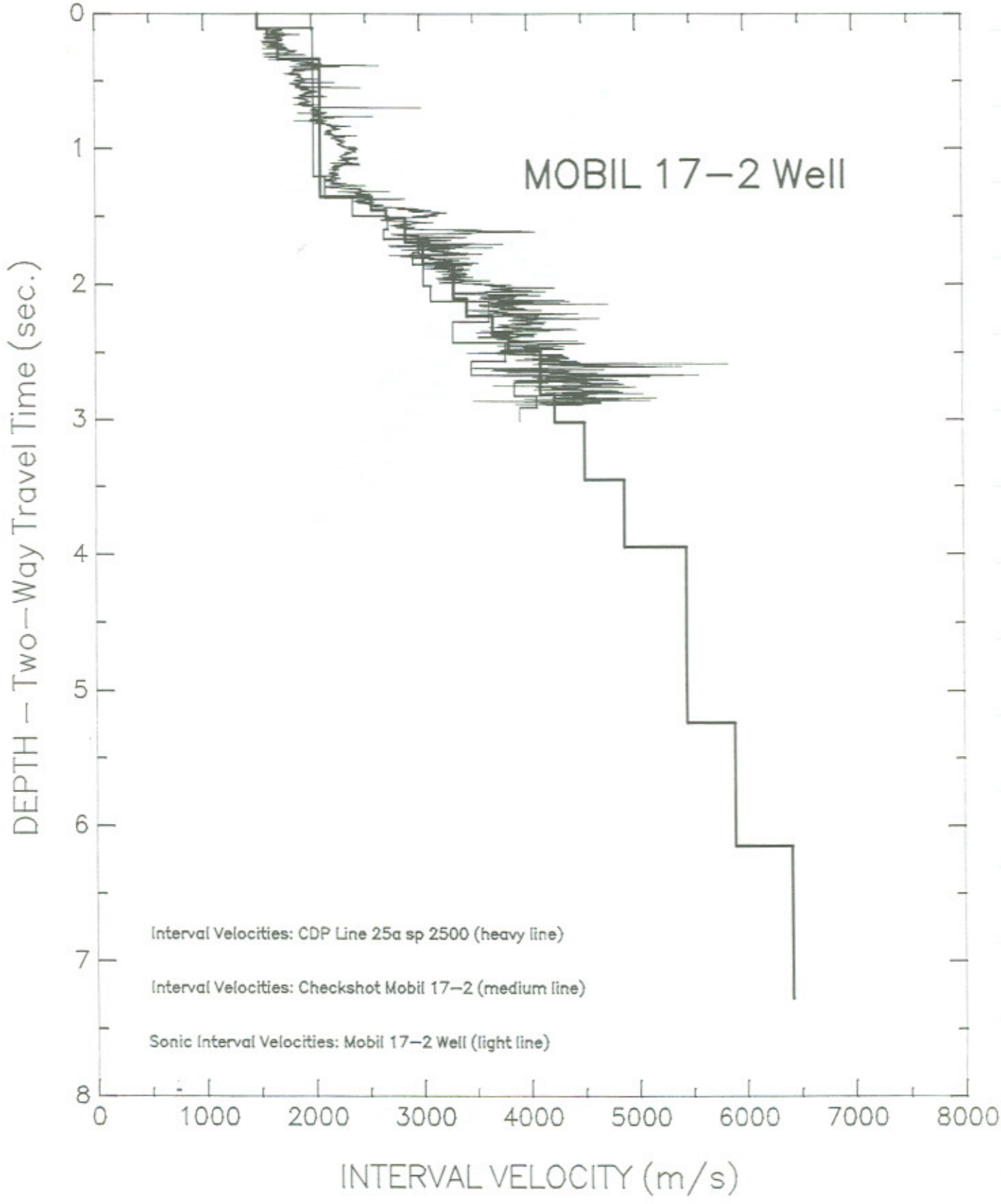
MOBIL 17–2 Well
DEPTH – Two–Way Travel Time (sec.)
INTERVAL VELOCITY (m/s)
0
1
2
3
4
5
6
7
8
0
1000
2000
3000
4000
5000
6000
7000
8000
Interval Velocities: CDP Line 25a sp 2500 (heavy line)
Interval Velocities: Checkshot Mobil 17–2 (medium line)
Sonic Interval Velocities: Mobil 17–2 Well (light line)

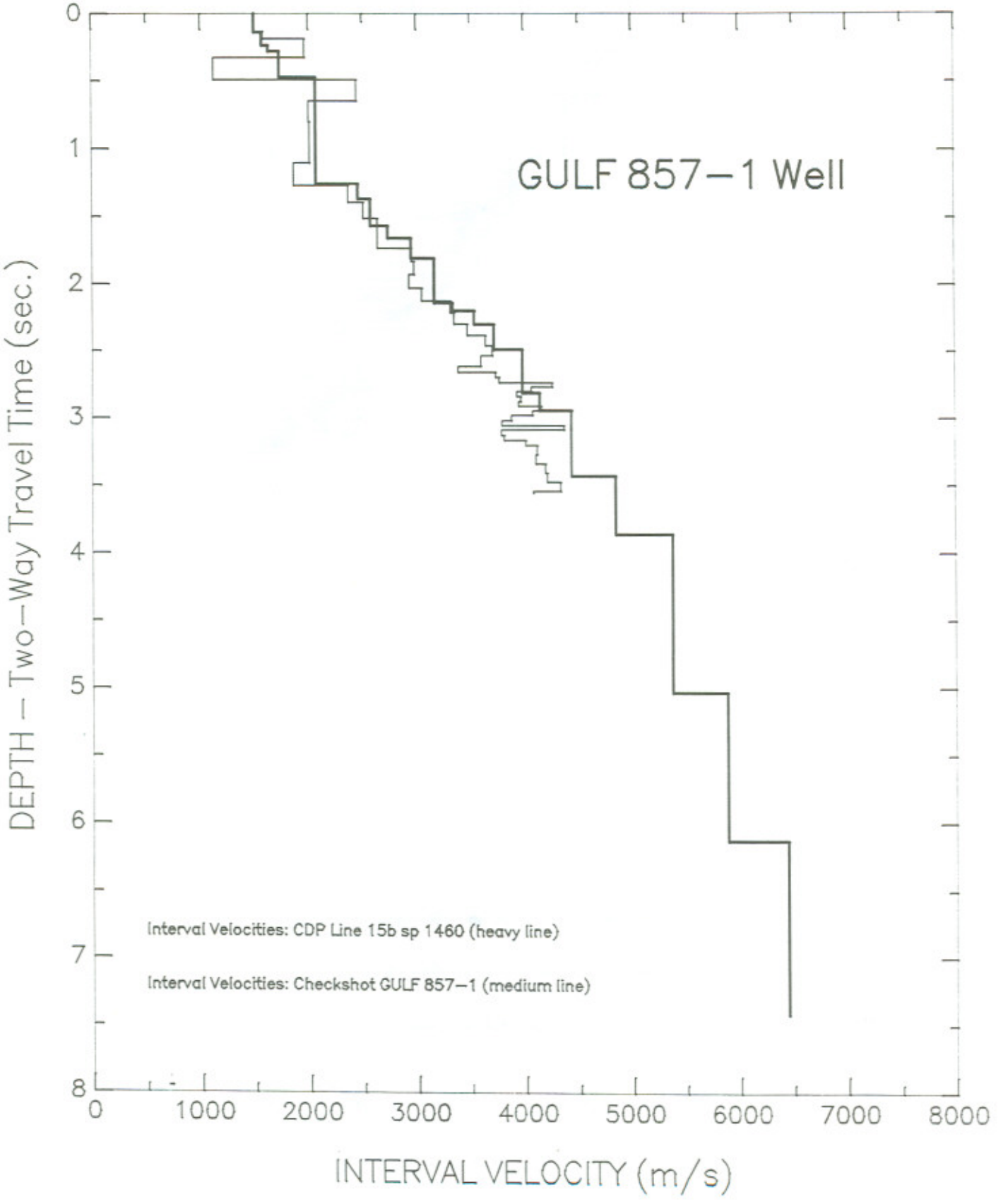
GULF 857–1 Well
DEPTH – Two–Way Travel Time (sec.)
0
1
2
3
4
5
6
7
8
0
1000
2000
3000
4000
5000
6000
7000
8000
INTERVAL VELOCITY (m/s)
Interval Velocities: CDP Line 15b sp 1460 (heavy line)
Interval Velocities: Checkshot GULF 857–1 (medium line)

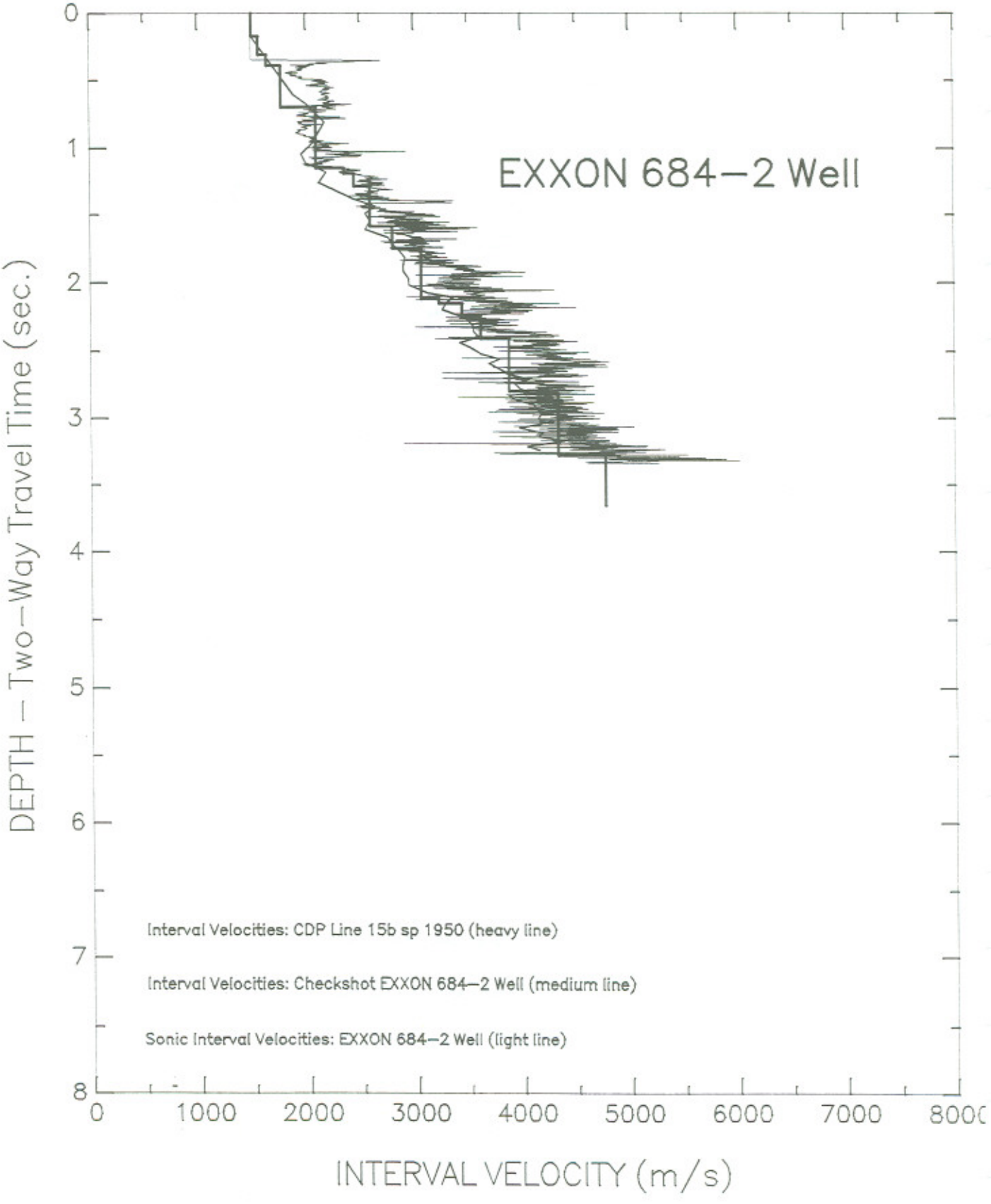
EXXON 684–2 Well
DEPTH – Two–Way Travel Time (sec.)
0
1
2
3
4
5
6
7
8
0
1000
2000
3000
4000
5000
6000
7000
8000
INTERVAL VELOCITY (m/s)
Interval Velocities: CDP Line 15b sp 1950 (heavy line)
Interval Velocities: Checkshot EXXON 684–2 Well (medium line)
Sonic Interval Velocities: EXXON 684–2 Well (light line)

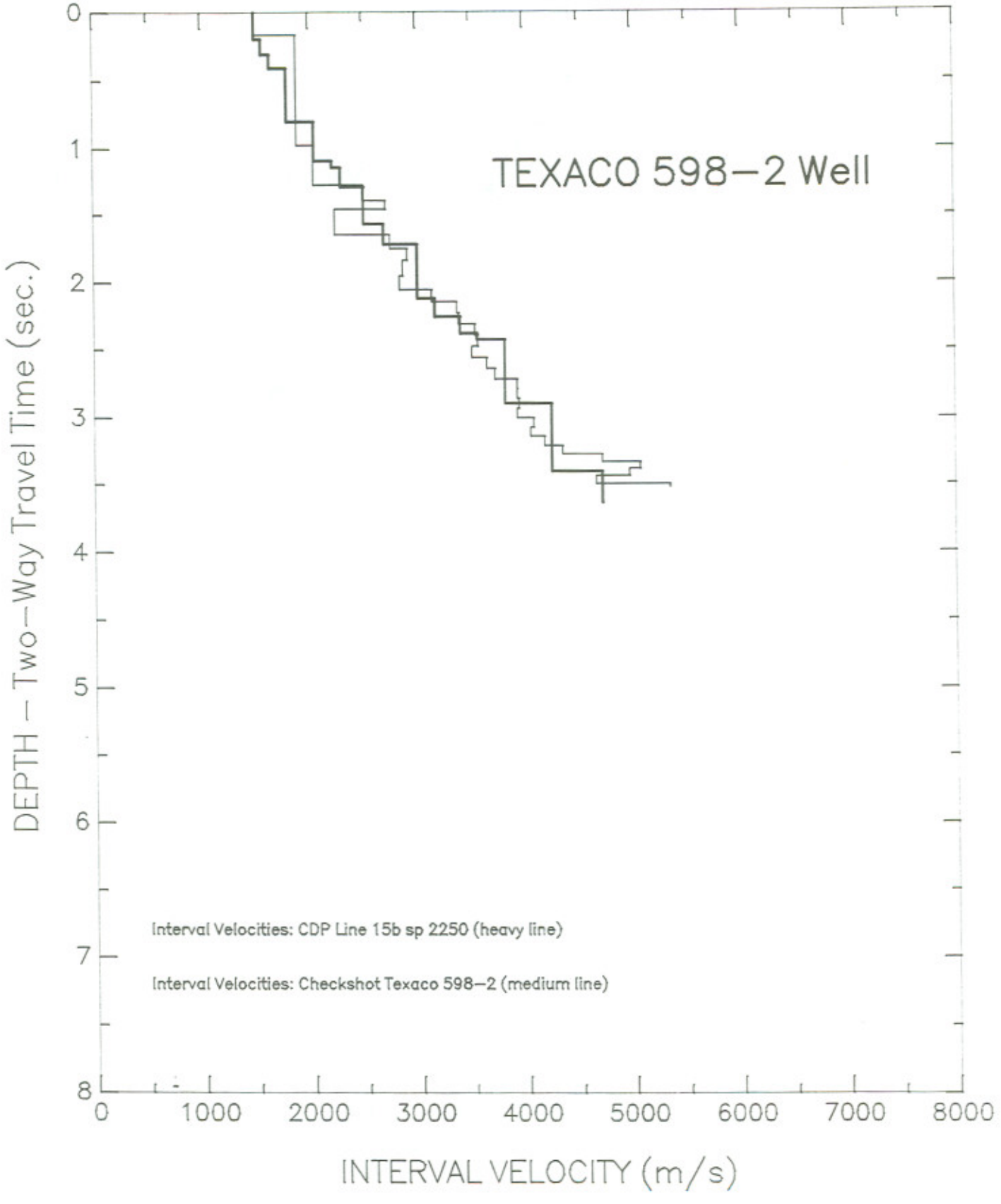
TEXACO 598–2 Well
DEPTH – Two–Way Travel Time (sec.)
0
1
2
3
4
5
6
7
8
0
1000
2000
3000
4000
5000
6000
7000
8000
INTERVAL VELOCITY (m/s)
Interval Velocities: CDP Line 15b sp 2250 (heavy line)
Interval Velocities: Checkshot Texaco 598–2 (medium line)

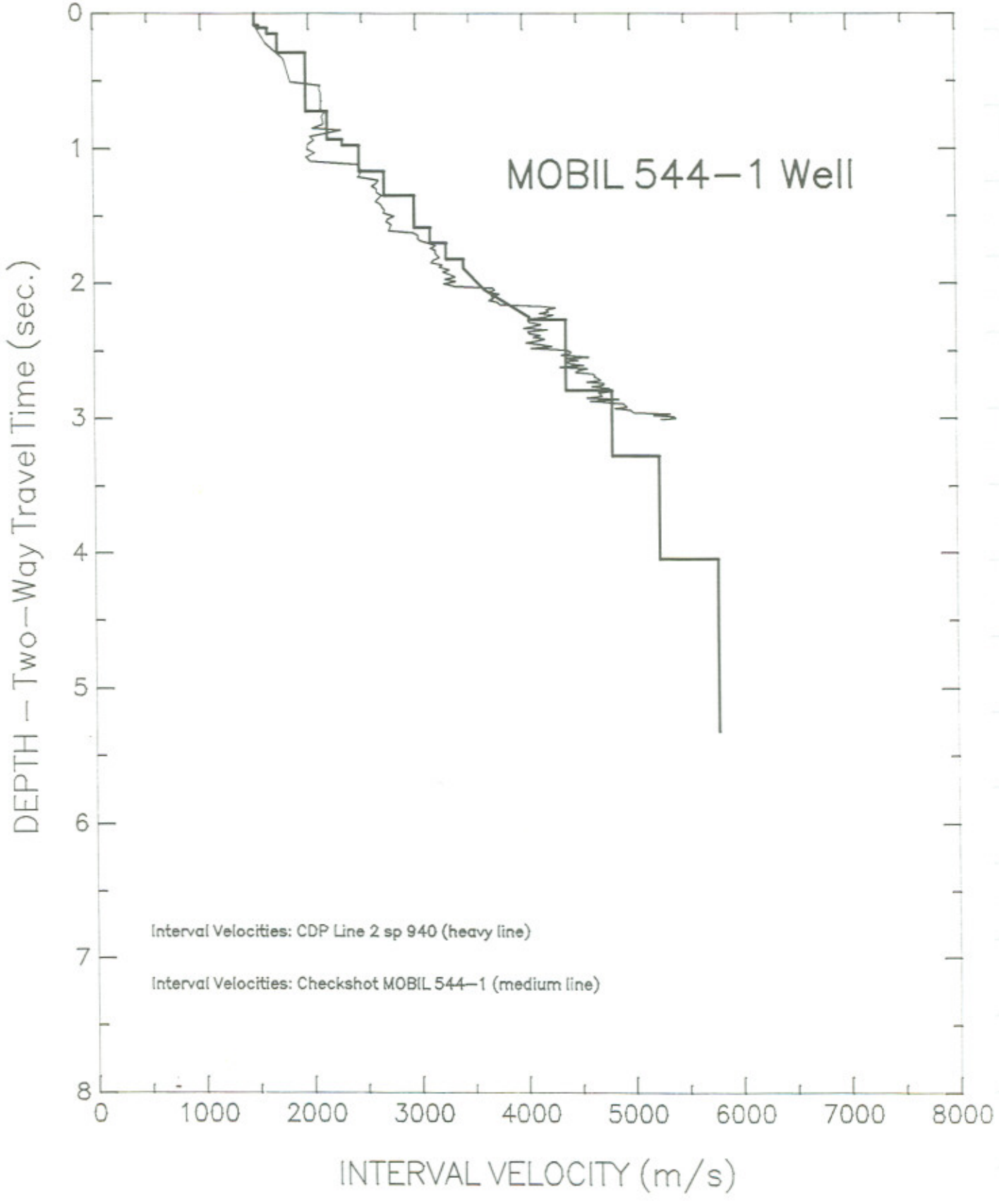
MOBIL 544–1 Well
DEPTH – Two–Way Travel Time (sec.)
0
1
2
3
4
5
6
7
8
0
1000
2000
3000
4000
5000
6000
7000
8000
INTERVAL VELOCITY (m/s)
Interval Velocities: CDP Line 2 sp 940 (heavy line)
Interval Velocities: Checkshot MOBIL 544–1 (medium line)

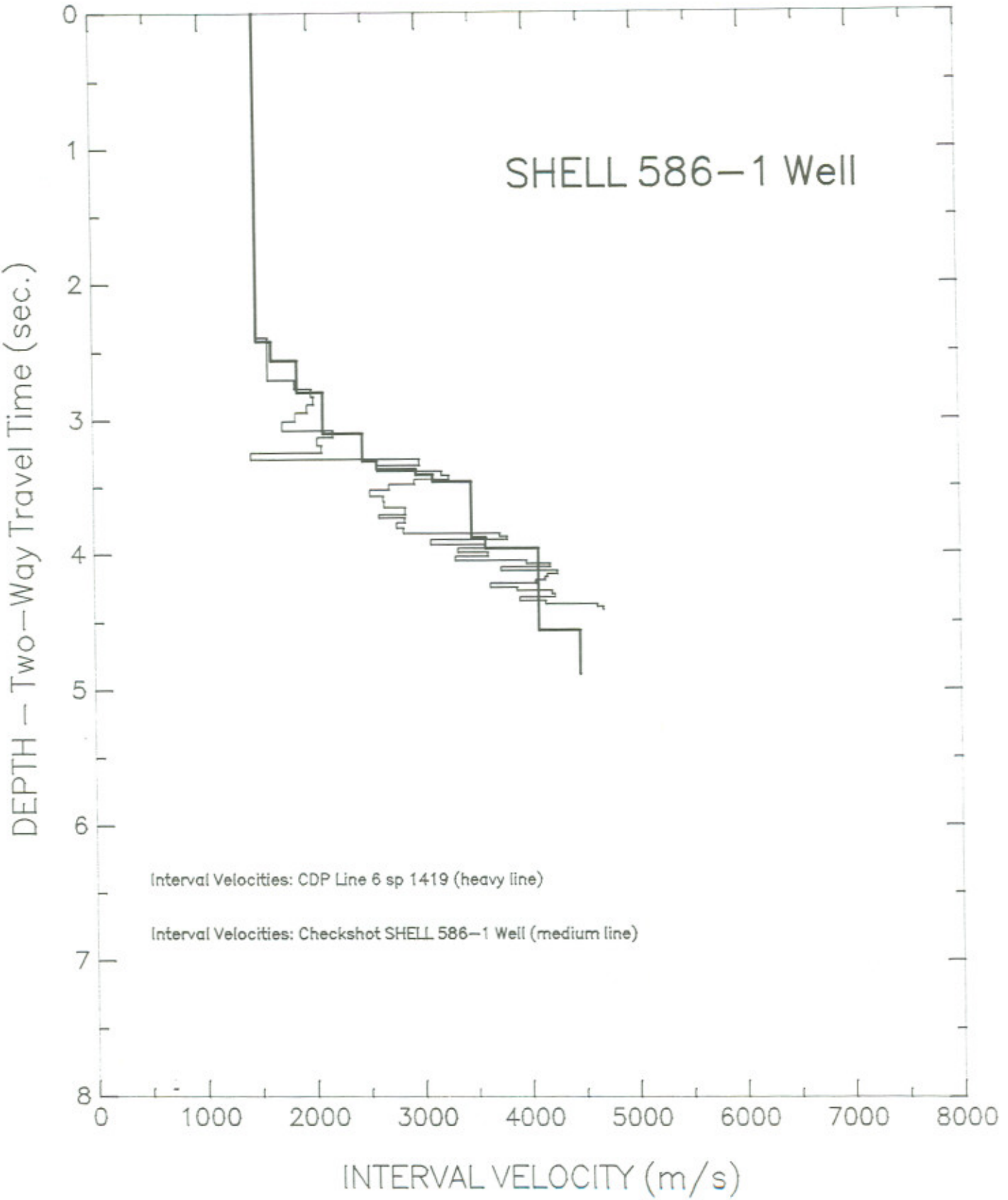
SHELL 586–1 Well
DEPTH – Two–Way Travel Time (sec.)
0
1
2
3
4
5
6
7
8
0
1000
2000
3000
4000
5000
6000
7000
8000
INTERVAL VELOCITY (m/s)
Interval Velocities: CDP Line 6 sp 1419 (heavy line)
Interval Velocities: Checkshot SHELL 586–1 Well (medium line)

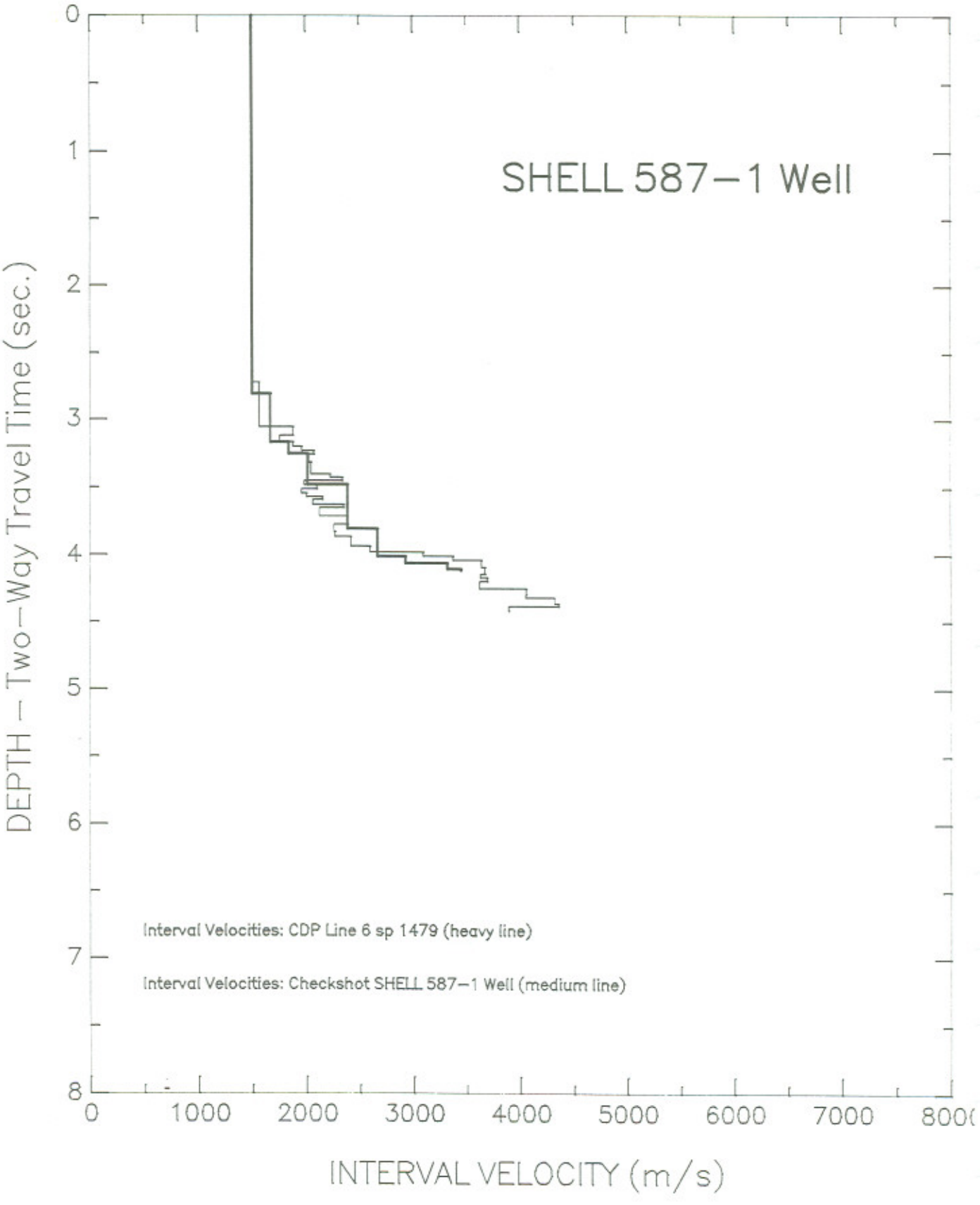
SHELL 587–1 Well
DEPTH – Two–Way Travel Time (sec.)
0
1
2
3
4
5
6
7
8
0
1000
2000
3000
4000
5000
6000
7000
INTERVAL VELOCITY (m/s)
Interval Velocities: CDP Line 6 sp 1479 (heavy line)
Interval Velocities: Checkshot SHELL 587–1 Well (medium line)

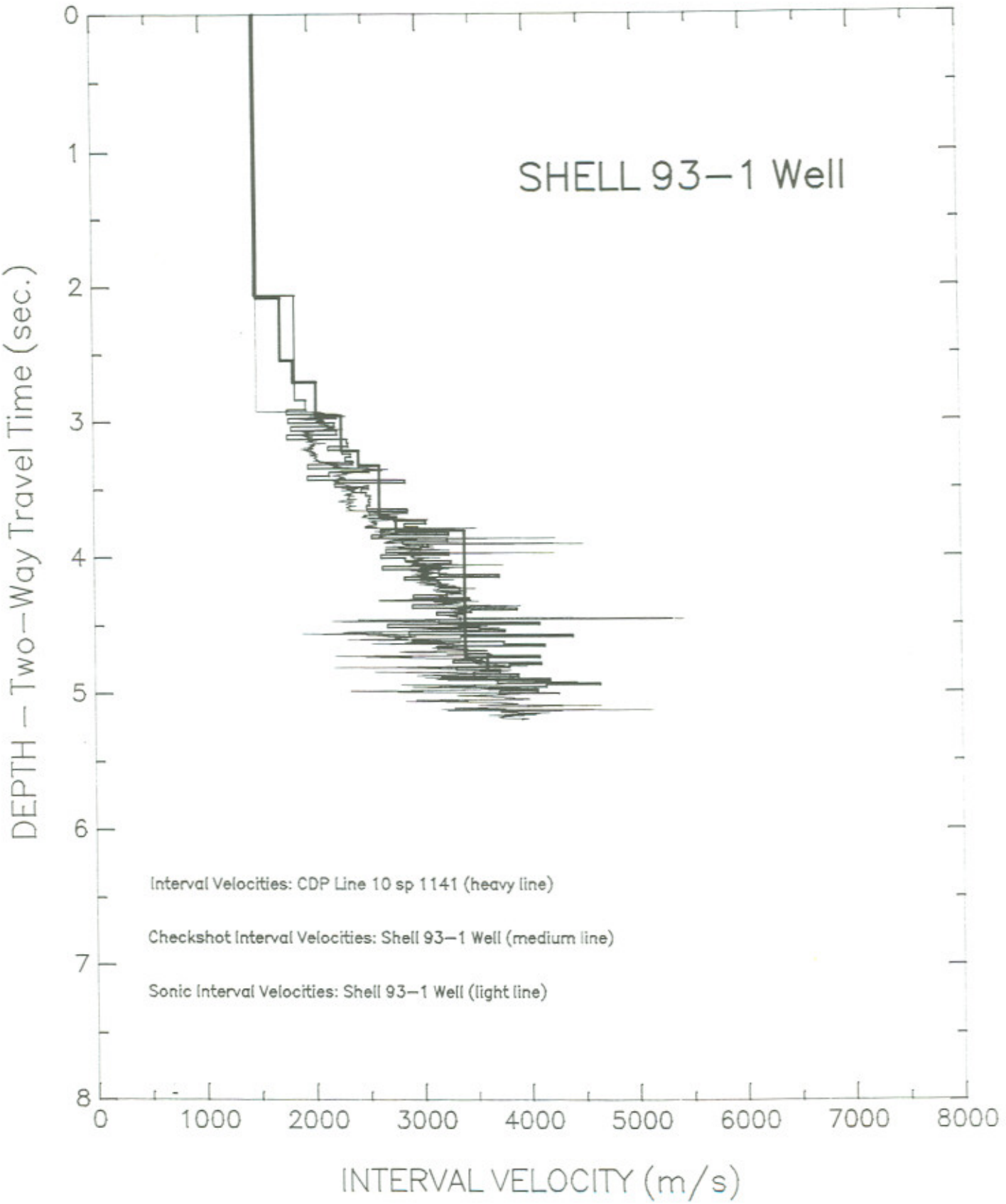
SHELL 93–1 Well
DEPTH – Two–Way Travel Time (sec.)
0
1
2
3
4
5
6
7
8
0
1000
2000
3000
4000
5000
6000
7000
8000
INTERVAL VELOCITY (m/s)
Interval Velocities: CDP Line 10 sp 1141 (heavy line)
Checkshot Interval Velocities: Shell 93–1 Well (medium line)
Sonic Interval Velocities: Shell 93–1 Well (light line)